Abstract

Title of Dissertation: INVESTIGATING THE REGULATION OF GROWTH MECHANISMS IN TWO DISTINCT BRANCHES OF PHOTOSYNTHETIC LIFE

John Sittmann, Doctor of Philosophy, 2019

Dissertation directed by: Professor Zhongchi Liu, Department of Cell Biology and Molecular Genetics

Photosynthetic organisms often have limited mobility and rely on a variety of environmental, physiological, and chemical signals to regulate aspects of growth and development. In this thesis, I investigated how two such organisms, one a flowering plant and the other a heterokont alga, incorporate external signaling cues to make decisions regarding reproduction. My dissertation research is focused on 1) investigating molecular mechanisms of crosstalk between photoperiod and shade in regulating asexual reproduction in the wild strawberry *Fragaria vesca,* and 2) elucidating the mechanism of a bacterium-derived agent in the stimulation of cell division in the marine diatom *Phaeodactylum tricornutum.*

First, strawberry, including woodland strawberry *Fragaria vesca,* is capable of a form of asexual reproduction by producing horizontal stems with daughter plants at the nodes. These horizontal stems, referred to as stolon, are derived from axillary meristems at the base of the leaves. Depending on the signals the axillary meristem receives, it will give

rise to either a branch crown (a flowering shoot) or a stolon. Stolon allows for asexual reproduction to maintain the superior hybrid genotype and hence is of great significance agriculturally. Daughter plants derived from stolon are sold and propagated in strawberry farming. In this work, I have shown that a key regulatory protein FveRGA1 in GA signaling pathway functions as a repressor of stolon development. I further expanded this work by showing that the light quality (shade) signaling pathway interacts with the GA signaling to regulate stolon development. I identified and demonstrated *FvePIF3* as a key transcription factor that positively regulates stolon initiation under far-red light (shade). Understanding the mechanisms underlying axillary meristem cell fate determination could advance biotechnology to increase strawberry production.

Second, I have discovered and characterized a bacterium-based growth stimulation of the diatom *Phaeodactylum tricornutum*. Specifically, I noticed that a culture of *P. tricornutum* that had been accidentally contaminated with bacteria exhibited faster growth. I subsequently identified the responsible bacterium as *Bacillus thuringiensis,* which stimulated rapid *Phaeodactylum* cell division when added to the *Phaeodactylum* culture. I experimentally determined that the growth stimulating agent was heat labile and proteinase K-resistant. Further, I showed that the mother cell lysate of *Bacillus thuringiensis* under sporulation was just as effective in promoting *Phaeodactylum.* In collaboration with Dr. Jon Clardy lab, we identified the growth-stimulating compounds as two distinct cyclic dipeptides. The work revealed that cyclic dipeptides may be previously under-reported signaling molecules for cross-kingdom communications. In addition to the fundamental discovery of novel signaling mechanisms between bacterium

and algae, this work may facilitate large-scale diatom culture in biomass production for biofuel and biopharma.

INVESTIGATING THE REGULATION OF GROWTH MECHANISMS IN TWO DISTINCT BRANCHES OF PHOTOSYNTHETIC LIFE

BY

JOHN SITTMANN

Dissertation submitted to the Faculty of the Graduate School of the University of Maryland, College Park. In partial fulfillment of the requirements for the degree of Doctor of Philosophy

2019

Advisory Committee:
Professor Zhongchi Liu, Chair
Professor Caren Chang
Professor Charles Delwiche
Professor Eric Haag
Professor Wade Winkler

Dedication

For my high school science teacher, Janyce Trampler, who fostered my interests, challenged my preconceptions and always made sure science was fun.

Acknowledgements

I first thank my advisor, Dr. Zhongchi Liu for her enduring mentorship. She taught me to think critically, challenge my own ideas and endure the highs and lows of graduate school. I thank her for encouraging the freedom to explore my academic interests, while also teaching me the value of perseverance and focus. I thank her for teaching me to craft a presentation and present my ideas to a variety of audience. Lastly, I thank her for all her guidance and insight during the thesis writing process.

I thank my committee members for their insight, challenge and encouragement throughout my work. Dr. Charles Delwiche for the use of and training on his microscopes. I thank Dr. Caren Chang for her enduring expertise and insight in experimental design. Dr. Eric Haag for always making time to talk as well as his experimental suggestions. I am also grateful to Dr. Wade Winkler for his much-needed expertise as well as for the resources of his lab.

I am grateful for the collaboration of Dr. Munhyung Bae, Dr. Emily Meyers and Dr. Jon Clardy for their work in natural product identification. Dr. Andrew Quinn and Dr. Ganesh Sriram for their work in GC MS. I am grateful to Dr. Lei Guo for his work and guidance in BiFC, plant transformation and Y2H.

I would like to thank all past and current lab members. Dr. Julie Caruana taught me the principles of molecular biology and fielded an unending onslaught of questions during my first 6 months in lab. Dr. Rachel Shahan for the laughs and encouragement.

I am incredibly grateful for the encouragement and support of our floor. I would like to thank Dr. Jose Feijo for always challenging me and to embrace the ignorance in science. Dr. Bill Snell, Dr. Robert Su and Dr. Heven Sze for their critical eyes and pushing me to dive deeper. I thank Dr. Steve Mount for the insightful conversations and challenging me to wonder what's next. I would like to thank every member on the floor for participating and orchestrating some much needed happy hours.

I would like to thank Drs. Alex Sohr and Cordelia Weiss for their friendship. Through the highs and lows of grad school we went through it in-step and I am grateful we get to defend at the same time.

I would like to thank my parents Robert and Cathy Sittmann for their love and support through my time at the University of Maryland. I thank my brother Thomas Sittmann for reminding me to never take myself too seriously.

This thesis would not be possible without enduring love and support of my wife Kim Sittmann. Her belief and steadfast presence carried me through research. She is my best friend and my (sometimes) willing audience.

Table of Contents

List of Figures

Chapter 1. Introduction

1.1 Overview

The United Nations proposes that the world's population will reach 9.8 billion by 2050 (UN 2009). Such a significant increase in world population demands greater worldwide resources such as food and fuel. To meet this projected demand, food production would need to increase by approximately 70% (FAO 2009). However, the effects of climate change driven by the burning of fossil fuels (Solomon, et al. 2007), could further compound this issue. Rising global temperatures are contributing to a reduction in plant pollination, potentially resulting in a decrease in crop production (Scaven and Rafferty, 2013). To cope with rising temperatures and prospective food shortages, advancements in renewable energy and plant production are needed now more than ever.

As of 2017 strawberry production and consumption was estimated to be a 3.5 billion dollar industry in the United States. Due to an increasing focus on healthier living and an expanding population, demand on strawberry production continues to grow (FAO 2009, NASS 2017). Fruit production in angiosperms is a consequence of sexual reproduction. The female gametophyte within the flower becomes fertilized and triggers a developmental cascade resulting in fruit production (Russel, et al. 2010; Liu and Franks. 2015). The wild strawberry *Fragaria* vesca is capable of undergoing both sexual and asexual reproduction. Sexual reproduction results in fruit production while asexual reproduction is driven by stolon, an above ground horizontal stem with genetically identical daughter plants at the internodes (Hytönen, et al. 2009; Mohou et al. 2013; Martins, et al. 2018). Interestingly, axillary branch crowns, which give rise to fruit-

producing inflorescence, and stolon both arise from the axillary meristem. All nurseries use stolon-based asexual reproduction to maintain superior high-yield strawberry lines and produce plantlets to sell to the farmers. However, it is important to maintain the balance between inflorescence and stolon formation as stolon production comes at the expense of fruit-producing inflorescence (Barrett, et al. 2015; Martins, et al. 2018). Chapter 2 of my thesis focuses on elucidating the molecular mechanisms that regulate stolon development in response to environmental signals. In this work, I use the wild strawberry *Fragaria vesca* as a model to study stolon development. *F.vesca* is a good model due to its diploidy, availability of molecular tools, and ease of growth (Kang, et al. 2013).

Algae are attractive as a source of biofuel due to their high-lipid content, fast growth rate, and photosynthetic capability. However, large-scale use of algal-derived biofuels is not yet economically sustainable (Hannon, et al 2010). Increasing algal biofuel yield has traditionally focused on increasing cellular lipid yield. However, increases in lipid yield are often accompanied by an overall decrease in algae growth and biomass (Tan and Lee. 2012). Developing strategies that result in a more rapid algae proliferation, while maintaining a high cellular lipid content, could lead to advancements in biofuel production. While most efforts towards increasing algae proliferation focus on targeted biological pathways, recent work has examined at algal-bacterial symbiosis to identify new molecular pathways to enhance algal growth (Tan and Lee. 2016; Yao, et al. 2019).

The marine environment is rife with different bacteria-alga interactions (Amin, et al. 2012). In mutualistic interaction, the bacteria typically provide micronutrients such as bioavailable iron or vitamin B12, and in return the algae provide sources of useable

carbon (Amin, et al. 2012; Croft, et al. 2005). In some instances, however, bacteria will produce signaling molecules to stimulate algae growth. In fact, recent work shows that the bacteria *P. multiseries* and *P. inhibens* produce phytohormone auxin to stimulate algae growth (Amin, et al. 2015; Segev, et al. 2016). In addition to auxin, bacterially produced quorum sensing compounds are thought to function in bacteria-alga signaling (Amin, et al. 2012; Zhou, et al. 2017).

Chapter 3 of this thesis focuses on investigating a novel bacterium-algae interaction between *Bacillus thuringiensis* and *Phaeodactylum tricornutum* that results in a rapid increase in *P. tricornutum* growth. Further I characterized the nature of the growth stimulating agent, and in collaboration with Dr. Jon Clardy's group, identified the compounds capable of stimulating *P. tricornutum* growth.

Since the two projects of my research are very distinct and concern different organisms, this introduction chapter are divided into sections on strawberry (sections 1.2-1.6) and on *B. thuringiensis*-*P. tricornutum* interaction (1.7-1.10).

1.2 GA Biosynthesis and Signaling

Gibberellins (GA) are a class of phytohormones that regulate a variety of plant developmental processes (Sun. 2011). Gibberellins were first discovered as a product of *Gibberella fujiuroi*, a pathogenic fungus. Rice infected by *G. fujiuroi* exhibited excessive elongation of the plant stem (Takashi. 1991; Sun. 2011). Since then, studies of GA-deficient mutants as well as the effect of exogenous GA treatment have revealed GA's role in plant growth, seed germination, stem elongation, flower initiation and fruit development (Yamaguchi. 2008; Pharis, King. 1985; Fleet, Sun. 2005; Kang, et al. 2013).

Since the discovery of GAs in *Gibberella fujiuroi,* 136 GAs have been discovered (Sun. 2008). However, only GA_1, GA_3, GA_4 and GA_7 are characterized as biologically active. The remaining GAs are either biosynthetic intermediates or catabolites of active GAs (Sun. 2008). GA biosynthesis begins with conversion of geranyl geranyl diphosphate*(*GGDP) to *ent*-kaurene in the proplastid. This initial conversion is a two-step process involving the enzymes *ent*-copalyl diphosphate synthase (CPS) and *ent*-kaurene synthase (KS). *Ent-k*aurene, then undergoes a stepwise oxidation and ring contraction, by *ent*-kaurene oxidase (KO) and *ent*-kaurene acid oxidase (KAO), to produce GA_{12} (Figure 1.1A) (Sun. 2008).

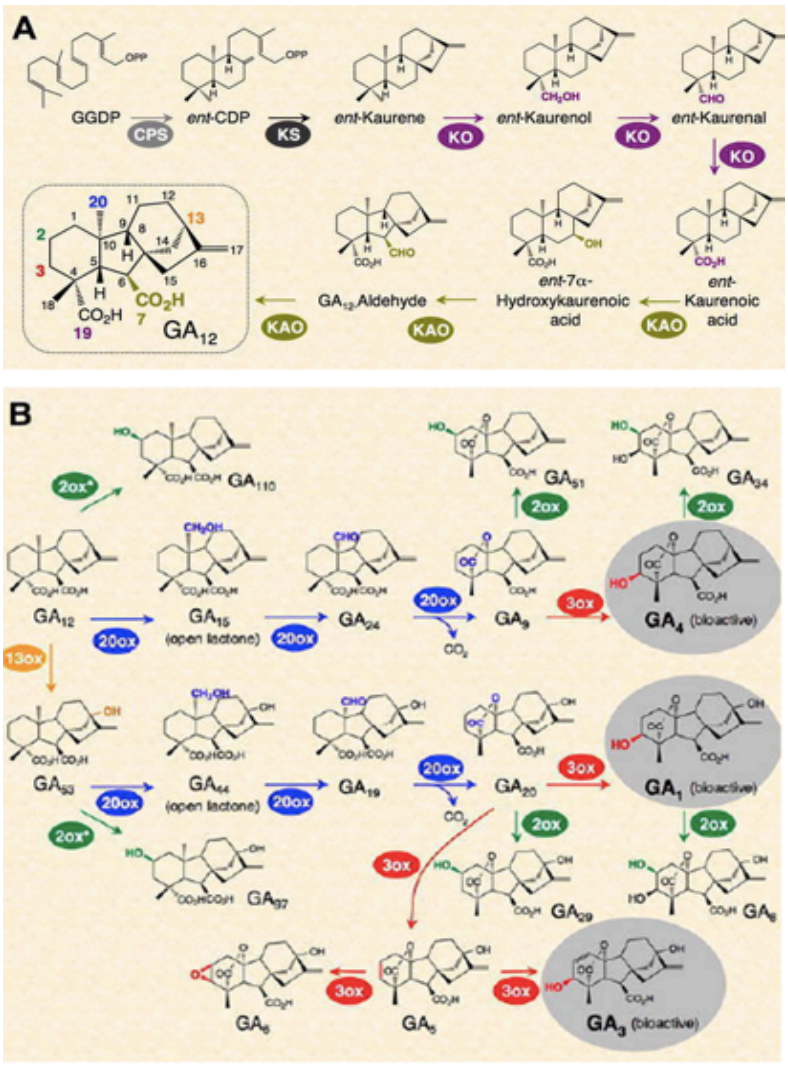

Figure 1.1: The GA biosynthesis pathway
GA biosynthesis is a multistep pathway originating in the proplastid in plants. A) Geranyl geranyl diphosphate (GGDP) is converted to GA_{12}. B) The GA biosynthesis enzymes GA3ox and GA20ox convert GA_{12} to the bioactive GA_1, GA_3 and GA_4. GA2ox converts bioactive GA's to inactive precursors (adapted from Sun, et al. 2008).

GA_{12} can undergo a 13'-hydroxylation to form GA_{53}. GA_{12} and GA_{53} are ultimately converted into the bioactive GAs by two parallel oxidative pathways that are regulated by the GA 20-oxidases (GA20ox) and the 3-oxidases (GA3ox) (Figure 1.1B) (Sun. 2008). A balance of GA biosynthesis and GA deactivation controls bioactive GA levels. While

GA20ox and GA3ox control the rate at which bioactive GAs are biosynthesized, GA 2-oxidase (GA2ox) is responsible for GA deactivation. GA2ox catalyze 2β-hydroxylation, a process that converts active GAs into their inactive precursors. The relative rates as well as the spatiotemporal expression of GA20ox/GA3ox vs GA2ox dictates the relative abundance of GA in plant tissue (Sun 2008; Wuddineh, et al. 2014). The GA-GID-DELLA module acts in the GA signaling pathway (Sun, 2011). In this module, GID (GA INSENSITIVE DWARF) functions as a GA receptor, with DELLA being the downstream transcription factor regulated by GA-GID (Figure 1.2). DELLAs are a class of proteins that are composed of two distinct domains. The C-terminal GRAS domain is responsible for transcriptional regulation, while the N-terminal DELLA domain is responsible for direct interaction with the GID receptor and mediates GA-induced degradation of the DELLA protein (Itoh, et al. 2002; Dill, Sun. 2001). In the absence of GA, the GRAS domain of the DELLA protein is free to bind and sequester away transcription factors, preventing them from functioning (Hirsch, et al. 2009; Lucas, et al. 2008). However, when GA is present, it complexes with the GID receptor and induces a conformational shift.

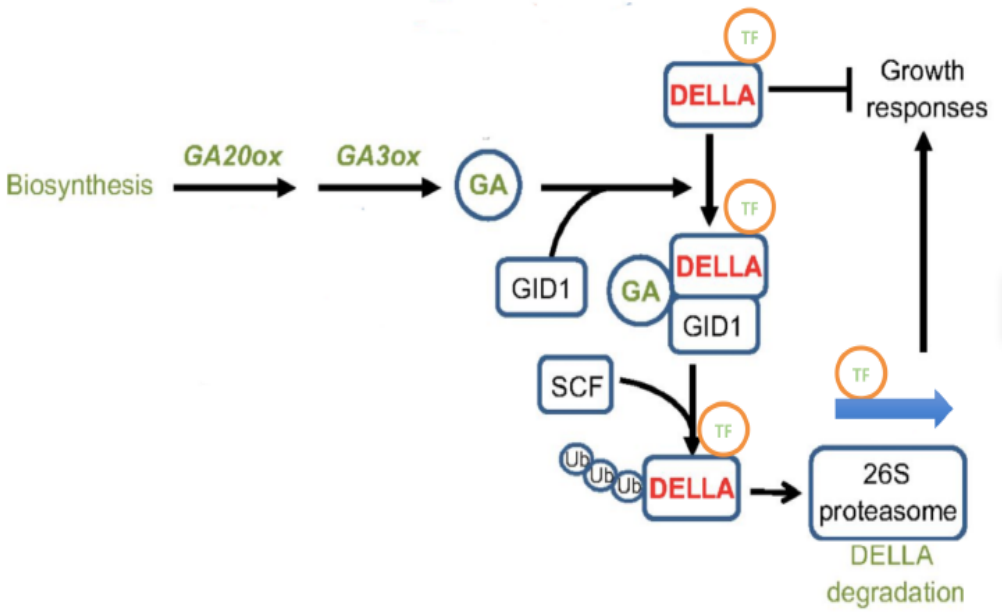

Figure 1.2: The GA signaling pathway is composed of the GA-GID-DELLA module DELLA proteins function as key regulators of the GA signaling pathway. In the absence of GA, DELLA proteins operate in the nucleus to bind and sequester TFs. When GA is present it complexes with GID, and GA-GID binds DELLA at the N-terminal DELLA-domain. The formation of the GA-GID-DELLA module facilitates the polyubiquitination and degradation of DELLA proteins. With DELLA degraded, target TFs are free to activate downstream target genes (adapted from Coldrbook et al 2014).

When DELLA is degraded, the transcription factors sequestered by DELLAs are now able to promote downstream GA responses. While most of our understanding of the GA signaling was elucidated in *Arabidopsis thaliana* and Rice, recent publications have begun to focus on the role GA in fruit-bearing plants including strawberry (Sun. 2011; Tenriera, et al. 2017; Caruana, et al. 2018).

1.3 GA controls stolon development in strawberry

Strawberry is one of the few plants that make stolons, which are horizontal stems consisting of units of internode and daughter plants (Figure 1.3). The daughter plants are also called runners, although recent literature uses runner and stolon interchangeably. In

strawberry, the axillary meristem in the axil of leaves has three alternative developmental fates, one being the development of stolon, a second being dormant, and the third being branch crown (a new plant resembling the mother plant). During the longer and hotter days of summer, the axillary meristem differentiates into above ground stolons. The stolon will grow away from the mother plant and eventually differentiate into a daughter plant at the end of each stem segment (Mouhu et al. 2014, Hytonen, et al 2004). Under the Short Day (SD) conditions of autumn, stolon development ceases and axillary meristems develop into branch crowns. At the same time the signals governing flower initiation are activated, and the branch crown will develop into a flowering shoot (Mouhu, et al. 2013; Hytonin, et al. 2004). Understanding the signals and mechanisms that govern the balance between branch crown formation and stolon development could lead to advancements in strawberry production as more branch crown will lead to more flowers and fruits (Barret. 2015, Hytönen, et al. 2004).

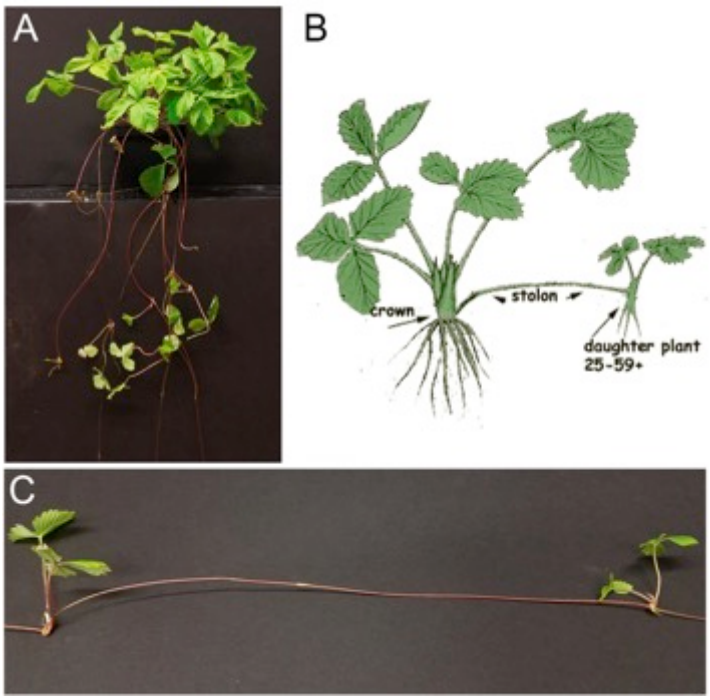

Figure 1.3: Stolon in *Fragaria vesca.*
Stolon are above ground stem-like structures that facilitate asexual reproduction in plants. A) A woodland *Fragaria vesca* (Hawaii 4) producing stolons. B) A diagram showing stolon originate from axillary meristems housed in the crown and grow away from the mother plant. Stolon eventually form a daughter plant. Drawing is from www2.mcdaniel.edu. C) A stolon internode between two daughter plants.

The phytohormone GA was previously shown to play a key role in runner development. A 9bp deletion was discovered in the GA biosynthesis gene GA20OX4 (gene09034), also referred to as the R locus, in the *Alpine* varieties of wild strawberry *Fragaria vesca*; this 9 bp deletion in GA20ox4 was attributed to the *runnerless* phenotype of the *Alpine* strawberry (Tenreira, et al. 2017). Further, the GA biosynthesis inhibitor Prohexadione-calcium (Pro-ca) has been shown to reduce stolon formation in the field (Black, 2004). Similar results were also observed in *Fragaria x ananassa,* the garden strawberry, when the application of Pro-ca reduced the number of stolons or inhibited stolon elongation (Hytonen, et al. 2009).

Through a chemical mutagenesis, our lab identified a suppressor mutant of the *runnerless* in *Alpine* strawberry; this suppressor mutant, previously referred to as *suppressor of runnerless (srl*), regains the ability to develop runners in the *Alpine* strawberry. We recently showed that the *srl* mutation resides in *FveRGA1* coding for the only DELLA protein in *F. vesca* (Caruana et al., 2018). My thesis research described in Chapter 2 contributed to further demonstration of FveRGA1 as a key regulator of stolon formation.

1.4 Environmental signals, photoperiod and temperature, regulate stolon development

In addition to GA, photoperiod is known to regulate stolon development. Typically, *F. vesca* plants will flower under Short Day (SD) photoperiod but produce stolon in Long Day (LD) (Hytönen, et al 2009). Prior work in *F. vesca* shows that the LD photoperiod promotes GA production (Mouhu et al. 2013). The floral repressor *SOC1 (Suppressor of Constans),* coding for a MADS box transcription factor, is induced under LD and is shown to be a facilitator of stolon development. *F. vesca* plants overexpressing *SOC1* produced stolon even under non-inductive SD photoperiod, while *SOC1*-RNAi plants exhibited a reduction in stolon development *(*Mouhu, et al. 2013). An increase in the expression levels of key GA biosynthesis genes was observed in the *SOC1-OX* plants while a corresponding reduction of GA biosynthesis gene expression was noted in *SOC1-RNAi* lines. The data suggests that LD induces the expression of *SOC1,* which activates GA biosynthesis needed for stolon development (Hytönen, et al. 2009; Mouhu, et al. 2013)(Figure 1.4). However, under SD *F. vesca* fails to produce stolon even with exogenously applied GA, suggesting that photoperiod may also either affect a plant's

sensitivity to GA, or that GA alone is insufficient to initiate stolon development under SD condition (Hytönen, et al. 2009).

In concert with photoperiod, temperature also plays a significant role in stolon development (Rantanen, et al. 2015; Hytönen, et al. 2004; Bradford, et al. 2010). Under LD, *Fragaria* plants grown at temperatures lower than 17^{o}C did not produce any stolons, while plants grown at 23-26C produced the optimal amount of stolon (Bradford, et al. 2010). Additionally, *SOC1* expression was found to be temperature dependent as well, suggesting that *SOC1* integrates environmental cues (photoperiod and temperature) to regulate GA biosynthesis and stolon formation (Rantanan, et al. 2015; Mouhu, et al.

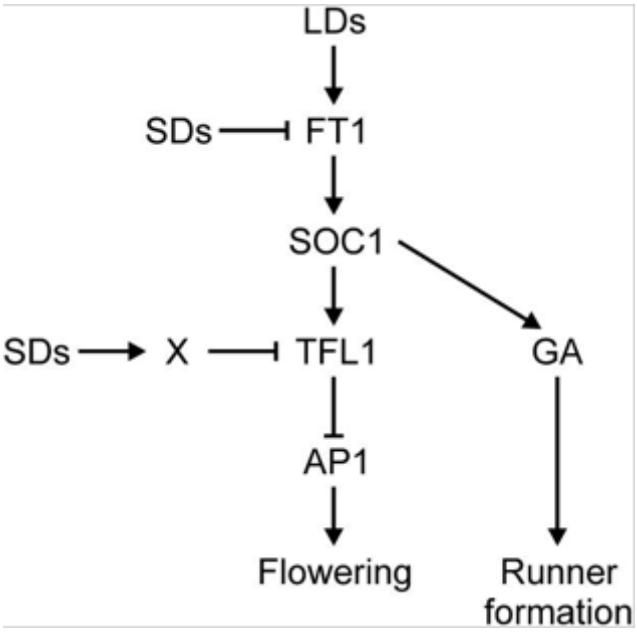

Figure 1.4: Long day conditions facilitate GA biosynthesis.

The MADS box transcription factor SOC1 is expressed during long day. SOC1 expression may facilitate the transcription of GA biosynthesis genes (Adapted from Mouhu, et al 2013).

2013).

1.5 Hypocotyl Elongation Serves as a Model for Stolon Development

Prior work suggests that stolon development requires a variety of molecular and environmental signals (Mouhu, et al. 2013). Our results, as well as recent work in the field, suggest that the GA pathway functions as the master switch for this process (Mouhu, et al. 2013; Tenriera, et al. 2017;Carauana, et al. 2018). To identify potential downstream effectors of GA/DELLA, we looked to hypocotyl elongation in Arabidopsis thaliana as a model. Like stolon formation, hypocotyl development is an elongative process that is ultimately governed by the GA signaling pathway. A review of the literature reveals brassinosteroid (BR) and light quality pathways interact with the GA signaling pathway to facilitate hypocotyl elongation (Willige, et al. 2007; Gallego-Bartolomé, et al. 2012;Depuydt and Hardtke. 2011).

Upon germination, the hypocotyl, a below ground stem, emerges from the seed and grows towards the surface. This developmental process is known as skotomorphogenesis and is characterized by the absence of light. Due to the absence of light, the growth-promoting Phytochrome Interacting factors (PIFs) build up in the hypocotyl and act as key transcription factors promoting elongation. To facilitate elongation, PIF proteins work in concert with the BR signaling protein Brassinazole Resistant1(BZR1) to promote hypocotyl growth (Oh, et al. 2012). Studies focusing on *pif* and *bzr* mutants notice changes in hypocotyl length as well as skotomorphogenic response. *A. thaliana* plants with a *pif* quintuple knock out (pifq), exhibit dwarfed hypocotyls. While a PIF4 overexpression allows for hypocotyl elongation even when grown in light.

Comparatively, a gain of function *BZR1 (bzr1-1D),* allows for hypocotyl elongation even in the presence of the BR biosynthesis inhibitor Brassinazole (BZR) (Oh, et al. 2012).

1.6 Light quality and brassinosteroid may regulate stolon development

Like stolon development, hypocotyl development is also an elongation process governed by the GA signaling pathway. In *Arabidopsis*, it was shown that brassinosteroid (BR) and light quality pathways operate downstream of GA signaling pathway to facilitate hypocotyl elongation (Willige, et al. 2007; Gallego-Bartolomé, et al. 2012; Depuydt and Hardtke. 2011). Therefore, BR signaling and light quality pathway may also play a role in stolon development. Light quality, specifically the Red (R) to Far-Red (FR) ratio, acts to influence hypocotyl elongation in Arabidopsis (Halliday, et al. 2009; Kim, et al. 2011). Phytochrome proteins are composed of a soluble chromoprotein covalently linked to a chromophore (Al-Sady, et al. 2006; Tu and Lagarias, 2005); they function as light quality sensors due to the interconversion between the active P_{Fr} and inactive P_r form when exposed to Red or Far Red light respectively (Quail and Peter. 2002). Under high R/FR, the Phytochrome B (PhyB), in its P_{fr} active form, binds and degrades the Phytochrome Interacting Factors (PIFs), causing a shortening of the hypocotyl in *Arabidopsis* (Monte, et al. 2004). When the R/FR ratio is low, PhyB enters its inactive P_r form, which is excluded from the nucleus and unable to bind PIFs. As a result, the nuclear PIFs accumulate and promote growth-related processes including hypocotyl elongation (Rockwell, et et al. 2006; Franklin and Quail. 2010; Castillon, et al. 2007; Oh, et al. 2012) (Figure 1.5). In addition to PhyB, PIFs are also bound and inhibited by DELLA proteins in the absence of GA as shown in *Arabidopsis* (Li, et al. 2016). When both low R/FR and GA are present, PIFs will be able to accumulate and free to stimulate hypocotyl

elongation. Therefore, cross-talk between light quality and GA occurs at PIFs to determine if elongation should proceed (Oh, et al. 2012; Oh, et al. 2014; Li, et al. 2016).

Upon germination, the hypocotyl, a below ground stem, emerges from the seed and grows towards the surface. This developmental process is known as skotomorphogenesis and is characterized by the absence of light. In the absence of light, PIF proteins accumulate and work in concert with the BR signaling protein Brassinazole Resistant 1 (BZR1) to promote hypocotyl growth (Oh, et al. 2012). *Arabidopsis* plants with a PIF quintuple knock out (*pifq)*, exhibit short hypocotyls. While a PIF4 overexpression allows for hypocotyl elongation even when grown in light. Similarly, a gain-of-function BZR1 (*bzr1-1D),* allows for hypocotyl elongation even in the presence of BR biosynthesis inhibitor Brassinazole (BZR) (Oh, et al. 2012). These prior studies motivated the study in stolon reported in chapter 2.

1.7 The BR signaling pathway and crosstalk with GA

In *Arabidopsis,* the GA and BR signaling pathways interact to affect developmental processes governing elongation (Thompson, et al. 1982; Bai, et al. 2012). The transcription factor BRASSINAZOLE RESISTANT (BZR1) functions to integrate the signaling pathways of both BR and GA (Li, et al. 2013). BR signaling begins with a signal transduction cascade that is initiated by the binding of BR to the cell-surface protein BRASSINOSTEROID INSENSITIVE 1(BRI1) (Zhu et al. 2013; Kim and Wang, 2010, Hothorn, et al. 2011). Upon recognizing BR, BRI1 begins a phosphorylation cascade that ultimately phosphorylates and activates BRI1 SUPPRESSOR (BSU1). BSU1 dephosphorylates and inactivates the protein BRASSINOSTEROID INSENSITIVE2 (BIN2), ultimately leading to BIN2 degradation (Kim, et al. 2011; Kim,

et al. 2009; Zhu et al. 2013). When BIN2 is degraded, BZR1 is allowed to enter the nucleus (He, et al. 2005; Sun, et al. 2010). However, when BR levels are low, BIN2 stays

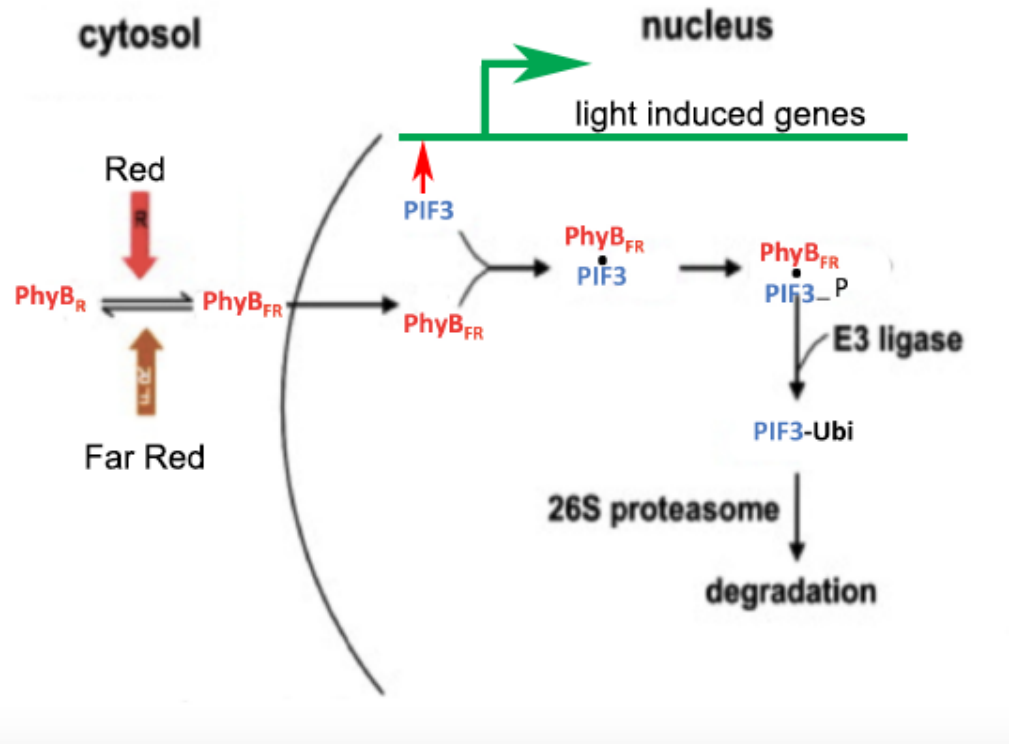

Figure 1.5: Overview of the light quality signaling pathway. The phytochrome (Phy) family of photosensors are chromoproteins composed of a polypeptide region covalently linked to a light-sensing chromophore (Tu and Lagrias. 2005). Exposure to red light converts phytochromes to their active P_{Fr} form (Al-Sady, et al. 2006). In the active form they translocate to the nucleus to bind and degrade PIF proteins. Conversely, exposure to far red light converts phytochromes to their inactive P_r form and maintains them in the cytoplasm (Al-Sady, et al. 2006).

activated and phosphorylates BZR1, preventing it from entering the nucleus (Figure 1.6)

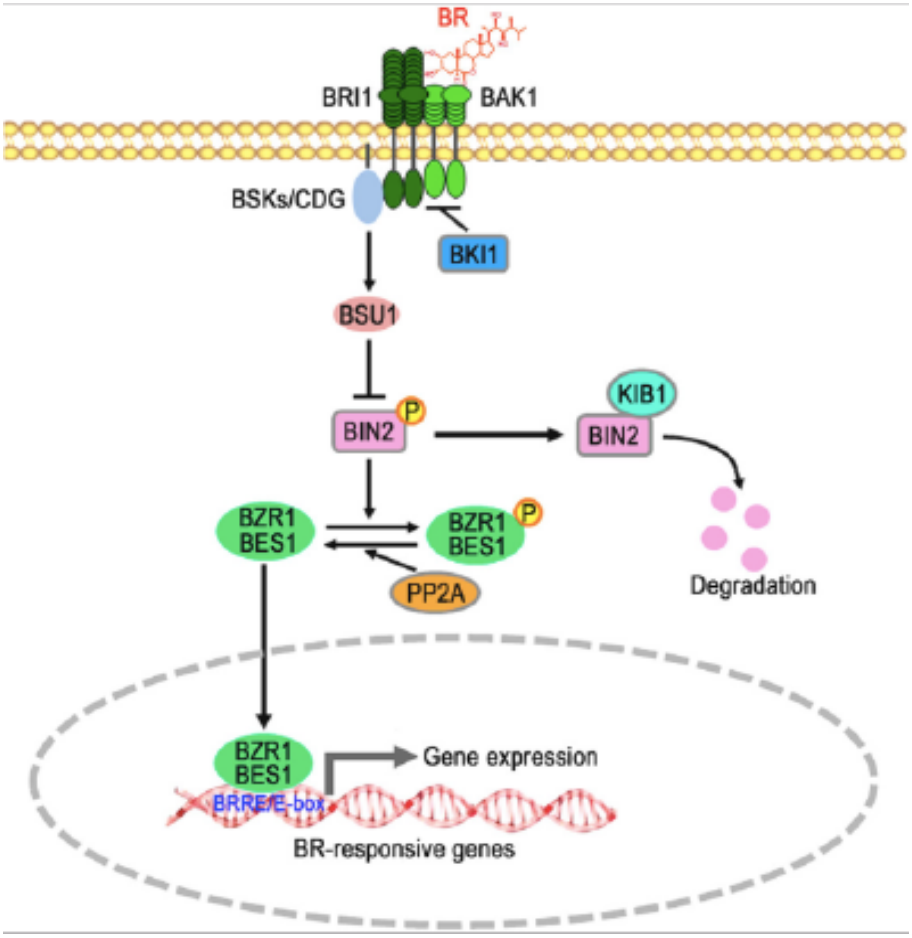

Figure 1.6. A current model for brassinosteroid (BR) signaling in *Arabidopsis*. BRs are perceived by the extracellular domain of the BR receptor BRI1. BR binding activates BRI1 through homodimerization and heterodimerization with its partner BAK1 and releasing it from its inhibitory protein BKI1. The activated BRI1 then sequentially phosphorylates and activates two downstream kinases BSK1 and CDG1 and a Ser/Thr phosphatase BSU1 that will inactivate the BIN2 kinase, a negative regulator of BR signaling. BR signal also activates PP2A, a phosphatase that phosphorylates and activates the transcription factors BZR1 and BES1. The dephosphorylated BZR1 and BES1 will bind the BRRE or E-box motif of their target genes and regulate their expression. When BR signal is absent, BRI1 is bound by BKI1 and cannot interact with BAK1. BIN2 is also in its active form that will phosphorylate and inactivate BZR1 and BES1. The phosphorylated BZR1 and BES1 are retained in the cytoplasm by 14-3-3 proteins and can be degraded by the 26S proteasome. Adapted from Li et al. 2013.

(Bai, et al. 2007; Gambala, et al. 2007; Zhu, et al. 2013). Once entering the nucleus,

BZR1 faces additional regulation by the presence of DELLA (Bai, et al 2012). DELLAs bind and sequester away BZR1 (Bai, et al. 2012; Zentella, et al. 2007; Gallego-Bartolomé, et al. 2012).

Understanding the environmental and molecular mechanisms that regulate stolon development is of significant academic and economic interests. The axillary meristem is capable of developing into either branch crown or stolon. Elucidating the regulators of stolon production could allow for insights into mechanisms of cell fate determination. Further, tools that could allow for facile switch between vegetative propagation and fruit production would be highly valuable for strawberry production and yield (Barrett. 2015; Martins, et al. 2018). In Chapter 2, I detail my work in incorporating the light quality pathway and the transcription factor FvePIF3 into stolon development. I also examined the role of Brassinosteroid signaling in the elongation of *F.vesca* stolons.

1.8 Diatom-bacterium interactions

Tara Oceans Expedition (2009-2013) completed massive samplings of world's oceans and provided rich open science resources for discovery and analysis (Pesant et al., 2015). These global expeditions revealed the incredible diversity of planktonic communities and highlighted the complex and diverse interactions that dictate marine ecology. With the sunlit ocean being one of the most ecologically and energetically important biomes on earth, understanding the interactions between its inhabitants is critical for understanding global food web. (Vargas, et al. 2015). Protists, archaea, and bacteria comprise a majority of the oceanic biomass (Amin, et al. 2012). Insight from the naturally occurring interactions among these microbes will shed light on how they shape the biogeochemical processes of the ocean (Falkowski, et al. 2008).

In the marine environment, specifically within the phycosphere, synergistic interactions exist between diatoms and bacteria. Typically, the photosynthetic algae provide bacteria a source of fixed carbon in exchange for micronutrients (Amin, et al. 2012). Examples of bacterial produced micronutrients include vitamins, hormones, antibiotics, nitrogen and trace metals such as iron (Boyd PW, et al. 2010; Foster, et al. 2011; Segev, et al. 2016; Seyedsayamdost, et al. 2011; Croft, et al. 2005). Although diatom-bacteria interactions were often reported, the mechanisms underlying interspecies communications between bacterium and diatom are poorly understood (Zhou, et al. 2017).

1.9 Quorum sensing in bacterium and inter-kingdom communication

Quorum Sensing (Qs) is a form of bacterium-bacterium communication. As bacterial populations grow and cell density increases, bacterial cells release chemical signals to coordinate gene expression and developmental behavior within a population (Miller and Bassler, 2001). In its most basic form a QS circuit is composed of a signal synthase, a chemical signal and a response regulator. The signal synthase produces the chemical signal and secretes it extracellularly. As the bacterial density increases, the chemical signal builds up within the population and eventually reaches a threshold, at which point, the signaling molecules bind response regulators and initiate transcription of genes involved in QS response (Hmelo, 2017).

Several different bacterial QS systems have been identified. In marine environment, the gram-negative bacteria use *Aceylated Homoserine Lactones* (AHLs) in marine bacterial communications (Hmelo, 2017). In the AHL system, the Lux I protein catalyzes the synthesis of AHLs. AHLs are hydrophobic compounds able to passively enter cells to bind to the response regulator LuxR (Amin, et al 2012). In the marine bacteria *Vibrio*

fischeri, when there is a high cell density, LuxR binds to AHKs and activates expression of genes involved in collective behavior, group metabolism of shared nutrients, Cyclic di-GMP signaling, biofilm production and secretion (Rutherford, et al. 2011; Ball, et al. 2017). In addition to the AHL QS system, gram-positive microbes employ a peptide-mediated QS strategy. In this system, the gram-positive microbe secretes a peptide autoinducer. The autoinducer binds a two-component sensor kinase and triggers a phosphorylation/dephosphorylation cascade culminating in the activation of the response regulator. Response regulators subsequently activate gene expression in the QS regulon. (Miller and Bassler, 2001).

1.10 Cyclic dipeptides facilitate interspecies communication

Cyclic dipeptides (CDPs) are a third and more recently discovered class of QS molecules found abundantly both as a naturally synthesized product and degradation products from longer peptides (Borthwick, 2012). CDPs are naturally produced from a wide range of species from bacteria and fungi to plants and mammals. Work in *Vibrio Fischeri* and *Pseudomonas aerogunosa* demonstrates that CDPs can interact with components of the AHL QS pathway to either increase or decrease the QS activities (Holden, et al 2002; Campbell, et al 2009). Although not extensively studied, work in model plant *Arabidopsis thaliana* provides an interesting insight into the role of CDPs in growth and division. *Arabidopsis thaliana* seedlings that are cultured with the bacterium *Pseudomonas aeruginosa* exhibited an increase in shoot and root biomass. CDPs produced by *P. aeruginosa* mimicked the effect of phytohormone auxin in promoting an increase in root biomass, potentially due to their heterocyclic ring, a structural motif common in many auxins (Ortiz-Castro, et al. 2011). This study suggests that some CDPs

may serve as a cross-kingdom signal capable of promoting cell-division in target species (Ortiz-Castro, et al. 2011). Due to their near-ubiquitous presence across kingdoms as well as their ability to activate AHL signaling, CDPs may play a role in allowing interspecies communication (Borthwick, 2012; Bellezza, et al. 2014).

1.11 Cyclic dipeptides in diatom reproduction

In the diatom *Seminavis robusta,* sexual reproduction and cell division is stimulated by the *S. robusta*-produced mating pheromone cyclic diproline. A consequence of cell division in many diatom species is the total reduction in diatom cell size (Chepernov, et al. 2004). Due to the biomineralizaton of their silicified cell walls, diatoms exhibit a

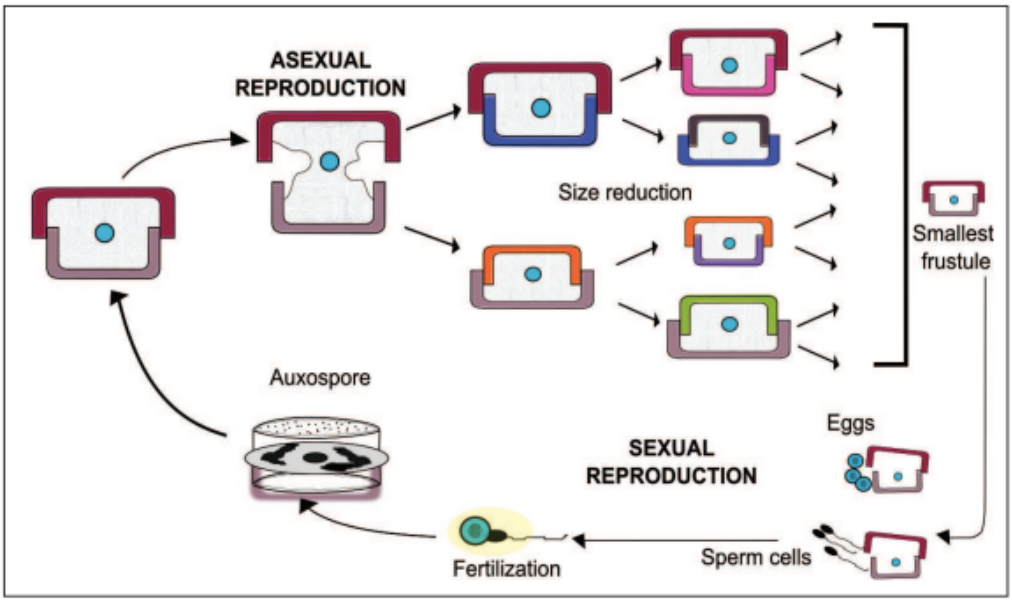

Figure 1.7: Cell division in diatoms results in a decrease in cell size. Due to the overlapping theca plates diatoms lose cell volume with each division. A common strategy for regenerating cell size is sexual reproduction
Adapted from Kale, et al. 2015

reduction in cell size with each mitotic division. To restore cell size many diatoms must find a mate and undergo sexual reproduction (Figure 1.7 (Chepernov, et al. 2004). Sexual reproduction in diatoms occurs when diatom cells become small enough to cross the

sexual size threshold (SST). The SST is the cell size in which diatoms begin the signaling processes that facilitate gamete fusion (Chepernoc, et al. 2004; Gillard, et al. 2013). In *Seminavis robusta,* once the cells have crossed the SST, individual *S. robusta* of mating type MT^- must find and mate with a compatible MT^+ type (Gillard, et al. 2013; Chepernov, et al. 2002; Chepernov, et al. 2004). Hence, MT^- cells produce and secrete cyclic diproline as a pheromone to attract MT^+ cells. MT^+ cells pair with MT^- cells, this pairing is followed by gametogenesis and formation of the zygote (Moeys, et al. 2016; Gillard, et al. 2013). Eventually the zygote will elongate resulting in a full-sized *S. robusta* cell, the resulting cell can now divide vegetatively (Moeys, et al. 2016). *S. robusta* cells that do not find a mate will continue to divide until they become too small and die (Moeys, et al. 2016). Considering the role cyclic diproline plays in regulating *S. robusta* behavior, CDPs may thus represent an under-investigated molecular signal for diatom as well as related organisms (Gillard, et al. 2013).

1.12 *Bacillus* cereus members exist in oceanic as well as terrestrial environments

Members of the *Bacillus* genus occupy ecological niches spanning both oceanic and terrestrial environments (Liu, et al. 2017; Turnbull, et al. 1996). *Bacillus* sp. are economically and ecologically noteworthy (Turnbull, et al.1996). Particularly, the *Bacillus cereus* group of microbes contributes to a wide variety of metabolically significant functions *B. thuringiensis* is used in agriculture as an insecticide, while *B. anthracis* is the causative agent of anthrax (Liu, et al. 2017; Rasko, et al 2006). Chief among the *B. cereus* members are *Bacillus anthracis, Bacillus cereus* and *Bacillus thuringiensis (*Rasko, et al.2005). Although well known for its terrestrial members, such as *B. cereus, B. thuringiensis* and *B. anthracis*, the *B. cereus* group members *B. mycoides,*

B. weihenstephanensis and some strains of *B. thuringiensis* occupy the marine environment (Liu, et al. 2017). How and if these *B. cereus* members interact with their oceanic neighbors are not known.

A characteristic shared by *Bacillus* is the ability to sporulation under nutrient-poor environment. During sporulation, *Bacillus* mother cell develops a metabolically inert and environmentally resistant endospore (Higgins and Dworkin. 2012). Sporulation begins with the formation of a septum within the mother-cell, which is predicated by an asymmetric cell division. The septum then curves to form the forespore that eventually becomes an endospore. Finally, the endospore is ejected from the mother-cell after mother cell lysis (Veening, et al. 2008); these spores will germinate only under suitable environment.

Chapter 2 Investigation of GA, BR, and light quality in stolon development

2.1 INTRODUCTION

As discussed in chapter 1, although GA and photoperiod are known to play critical roles in stolon development, the downstream regulators of stolon development are not well understood (Figure 2.1A). To investigate the downstream effectors that may promote stolon formation we drew insights from hypocotyl elongation in *Arabidopsis*. As with stolon development, hypocotyl elongation is a developmental process that relies upon GA signaling in combination with photoperiod and light quality (Oh, et al. 2014).

In *Arabidopsis thaliana,* the transcription factors PIFs and BZR1 are known to act in the light quality and BR signaling pathways, respectively. Furthermore, both Arabidopsis PIF and BZR1 are known to be bound and inhibited by DELLA proteins through direct

protein-protein interactions (Oh, et al. 2014; Bai, et al. 2012). These prior studies in *Arabidopsis* provide us testable hypotheses regarding the downstream processes that may regulate stolon development in strawberry.

As described in the introduction, the axillary meristem could adopt three different developmental fates: dormant bud, branch crown, or stolon. In order for an axillary meristem to develop into a stolon, the first critical decision is to adopt the stolon fate, which is followed by the activation of genes for horizontal growth and elongation as well as for acquiring the indeterminacy. While prior literature points to GA as the most critical factor downstream of LD and SOC1 to activate "stolon" identity, it is not known how GA acts to promote and maintain "stolon" fate. This chapter is aimed at addressing this question.

Through a chemical mutagenesis, our lab previously identified a suppressor mutant of the *runnerless* in alpine strawberry (Figure 2.1A); this *suppressor of runnerless* mutant, named as *srl-1*, regains the ability to develop runners in the alpine strawberry which is defective in GA biosynthesis due to a 9 bp deletion in the *GA20OX4* gene (Tenreira, et al. 2017). We showed that the *srl-1* mutation causes a W601X mutation in the *FveRGA1* gene (gene 06210) (Figure 2.1B), which codes for the only DELLA protein in *F. vesca* (Caruana et al., 2018). Since this *srl-1* mutation only removes the last 10 amino acids of the FveRGA1 protein and it is only a single allele, it requires further experimental evidence supporting its the molecular identity.

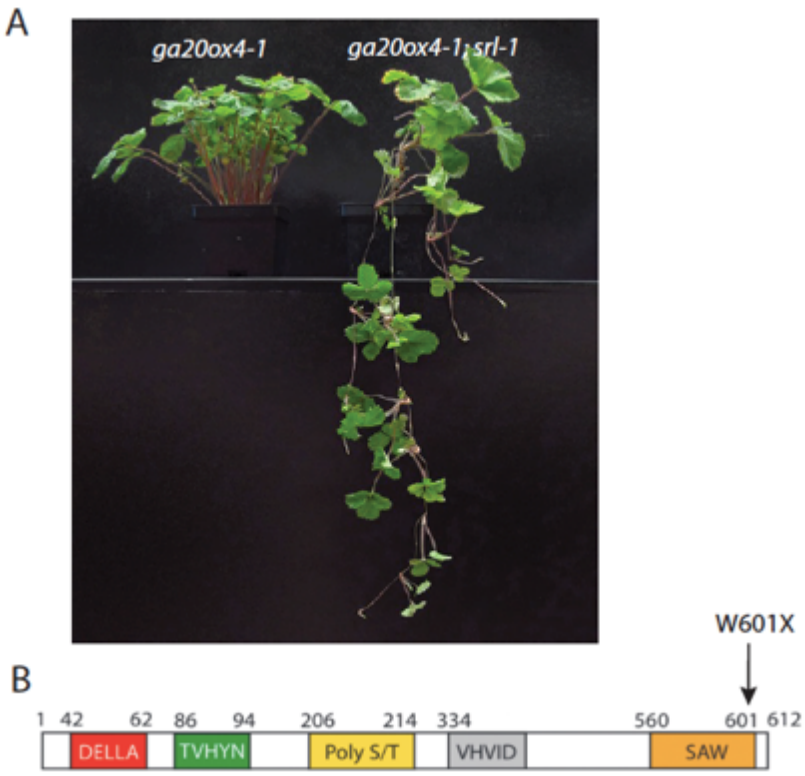

Figure 2.1: *Suppressor of runnerless* (*srl-1)* mutation resides in *FveRGA1*

A) Photograph of YW5AF7 (left), which is runnerless and carries *ga20ox4-1* mutation and (right) *suppressor of runnerless (srl-1)* mutant in YW5AF7 background.

B) Diagram of FveRGA1 protein and the *srl-1* mutation (W601X).

2.2 METHODS

2.2.1 Plant materials and growth conditions

Diploid wild strawberry, Yellow Wonder 5AF7 (YW5AF7) and Hawaii 4 (H4), are the two *Fragaria vesca* varieties used for this study. YW5AF7, an alpine strawberry, is *runnerless* and harbors the 9 bp deletion in the *GA20OX4* (gene09034) gene. H4 is a woodland strawberry and does not harbor the *ga20ox4* mutation.

Plants are generally grown in a growth chamber at a temperature of 22 °C and 16 hr light followed by 22 °C and 8 hr darkness. The plants were grown in a relative humidity of 50%.

For Red light (R) treatment, H4 plants were exposed to 12W of red light (ABI PAR38 LED GROW bulb 620-630nm) for the last 3 hours of a 16 hour light period. 12 plants were subjected to red light treatment and 12 plants served as white light only controls. For Far Red (FR) treatment, YW5AF7 plants were exposed to 15W of FR light during an entire 16 hour light period (Hydrofarm power PAR 730-740nm). 20 plants were subjected to far red light treatment with 14 plants subjected to only white light. The temperature was set at 23.5 C (20 C at night) with a light intensity of 115µmol/m^2s. Statistical analysis was performed using the t.test function in Rstudio (Version 1.2.1335) $p<.05$. Number of stolon was counted were counted at 1 month, 2 month and 3 month intervals. Internode distance is defined as the length (in cm) between daughter plants on a stolon.

2.2.2 Propiconazole treatment to inhibit BR

H4 plants were germinated and grown for 5 weeks in 1/2MS culture media. Plants were then transferred to soil and allowed to grow for 7-10 days. Plants were watered with a 50uM Propiconazole solution 1/week and had 50uM Propiconazole applied directly to the crown and runner 3x/wk(N=11). Mock treated control plants were treated with water (N=13). All treatments lasted for 6 weeks throughout the experiment. Plants were grown in 16 hour white light days. The temperature was set at 22.5 C (20 C at night) with a light

intensity of 115μmol/m^2s. Statistics were performed using the t.test function on Rstudio (Version 1.2.1335)

2.2.3 Y2H constructs and assay

Y2H was performed using the vectors pGADT7 and pGBTK7. Gibson assembly was used to clone full length CDS of FvePIF3 (gene 22963) and FveBZR1 (gene15105) into pGADT7 and full length CDS of FveRGA1, *rga1-1* and M5 into PGBTK7. Genes were cloned off of *Fve* cDNA. Primer sequence are listed in Table 1. Yeast strain PJ69-4A was transformed with the vectors following protocols in Matchmaker Gold Yeast Two Hybrid System User Manual by Clontech. Perspective transformants were plated on –LW dropout SD medium and allowed to grow for 2 days. Colonies were screened for transgenes by PCR and positive colonies were plated on –LWH SD medium and grown for 3-5 days to detect interaction.

2.2.4 BiFC constructs and assay

Full length CDS of FveBZR1 and FvePIF3 as well as full length FveRGA1 and various truncation of FveRGA1 were Gibson cloned into the BiFC vectors pXY106 and pXY105 respectively. Primers are listed in are listed in Table 1. Agrobacteria containing these constructs were infiltrated into young *Nicotiana benthamiana* leaves. After 2 days, the leaves were imaged under a Leica SP5X Confocal microscope (Leica Co. USA).

2.2.5 Vector construction and transformation of *FveRGA1-ΔDELLA _GR* as well as DEX treatment

To produce the inducible *35S::FveRGA1-ΔDELLA _GR* construct, *FveRGA1* was PCR amplified from YW5AF7 genomic DNA using the primer pair 06210_Fwd/06210_Rv (Table 1). The ligand binding domain of the rat glucocorticoid receptor (GR) was amplified from *pBI-ΔGRBX* (Lloyd et al., 1994) with the primer pair Fwd_GR/Rv_GR. The backbone vector *pCR8/GW/TOPO* (Invitrogen) was amplified using the primer pair Fwd_TOPO/Rv_TOPO. The *FveRGA1* and *GR* PCR products and the linearized pCR8/GW/TOPO backbone vector were then combined via Gibson assembly (https://www.neb.com/protocols/2012/12/11/gibson-assembly-protocol-e5510). To delete the DELLA domain from *FveRGA1,* the primer pair Fw06210_DELLA_Del:Q5/ Rv06210_DELLA_Del:Q5 was used with the Q5 site-directed mutagenesis kit (New England Biolabs). Upon completion, *pTOPO:FveRGA1-ΔDELLA_GR* was sequenced to confirm correct configuration and then recombined with the destination vector *pMDC32* (Curtis and Grossniklaus, 2003) using the Gateway LR Clonase II Enzyme mix (Invitrogen), leading to the final binary vector *pMDC32:FveRGA1-ΔDELLA _GR.* All primer sequences are listed in Table 1.

Three independent transgenic lines (#1-3) were obtained for *pMDC32:FveRGA1-ΔDELLA _GR* construct, and individual plants were verified as transgenic using PCR with the primer pair Rv_GR/Fw_06210_1680bp. Multiple T0 plants derived from three transgenic lines (lines #1-3) were sprayed daily for 27 days with 150 uM DEX in 0.5% ethanol with 0.02% silwet. Corresponding mock treatment contained 0.5% ethanol with 0.02% silwet.

2.2.6 FvePIF3 and FveBZR1 RNAi construction and transformation

A RNAi fragment targeting base pairs 58 to 425 of gene22963 was cloned into pENTR2B (primer sequence listed in Table 1.) LR clonase was used to transfer the RNAi target from pENTR2B into the RNAi vector ph7gwiwg2-7721. Potential transgenic plants were screened for the GFP fluorescence. We obtained 20 plants originating from two callus. Plants representing a weak, medium and strong RNAi phenotype had their RNA extracted and *FvePIF3* transcript abundance was determined by qRT PCR(Figure Supplementary table 1).

A RNAi fragment targeting base pairs 568 to 928 of gene 15105 was cloned into pENTR2B using primers listed in Table 1. LR clonase was used to transfer the RNAi target from pENTR2B into the RNAi vector ph7gwiwg2-7721. Potential transgenic plants were screened for the GFP fluorescence. We obtained 10 plants originating from two callus. Transgenic plants had their RNA extracted and *FveBZR1* transcript abundance was determined by qRT PCR.

2.2.7 Transformation of *F. vesca* (done by Drs. Julie Caruana and Lei Guo)

Vectors were transformed into *F. vesca* as previously described (Kang et al., 2013) with the modification of using young cotyledons as the starting material. Specifically, callus was induced from cut cotyledons on the 5^{++} medium (1 x MS, 2% sucrose, 3.4 mg/L benzyladenine, 0.3 mg/L indole-3-butyric acid, 0.7% phytoagar, pH5.8) for two-to-three weeks in the dark and then co-cultivated with *agrobacterium* GV3101 harboring PIF3-RNAi in the dark for 1 hour in the co-cultivation buffer (1 x MS, 2% sucrose, 0.4 mg/ml acetosyringone) with gentle shaking. Then transformed callus were kept on the 5^{++} medium for three days in the dark and subsequently washed with sterile water and

moved on MS medium with antibiotics (250 mg/L timentin + 250 mg/L carbnicillin) for 2 weeks in the dark. Transformed callus were moved to the medium 5^{++} with 250 mg/L timentin, 250 mg/L carbnicillin and 4 mg/L hygromycin. The callus were changed to the same fresh medium every 2-to-3 weeks until shoots appear. When shoots are induced from callus, they are moved the rooting medium (0.5 x MS, 0.01 mg/L IBA, 2% glucose, 0.7% phytoagar, pH5.8) with 4mg/L hygromycin. After about 1-to-2 months, the plants will generate roots and transferred to soil and genotyped.

2.2.8 Primer Table

Primer Name	Primer sequence	Purpose
GBTK7_M5_06210_F	5’ CATATGGCCATGGAGGCCGAATTCTTCGATTCTTCCCCAAGAG 3'	Cloning M5 06210 into PGBTK7
GBTK7_BamH1_06210_R	5’ CCGCTCCAGGTCGACGGATCCTCAGTGAGTCATCACCGCTT ‘3	Cloning 06210 into PGBTK7
GADT7-BZR1-F	5' gccatggaggccagtgaattcATGACGTCAGACGGAGCCAC 3'	Cloning 15105 into PGADT7
GADT7-BZR1-R	5' CAGCTCGAGCTCGATGGATCCTTAACTTCGAGGCTTACCATTG 3'	Cloning 15105 into PGADT7
GADT7-PIF3-F	5' gccatggaggccagtgaattcATGCCTTTATCAGAGCTATTATC 3'	Cloning 22963 into PGADT7
GADT7-PIF3-R	5' CAGCTCGAGCTCGATGGATCCTTACTCATAACTAGCTGGTC 3'	Cloning 22963 into PGADT7
DELLAlessBamH1BIFC-FWP	5' - CTGTACAAGGCCGGCGGATCCCTTGAAGAGTTCATGGGGAC 3'	Cloning 06210 into pXY105
NtermlessBamh1BIfc_FWP	5' CTGTACAAGGCCGGCGGATCCCTCCAGCCCGTCTCCCTCCC 3'	Cloning 06210 into pXY105
380bplessBamh1BiFC_FWP	5' CTGTACAAGGCCGGCGGATCCCCGTCGGATCTGTCGAATTG '	Cloning 06210 into pXY105
430bplessBamh1BiFC_FWP	5' CTGTACAAGGCCGGCGGATCC ATAGATTTTGCAGATCAAAGC 3'	Cloning 06210 into pXY105
SAWlessBIFC-Xba1RVP	5' CTCTGCAGGTCGACTCTAGATCACGCGTTGGAACCGAGATGAA 3'	Cloning 06210 into pXY105
pXY105_15105_F	5' CTGTACAAGGCCGGCGGATCCATGAAAAGAGAGCATCACAG 3'	Cloning 15105 into pXY105
pXY105_15105_R	5' CTCTGCAGGTCGACTCTAGATCAGTGAGTCATCACCGCTTG 3'	Cloning 15105 into pXY105
VHVIDlessBIFCXba1-RVP	5' CTCTGCAGGTCGACTCTAGATCAGCCTTGGAAACCTTCTAGAAT 3'	Cloning 06210 into pXY105
PXY106-PIF3-F	5' CGAGGACGCCGGCGGATCCATGACTAGAAAGAAGGTGAAAC 3'	cloning 22963 into pXY106
PXY106-PIF3-R	5' CTCTGCAGGTCGACTCTAGATCAAGGAAAATTAAAGCCATTAG 3'	cloning 22963 into pXY106
BZR1_RNAi_F	5' GTCGACTGGATCCGTACCGATGGCCTCTTTCAATTACCC 3'	Cloning RNAi fragment 15105 into ph7gwiwg2-7721
BZR1_RNAi_R	5' ATATCTCGAGTGCGGCGGCGCATTGCCAAGTGTGAGCTCTA 3'	Cloning RNAi fragment 15105 into ph7gwiwg2-7721
PIF3_RNAi_F	5'GACTGGATCGGTACCgAATACCTTTGAGTGATTTTGGTTG 3'	Cloning RNAi fragment 22963 into ph7gwiwg2-7721
PIF3_RNAi_R	5' ATCTCGAGTGCGGCCGCGAAGTCGATTGGCGTGAGATTTC 3'	Cloning RNAi fragment 22963 into ph7gwiwg2-7721
06210_fwd	5’ CAGGCTCCGAATTCGCCCTTATGAAAAGAGAGCATCACAG-3’	Amplifies 06210 off of Fv genome. Overlaps with TOPO.
06210_Rv	5’ CAGGCTCCGAATTCGCCCTTATGAAAAGAGAGCATCACAG-3’	Amplifies 06210 off of Fv genome. Overlaps with GR.

Fw_GR	5’ GATGACTCACGAAGCTCGAAAAACAAAG-3’	Amplifies GR off of PBR1221. Overlaps 06210.
Rv_GR	5’ GCTGGGTCGAATTCGCCCTTAGATTTTTGATGAAACAGAAG-3’	Amplifies GR off of PBR1221. Overlaps TOPO.
Fw_TOPO	5’-AAGGGCGAATTCGACCCAG-3’	Amplifies PCR8/GW/TOPO.
Rv_TOPO	5’- AAGGGCGAATTCGGAGCC- 3’	Amplifies PCR8/GW/TOPO
Fw06210_DELLA_Del:Q5	5’ GATGACTCACGAAGCTCGAAAAACAAAG-3’	Used in Q5 mutagenesis to remove DELLA domain from gene 06210.
Rv06210_DELLA_Del:Q5	5’CATGCCGTCGTCGTGCT-3’	Used in Q5 mutagenesis to remove DELLA domain from gene 06210.
Fw_06210_1680bp	5’-GGTTCATCTCGGTTCCAACGCG-3’	Anneals at the 1680bp point in 06210.
Fwp-22963 for RNAi	5' gactggatccggtaccgaatACCTTTGAGTGATTTGGTTG 3'	Fragment targeting 22963 for RNAi
RVP- 22963 for RNAi	5' atctcgagtgcggccgcgaaGTCGATTGGCGTGAGATTTC 3'	Fragment targeting 22963 for RNAi

2.3 RESULTS

2.3.1 Confirmation of FveRGA1 as a major switch in stolon identity

To confirm that FveRGA1 indeed controls stolon identity in strawberry, I constructed a GA-resistant FveRGA1 protein by deleting the N-terminal DELLA domain to yield construct pMDC32: FveRGA1-ΔDELLA. Additionally, I fused the ligand binding domain of the rat glucocorticoid receptor (GR) to pMDC32:FveRGA1-ΔDELLA (Figure 2.2A). The resulting FveRGA1-ΔDELLA-GR fusion protein will only enter nucleus upon the application of ligand Dexamethasone (DEX), allowing manipulation of this dominant

negative FveRGA1-ΔDELLA to exert its inhibition of GA signaling upon DEX treatment (Caruana, et al. 2018).

We introduced the pMDC32: FveRGA1-ΔDELLA-GR construct into the stolon producing *F. vesca* woodland strawberry H4. Transgenic plants treated with DEX stopped producing stolons, while mock treated transgenic plants continued stolon production (Caruana, et al. 2018) (Figure 2.2B). This data suggests that FveRGA1

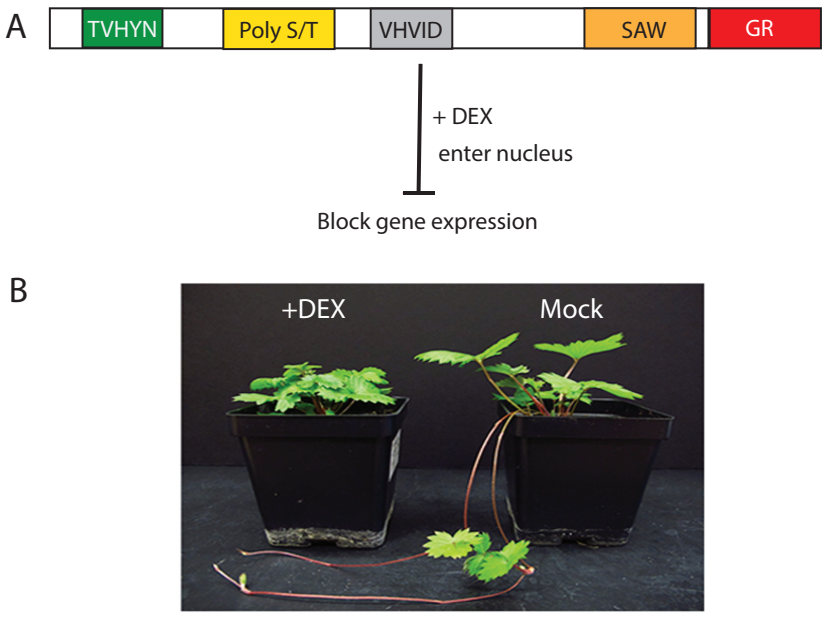

Figure 2.2 Demonstration of *FveRGA1* in suppressing stolon formation in transgenic *F. vesca*

(A). Diagram of FveRGA1-ΔDELLA-GR, which is transformed into Hawaii 4 plants.

(B). Transgenic H4 plants treated with DEX (left) and mock (right). DEX treatment blacks stolon formation in H4 plants.

functions to suppress stolon development. And *srl-1* is indeed caused by the W601X mutation in FveRGA1.

2.3.2 *ga20ox4-1* mutation controls stolon internode length in *srl-1* background

Although *srl1-1; ga20ox4-1* plants produce stolon in YW5AF7, the internode length is characteristically shorter than that of H4 plants (Caruana, et al. 2018) (Figure 2.3A-B). To determine if the short internode was a consequence of the *srl1-1* mutation or the *ga20ox4-1* mutation in the YW5AF7 background, we crossed *srl-1*; *ga20ox4-1* to *+/+; +/+* (H4 plants carrying wild type alleles at the both loci). F2 progeny was screen with PCR markers to identify *srl-1/srl-1*; *ga20ox4*/+ plants, which carry a wild type copy of *GA20OX4* and are homozygous for *srl-1*. Interestingly, the *srl-1/srl-1*; *ga20ox4*/+ plants develop stolon of normal internode length (Figure 2.3A-C). This suggests that the short internode in *srl-1*; *ga20ox4-1* was due to the *ga20ox4-1* mutation. This result suggests that stolon elongation and stolon identity can be separately regulated. While stolon elongation is defective due to the *ga20ox4-1* mutation in YA5AF7, stolon identity is switched on due to the *srl-1* mutation. Another interesting observation is that *ga20ox4* appears to affect internode length only in stolon but not in stem for plant height.

Taken together, GA induces stolon development by facilitating the degradation of the repressive DELLA protein FveRGA1. Removing *RGA1* activity in the *sr1-1* mutants could cause runner formation even in the absence of GA. The fact that *srl-1* makes normal internode length when GA biosynthesis is normal (ie. wild type GA20OX4) but short internode when GA20OX4 is mutated in YW5AF7 indicates that GA is required to stimulate internode length even when *srl-1* is mutated. One explanation is that FveRGA1 carrying the *srl-1* mutation can still respond to GA as it only misses the last 10 amino acids at the C-terminus. Therefore, FveRGA1 function maybe affected in stolon identity but not affected in stolon elongation.

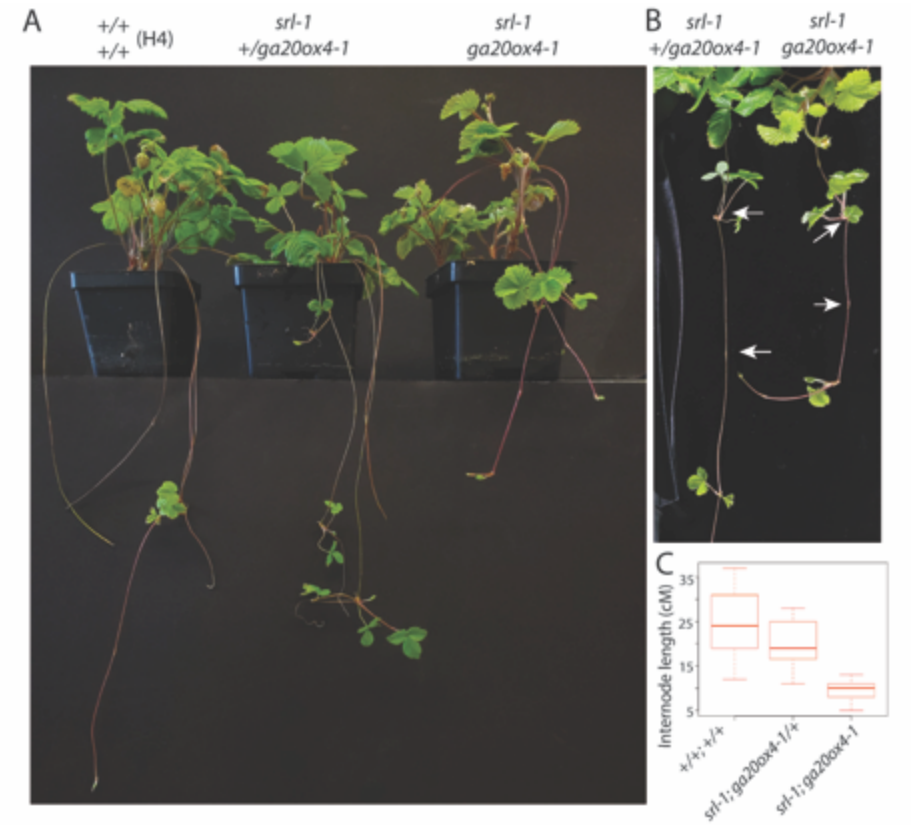

Figure 2.3 *GA20OX4* gene regulates internode distance in *srl-1* background
A) *srl-1; ga20ox4-1* plants develop stolon with shorter internode distance when compared to *srl-1/srl-1; ga20ox4-1/+* as well as *+/+; +/+* (Hawaii 4) plants. B) Closeup photo of the internode between daughter plants in *srl-1; ga20ox4-1* and *srl-1/srl-1; ga20ox4-1/+* plants. The pair of arrows indicates internode length in the two genotype. C). Quantitative measure of internode length of the three genotypes. Forty stolon were measures off of twenty-four *+/+;+/+* plants. Forty-nine stolon were measured off of thirteen *srl-1/srl-1; ga20ox4-1/+* plants. Forty-three stolon were measured off of nineteen *ga20ox4-1/+* plants. Internode distance was measured as the distance between daughter plants. All internodes were measured. The distance between the mother and the first daughter plant were not measured.

2.3.3 Stolon development is affected by the light quality pathway

To evaluate if light quality also plays a role in stolon development, we took three different approaches. First, we determine how the R/FR ratio affects stolon formation. Second, we evaluated a mutant photoreceptor *PhyB* on stolon development. Finally, we tested the effect of PIF3 knockdown on stolon development.

We first grew woodland strawberry H4 under 16 hr light (LD) condition supplemented with 3 hours of red light at the end of each day. Plants were evaluated after 1 month, 2 months and 3 months on stolon development. Both the number of stolon per plant and the internode length (distance between daughter plants) were measured. Red light treatment caused a significant reduction in stolon formation in H4 during the first two months (Figure 2.4A-B, C). However, this difference is diminished at month 3 (Figure 2.4C), suggesting that red light may deter stolon formation. Furthermore, no significant difference in internode length was observed (Figure 2.4D). This suggests that the light quality pathway may deter the initiation of stolon, but once initiated, it does not affect its subsequent development.

Second, YW5AF7 (*ga20ox4-1*) was grown under continuous FR light for two-month to see if FR could restore runner formation. Plant stems become green under far red light, however stolon does not form even under FR treatment (Figure 2.4E).

2.3.4 *F. vesca phyb-1* mutant develops stolon-like structures

While light treatment is a great first test of stolon development, the specific genes involved in the regulation of stolon is unclear. Mutants in the photo-receptors will be more effective in evaluating the effect of light on stolon. As a gift from our collaborator Chunying Kang, we received a loss-of-function mutant of *phyB-1 (gene36731/*gene05117) with a premature stop (W375X) in the first exon in an *alpine* strawberry Rugen. Like YW5AF7, Rugen also carries the *ga20ox4-1* allele and does not make runner (Figure 2.5A).

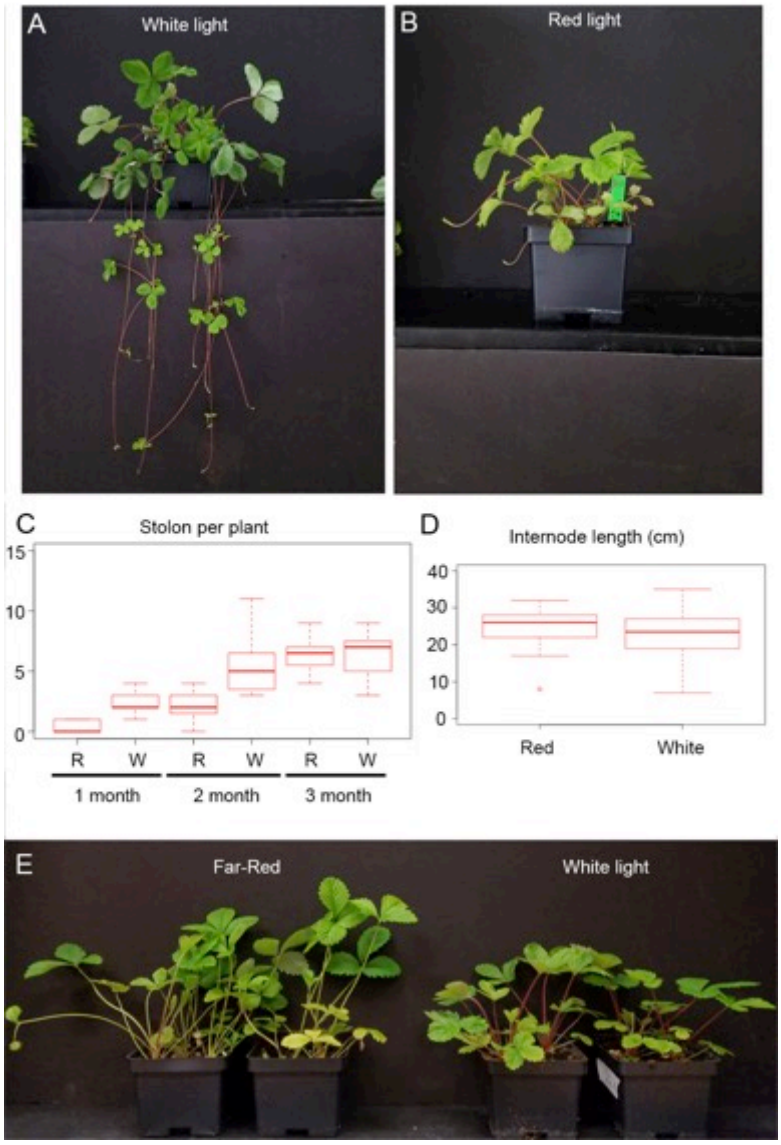

Figure 2.4 Red light treatment of Hawaii 4 plants deter stolon formation.
(A) H4 plants under LD condition. (B) H4 plants under LD condition with 3 hour red light treatment at the end of each day. Stolon formation is reduced at months 1 and 2 of the red light treatment. (C) Number of stolon per H4 plant under white light or red light condition. (D) Internode length of stolon in H4 plants under white light or red light conditions. (E) YW5AF4 (*ga20ox4-1*) plants growing under the LD white light or Far-red light for two months. No stolon is observed but the far-red treated plants have green petioles.

Interestingly, *phyb-1; ga20ox4-1* plants form short stolon as well as indeterminate flowering shoot (Figure 2.5B-C). Specifically, when the primary axillary shoot terminates in a flower, its secondary axillary shoot repeats the same pattern, eventually producing a long chain of daughter plants on a shoot. Hence, a loss-of-function *FvePhyB* in

strawberry might result in the sensing of allow R/FR ratio, which may mimic shade, leading to stolon formation and indeterminate flowering shoots. This suggests that *FvePhyB* may normally function to terminate development and suppress the repetitive structure of stolon. In addition, *phyb-1* plants showed loss of red pigment in the stems (Figure 2.5B-C), similar to the FR treated plants (Figure 2.4E).

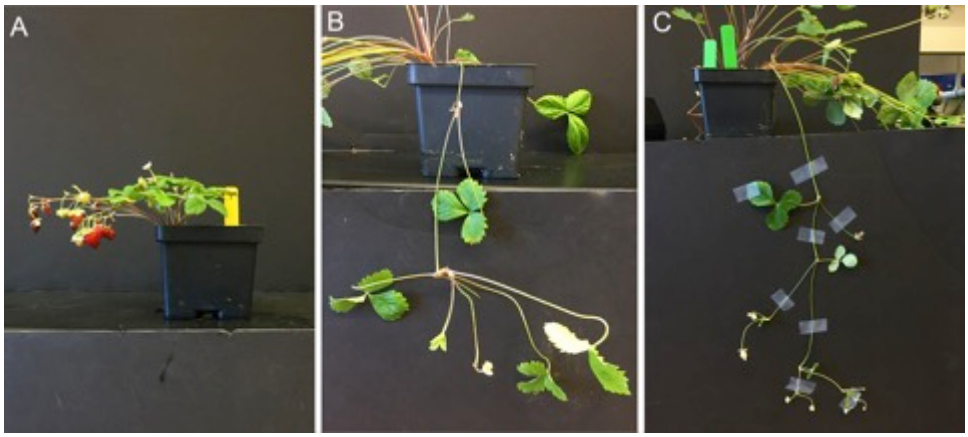

Figure 2.5 *phyb-1* plants produce stolons in a non-stolon producing background
A) Rugen is a non-stolon forming variety of *F. vesca* as it carries *ga20ox4-1*. B) *phyb-1; ga20ox4-1* plants (Rugen background) produce short stolons. C) *phyb-1*; *ga20ox4-1* plants form stolon-like structures out of the flowering shoots.

To sum up, my work indicates that while GA mediates photoperiod signal, *FvePhyB* may mediate light quality/shade signal. These two pathways may converge to regulate the switch between branch crown and stolon.

2.3.5 Propiconazole, A BR biosynthesis inhibitor, reduces stolon length

The Brassionsteroids are a class of plant hormones that regulate processes involved in elongation (Willige, et al. 2007; Gallego-Bartolomé, et al. 2012). To evaluate if brassinosteroid signaling impacts stolon development we sought to disrupt both BR

biosynthesis and BZR1 expression. Propiconazole is a pharmacological agent that functions to inhibit BR biosynthesis (Hartwig, et al. 2012). Here we used 5 week old H4 plants and similar size *rga1-1* plants (7 week old due to slower growth) to investigate whether inhibiting BR biosynthesis would alter runner development in *F. vesca.* Over the course of 7 weeks, plants were treated with propiconazole and compared to the mock treated controls. Treated plants were watered in 50µm 1x/week and 3x/week had propiconazole applied directly to the crown. The H4 plants exhibited a significant reduction in stolon length as well as internode distance between daughter plants (Figure 2.6A-D). In addition, the total plant height is reduced (Figure 2.6A). These effects are consistent with BR playing a critical role in stem and petiole elongation. In contrast, the number of stolon formed was slightly reduced but insignificant ($p>.05$) perhaps due to slower emergence of new stolons (Figure 2.6).

Similar results were observed when *rga1-1* mutants were treated with propiconazole (Figure 2.7). However, we were unable to obtain data on internode distance of propiconazole-treated *rga1-1* plants as the *rga1-1* plants did not develop a second daughter plant within the time frame of the experiment. *rga1-1*; *ga20ox4-1* already possessed short internode due to the *ga20ox4* mutation, propiconazole further inhibited stolon length. Together, the data suggests that BR may be specifically involved in promoting elongation in stolon, stem and petioles.

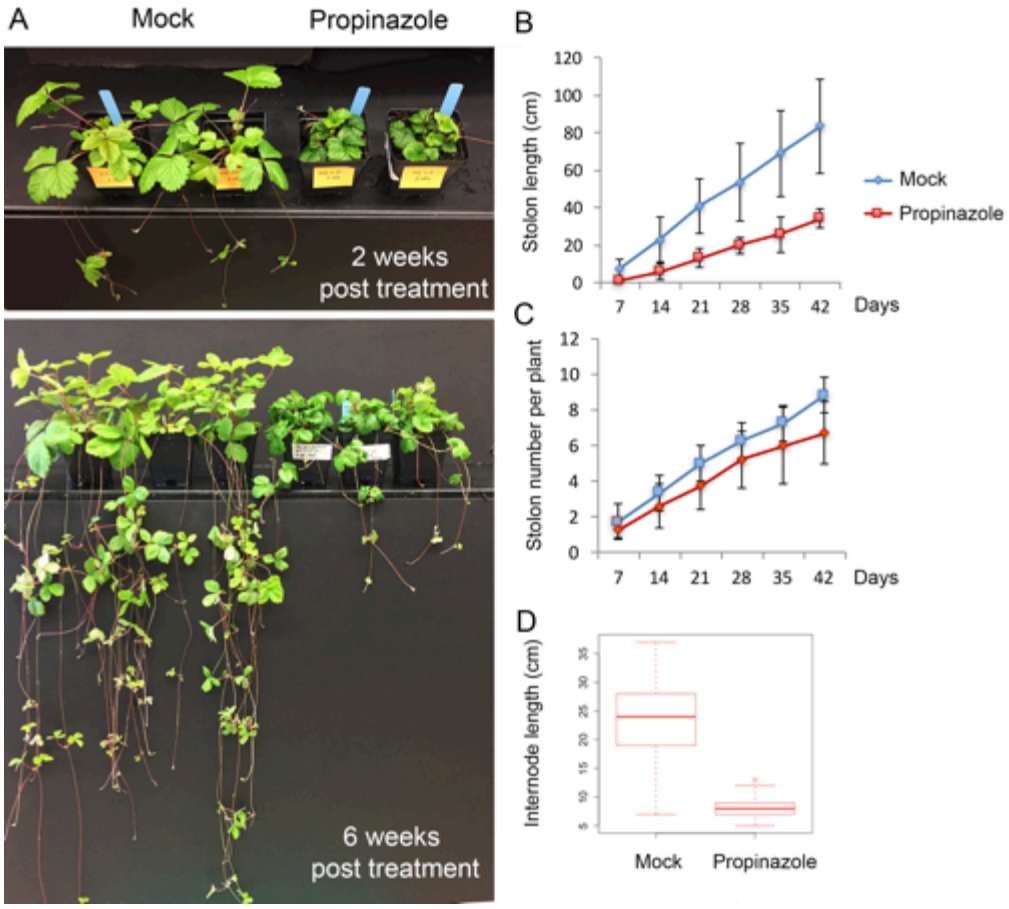

Figure 2.6 Brassinolide (BR) affects stolon elongation in Hawaii 4
A) H4 plants were treated with a mock solution and the BR biosynthesis inhibitor propiconazole. Images were taken at 2 weeks and 6 weeks post-treatment. B) Propiconazole significantly reduces stolon length. C) Propiconazole does not significantly affect stolon number per plant. D) Propiconazole significantly reduces internode length between daughter plants.

2.3.6 FveRGA1 interacts with FveBZR1 and FvePIF3

How does GA signaling crosstalk with light quality and BR signaling pathways at the molecular level? To identify potential genes in the light quality and BR pathway that impact stolon development, I identified *F. vesca* homologs of well-studied Arabidopsis genes At*BZR1, AtPIF1, AtPIF3,* and *AtPIF4* through blasting against the *Fragaria vesca*

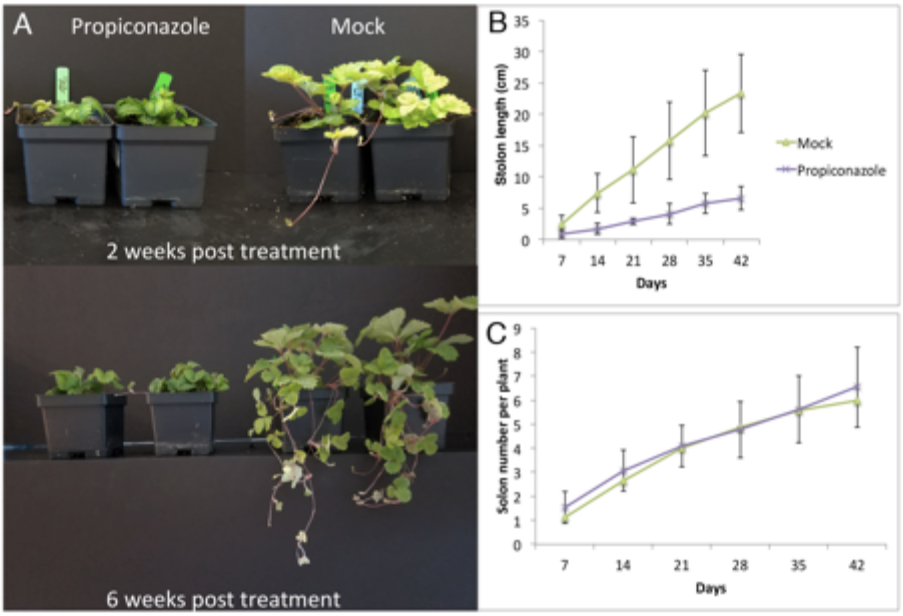

Figure 2.7 Brassinolide (BR) affects stolon elongation in *srl-1*
A) *srl-1* plants were treated with a mock solution or propiconazole. Images were taken at 2 weeks and 6 weeks post-treatment. B) Propiconazole significantly reduces stolon length in *srl-1* plants. C) Propiconazole does not significantly affect stolon number of *srl-1* plants.

genome V1.1 in Plaza. Two *FveBZR1* and four *FvePIFs* were identified. The expression of these candidate genes was examined based on RNA-seq data from *Fragaria vesca* crown tissues (Caruana and Liu, unpublished). *FveBZR1(gene15101), FveBZR1-Like (gene29525), FvPIF1(gene08411)* and *FvePIF3(gene22963)* were found to be expressed in the crown tissues (Figure 2.8) and were identified as potential transcription factors with roles in stolon development. I have since focused on the characterization of *FveBZR1* and *FvePIF3*.

RGA proteins are known to repress gene expression by binding and sequestering TFs (Sun, et al. 2011; Oh, et al. 2014; Gallego-Bartolomé, et al. 2012). To test if FveRGA1 directly interacts with FveBZR1 and FvePIF3 to sequester them away from their targets, I performed Yeast 2 Hybrid (Y2H) experiments. I cloned full length CDS of FveBZR1 and

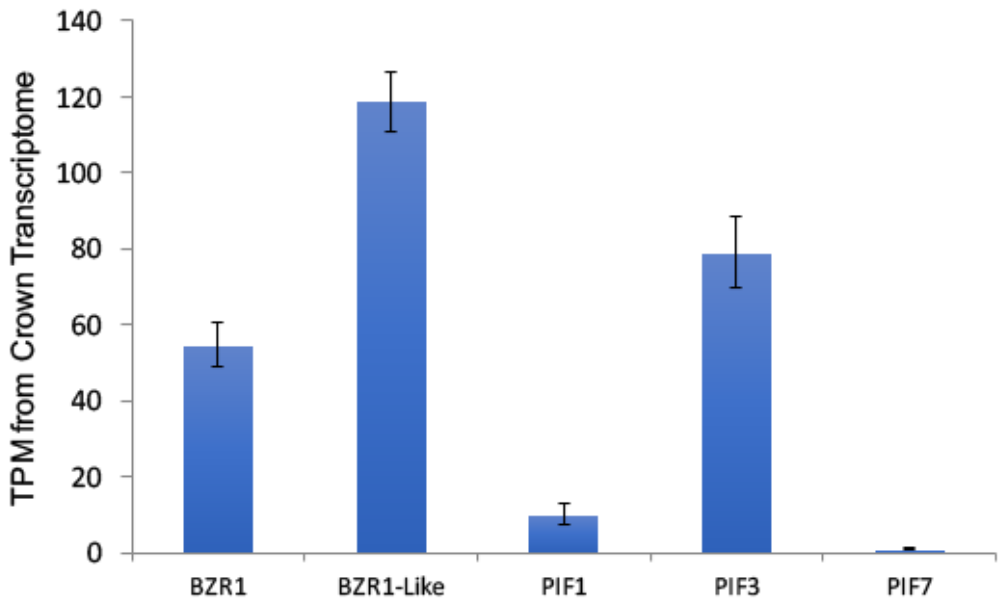

Figure 2.8 Expression of candidate BZR1 and PIF genes in crown tissues. Read counts per million (TPM) for each queried gene. The data is obtained by mining RNA-seq data derived from crown (stem) tissues of the stolon producing *F. vesca vesca*.

FvePIF3 into the pGADT7 and full length FveRGA1 into pGBTK7. To overcome self-activation exhibited by pGBTK7-RGA1 (Figure 2.9), I created a series of N-terminal deletions of FveRGA1 (Figure 2.9). The truncation at -564 bp (-188 aa) (also called M5) lost its auto-activation and was used to test for interactions. RGA1 (M5) was able to interact with FveBZR1 and FvePIF3 in the Y2H assay (Figure 2.10A, B). This was confirmed in BiFC assay (Figure 2.10C).

2.3.7 Domain-specific interactions of FveBZR1/FvePIF3 with FveRGA1 using BiFC

DELLA proteins, like FveRGA1, affect many different developmental pathways due to their ability to bind a variety of transcription factors (Oh, et al. 2012; Oh, et al. 2014; Li, et al. 2016). To determine which domain of FveRGA1 was responsible for interacting

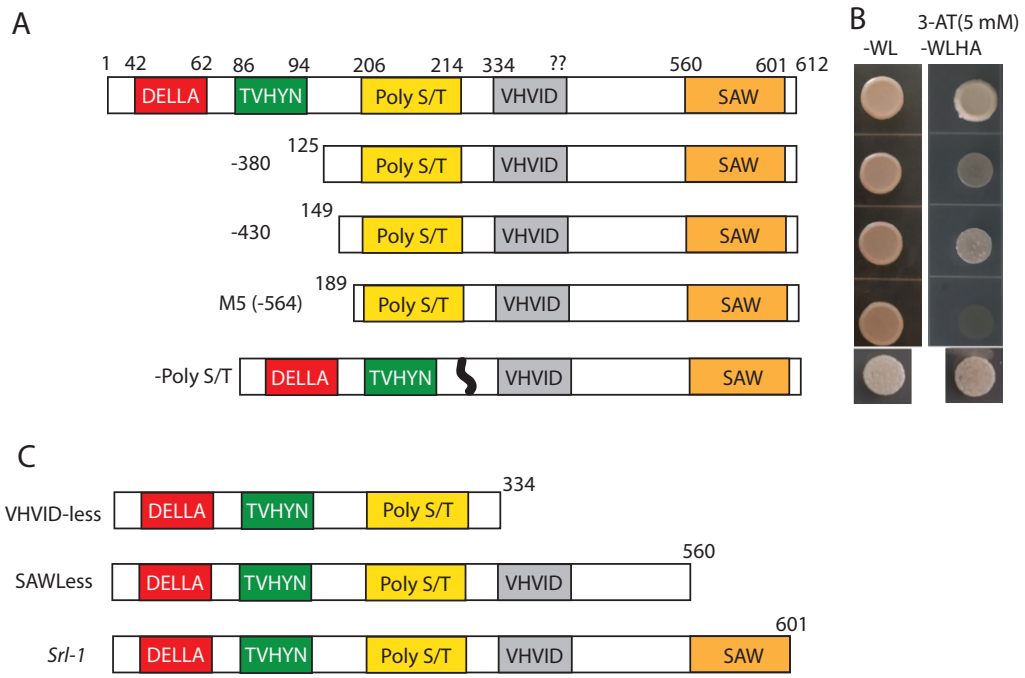

Figure 2.9: Dissection of FveRGA1 protein domains
A) Diagram of various N-terminal truncations of FveRGA1 that were cloned into vector pGBTK7. Numbers above protein domains are amino acid number from Start codon. B) Test results of self-activation of reporter His3 by FveRGA1 N-terminal truncations fused to GAL4 BD in pGBTK7. M5 is the only N-terminal deletion that failed to self-activate. C) Diagram of various C-terminal truncations of FveRGA1.

with FvePIF3 or FveBZR1, a series of FveRGA1 truncations were cloned into pXY105 (Figure 2.10A). Co-infiltration of agrobacteria containing pXY106-FveBZR1 or pXY106-FvePIF3 against pXY105-FveRGA1 deletion series was performed. After 48 hours, tobacco leaves were imaged under a confocal microscope to assay for fluorescence.

A series of N-terminal deletions were constructed and tested (Figure 2.10A). RGA1 truncations with its DELLA domain removed (-DELLA) or N-terminal 430 bp removed (-430N) were still able to interact with FveBZR1 and FvePIF3 (Figure 2.10D) suggesting that the N-terminus is not involved in binding to these two TFs. Interestingly, the RGA1

(-430N) truncation showed a stronger interaction with PIF3, perhaps due to a more stabilized RGA1 (-430N) than the full length or RGA1 (-DELLA).

Next, FveRGA1 with the C-terminal half removed (from 334aa to the end at 612aa; -334C) was tested against full length FveBZR1 and FvePIF3, neither of which interacted with this C-terminal truncated RGA1(-334C) (Figure 2.10D). This suggests that both FveBZR1 and FvePIF3 interacted with the C-terminal GRAS domain of FveRGA1.

The *rga1-1* allele of *FveRGA1* with its last 10 aa deleted was tested to determine if it affects FveRGA1's ability to interact with FveBZR1 and FvePIF3. Interestingly, FvePIF3 failed to interact with *rga1-1*, while FveBZR1 still interacted (Figure 2.10D), indicating that PIF3 likely interacted with the SAW domain of FveRGA1 at the C-terminus and that a loss of interaction with PIF3 might mediate the constitutive runnering phenotype of *rga1-1*.

Taken together, these results suggest that FvePIF3 interacts with the SAW domain at the C-terminus of the FveRGA1, while FveBZR1 interacts with the C-terminal half (from VHVID to SAW) of FveRGA1. These different domains of interaction may allow RGA1 to simultaneously regulate multiple TFs in different signaling pathways.

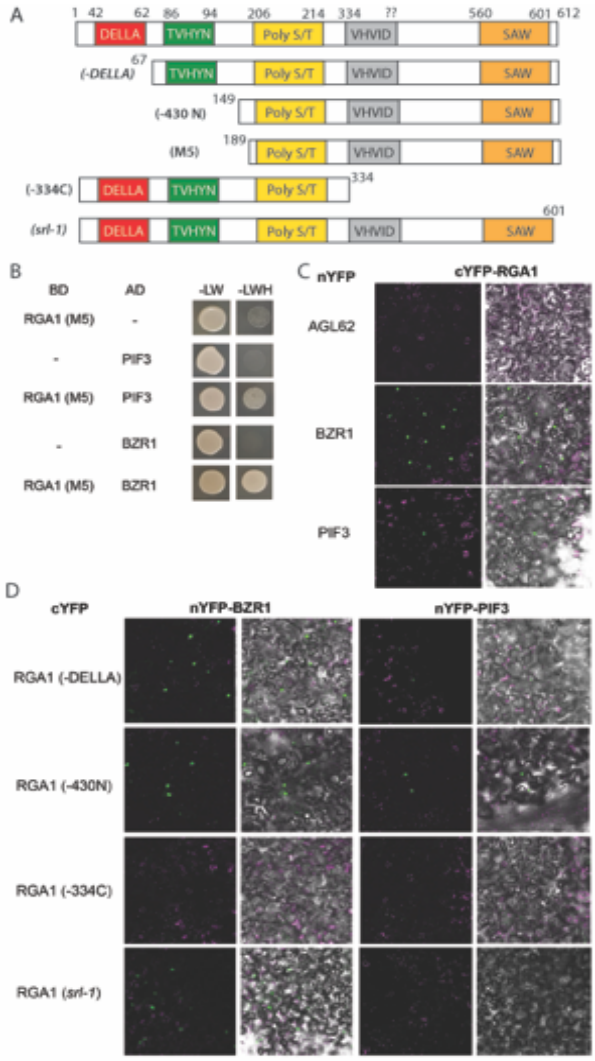

Figure 2.10 FveRGA1 interaction with FvePIF3 and FveBZR1 in yeast and tobacco

A) Diagram of various N-terminal and C-terminal truncations of FveRGA1. Numbers above protein domains are amino acid number from Start codon. -430N and -334C represent N-terminal and C-terminal deletions, respectively, in nucleotide sequence. *srl-1* represents the mutant FveRGA1 protein with the last 11 amino acid deleted. B) Y2H and BiFC both confirm the direct interaction between RGA1 (M5) and FveBZR1 and PIF3 respectively. C) BZR1-nYFP and PIF3-nYFP interacted with c-YFP-FveRGA1 in the nucleus of tobacco cells. AGL62-nYFP serves as a negative control. D) N-terminal deletions of FveRGA1 (-DELLA and -430N) fused to cYFP still interacted with nYFP-BZR1 and nYFP-PIF3. However, C-terminal deletion -334C abolished the interaction. Mutant FveRGA1 (*srl-1*) lose its interaction with PIF3 but can still interact with BZR1.

2.3.8 RNAi knockdown of *FvePIF3* results in a decrease in stolon number

To assess the role of FvePIF3 (gene22963) in stolon development I constructed an RNAi vector ph7gwiwg2-7F2,1 targeting *FvePIF3* and transformed the RNAi vector into H4. We obtained 20 plants originating from two calli. Plants representing a weak, medium and strong RNAi phenotype were tested for their *FvePIF3* transcript abundance by qRT PCR. Over a period of 6 weeks, stolon production was observed in 20 H4 transgenic plants harboring the construct and compared to 25 H4 plants that did not contain the

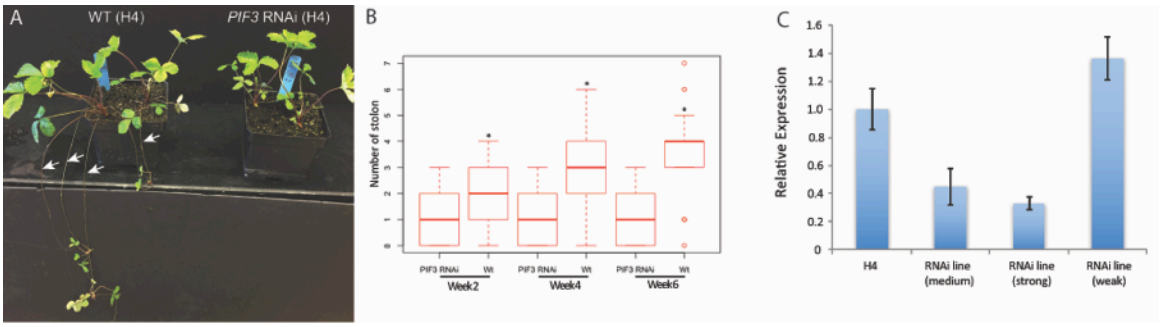

Figure 2.11 RNAi knockdown of PIF3 resulted in a reduction of stolon
A) WT (H4) and an RNAi line of *FvePIF3* at similar age after being transferred from rooting medium to soil. H4 plants already made several stolons (arrows), while the RNAi line of FvePIF3 has not made any stolon. (B) Quantitation of stolon number in WT and RNAi lines of FvePIF3. Twenty one *FvePIF3* RNAi plants originating from two callus and twenty-four Wt (H4) plants were used in this experiment. C) Relative PIF3 mRNA expression PIF3 RNAi plants representing a medium, strong and weak stolon phenotype.

RNAi construct. Some plants containing the RNAi vector exhibited a significant reduction in stolon formation when compared to the control plants (Figure 2.11A-B). Some other transgenic plants produced normal number of stolons. qRT-PCR experiments will determine if the reduction in stolon formation correlates with the reduction of *FvePIF3* expression on individual plant basis. The result suggests that *FvePIF3* likely promotes stolon development.

2.3.9 RNAi targeted FveBZR1 results in no difference in stolon development.

We next sought to determine the role *FveBZR1* (gene15105) may play in stolon development. Here I constructed an RNAi vector in ph7gwiwg2-7F2,1 targeting base pairs 568 to 928 of *FveBZR1* and transformed it into H4. We obtained 10 plants

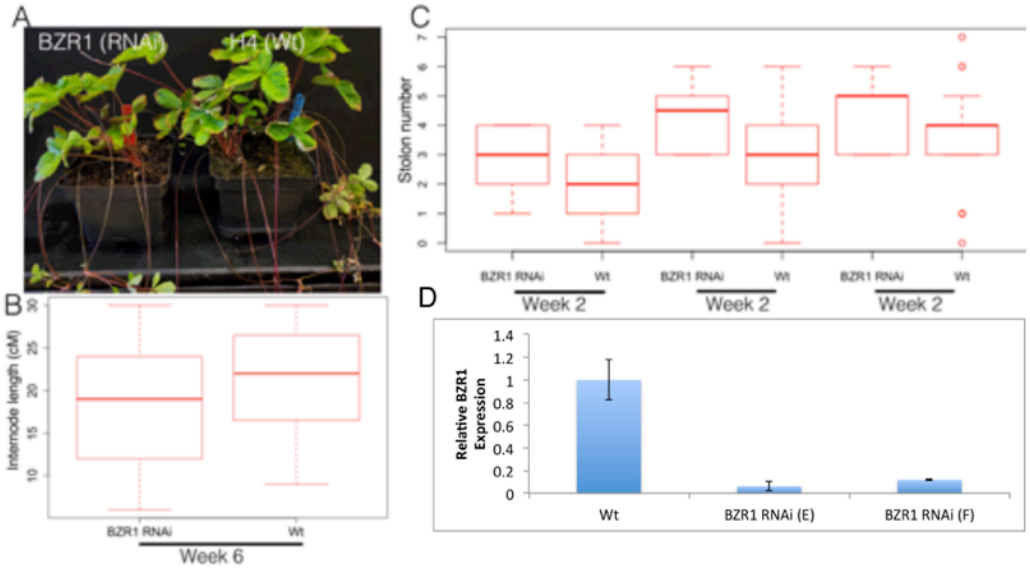

Figure 2.12 RNAi knockdown of BZR1 failed to cause any phenotype

A) WT (H4) and an RNAi line of *FveBZR1* at similar age after being transferred from rooting medium to soil. (B) Quantitation of stolon length in WT and RNAi lines of FveBZR1. C) Quantification of stolon number produced in Wt (H4) and *FveBZR1* (RNAi). Ten *FveBZR1* RNAi plants originating from two callus and fifteen Wt (H4) plants were used to quantify internode distance. Ten *FveBZR1* RNAi plants originating from two callus and twenty-six Wt (H4) plants were used to quantify stolon production.

originating from two calli and compared them to 20 H4 WT plants for stolon number and 10 WT plants were used for calculating internode length. Every 2 weeks for a 6-week period, plants were screened for the number of stolon produced as well as internode length. During the timeframe of the experiment we failed to notice any difference in stolon produced or internode distance (Figure 2.12 A-C). The lack of BZR1 RNAi runner

phenotype maybe due to the presence of a second BZR1 gene *FveBZR1-Like (gene29525)* which may provide redundant function.

2.4 DISCUSSION

A Proposed Model for Stolon Development in *Fragaria vesca*

Based on the results described above, I have proposed a model of *Fragaria vesca* stolon development (Figure 2.13). The light quality pathway and Brassinosteroid signaling are responsible for stolon initiation and elongation respectively. Specifically, the transcription factor FvePIF3 may function downstream of PhyB and promotes stolon initiation (Figure 2.13). BZR1 or related TFs may mediate BR signaling to promote internode elongation. Further, the photoperiod pathway, acting through GA and RGA1, cross-talks with light quality and BR pathway through direct protein-protein interaction between FveRGA1 and FvePIF and FveBZR (Figure 2.13). In the absence of GA such as in the *alpine* strawberry when *GA20OX4* is mutated, FveRGA1 interacts with and sequesters away FvePIF3 and FveBZR1 with specific sub-domains. FvePIF3 interacts with the C-terminal end of FveRGA1 and FveBZR1 interacts with the middle region of FveRGA1, between Poly S/T and right before SAW (Figure 2.13). Therefore, there will be no runner formation. In the presence of GA, FveRGA1 is degraded, freeing FvePIF3 and FveBZR1. However, BR and low R/FR ratio will be required to ensure the continuous supply of FvePIF3 and FveBZR1 into the nucleus. Together, the three signaling pathways work in concert to enable normal stolon formation. In *rga1-1* mutants carrying a FveRGA1 with a defective SAW domain, PIF3 is released, which facilitates stolon initiation even in the absence of GA biosynthesis. However, BZR1 is still bound

by FveGRA1 and could not promote stolon internode elongation unless GA is produced. As a result, *rga1-1* develops stolon with short internode.

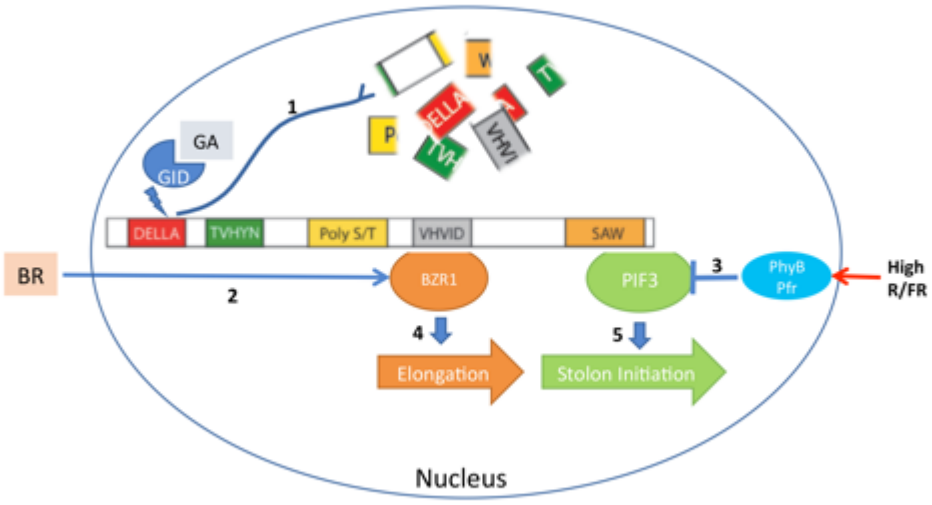

Figure 2.13: A proposed model for stolon development in *Fragaria vesca*
A proposed model based on crosstalk among GA, BR, and light (PhyB). In the absence of GA, FveRGA1 binds and inhibits the transcription factors FveBZR1 and FvePIF3. However, when GA is present, which binds its receptor GID and interacts with RGA1 via its N-terminal DELLA domain. This interaction results in ubiquitination and degradation of the RGA1 protein (1). As a result, FvePIF3 and FveBZR1 are released and able to promote stolon initiation (5) and stolon elongation (4), respectively. However, additional factors including shade under low R/FR light (3) and BR (2) are required to ensure the steady supply of FvePIF3 and FveBZR1 in the nucleus. *srl-1* mutant RGA protein may have lost the ability to inhibit FvePIF3 but still is able to bind FveBZR1, accounting for the reduction in stolon internode distance in the *srl-1* plants.

2.4.1 Stoloniferous reproduction in other plants

Stolon production is not a trait exclusive to *Fragaria*. Stoloniferous reproduction is observed in a variety of plants including grasses, tubers, as well as other angiosperms (Burgess and Huang. 2014; Gao, et al. 2014; Marhold, et al. 2010). Stolons are

responsible for a variety of plant behaviors that have significant impact on human health and agriculture (Marhold, et al 2010, Gao, et al. 2014; Neuhaus, et al. 2013). Stoloniferous reproduction in the turfgrasses is essential to its environmental functions such as erosion control, carbon capture and surface water detox (Beard and Green. 2004; Burgess, et al. 2014). Specifically, the grass *Agostis stolinifera* was found to exhibit an increase in biomass, by way of stoloniferous reproduction, in response to increased CO_2 levels (Burgess, et al. 2014). In addition to the environmental benefits of stolon production, stolons are also a source of food. In the potato, *Solanum tuberosum,* tubers are formed from swollen below-ground stolons (Gao, et al. 2014). Despite their environmental and agricultural significance, the molecular mechanisms governing stolon production is not well studied outside of *Fragaria vesca* (Gao, et al. 2014; Burgess, et al 2014).

Cardamine amara, a member of the Brassicaseae family, offers a unique perspective in studying the environmental and molecular signals that give rise to stolon production. *C. amara* and the extensively studied non-stolon producing *Arabidopsis thaliana* are both members of the Brassicaseae family of angiosperms (Marhold, et al. 2010; Johnston, et al. 2005). Unraveling the molecular signals and mechanisms that dictate stolon development in *C. amara* could be compared with the signals and mechanisms we discovered in strawberry. Such insights may guide future engineering to produce stolon in *A. thaliana* as well as other non-stoloniferous plants. This could also serve as a template for studying the evolution of stolon development.

2.4.2 Future works in studying stolon development in *Fragaria vesca*

While this work focuses on the signals that dictate stolon initiation, other aspects of stolon development remain to be investigated. In addition to initiation; the factors that govern stolon elongation, gravitropic horizontal growth, and stolon meristem differentiation are likely next steps in studying stolon development. Although we identified the BR signaling pathway as a putative regulator of stolon elongation, the lack of *bzr1* RNAi line phenotype indicates that we have yet identified the genes in the BR pathway regulating this elongation; future work would include knocking out the second BZR-like gene in the BZR1 RNAi background. Following elongation, the stolon meristem tip differentiates into a strawberry plantlet. Next steps could be to study the environmental and molecular cues that 1) regulate the timing of meristem differentiation as well as 2) the developmental signals that differentiate the stolon meristem into the plantlet. Advancements in understanding stolon development could allow for more rapid reproduction of fruit bearing crops. Further, as stolon development is a form of clonal propagation, methods developed towards genetically manipulating the stolon could serve as a faster means for developing a transgenic plant.

Chapter 3 Cyclic dipeptides of bacterium origin as a growth stimulating agent for a marine diatom *Phaeodyctylum tricornutum*

3.1 INTRODUCTION

Diatoms are photosynthetic green algae with critical ecological and global implications. Thriving in a variety of oceanic environments worldwide, diatoms are responsible for 20-40% of the yearly global carbon fixation (Hopkinson, et al. 2011). In addition to their role as a primary producer, diatoms are investigated as a source of renewable energy due to

their high lipid content and photosynthetic capability (Vega-Sanchez, et al. 2010). Diatom are a rich source of fatty acids for human nutritional supplement such as Eicosapentaenoic acid (EPA) and Palmitoleic acid (Pérez-López, et al. 2013; Yang, et al. 2017). These valuable fatty acids are increasingly produced from algae instead fish to curb over-fishing (Worm, et al. 2006; Adarme-Vega, et al. 2012).

Phaeodactylum tricornutum (P. tricornutum) is a model species of diatom, due to its sequenced genome, single-cellularity, and availability of molecular tools including transformation (Bowler, et al. 2008; Zhang, Hu. 2013). New knowledge that improves the growth and yields of *P. tricornutum* will be highly valuable both for basic understanding of how diatom sustains its growth in nutrient poor ocean as well as new strategies to enhance algal-based production of biomass for biofuel and nutritional products.

In this study, we characterized a beneficial interaction between *Bacillus cereus* and diatom *Phaeodactylum tricornutum.* Multiple sporulating *B. cereus* species were found to release a heat labile agent that significantly stimulates the growth rate of *P. tricornutum*. Characterization and purification identified two CDPs responsible for the stimulating activity. Our work highlights CDPs as an inter-kingdom communication signal that may be applied to enhancing algal-based biomass production as well as understanding of inter-kingdom communications.

3.2 METHODS

3.2.1 *Bacillus* strains and culture conditions

Bacillus thuringiensis israelensis was isolated from spores in the larvicide Gnatrol (Valent, United States). *Bacillus subtilis* 168 and *Bacillus velezensis* FZB42 were from

Dr. Wade Winkler at the University of Maryland, College Park. *Bacillus cereus 6A1, Bacillus thuringiensis 4A4* and *Bacillus thuringiensis 4Q7* were purchased from the Bacillus Genetics Stock Center (BGSC). All *Bacillus* species were cultured in LB medium. A single colony of *Bacillus* was added to 10mL LB, which was grown in a 37^{o} C shaker at 200RPM overnight.

3.2.2 *Phaeodactylum tricornutum* strain, culture condition, and cell counts

P. tricornutum is cultured in the L1 medium, a salt water solution containing 32g/L of Instant Ocean sea salt (Instant Ocean, United States) supplemented with 1ml (per liter salt water) trace metal solution (NCMA) as well as 8.82 x 10^{-4} M NaNO3, 3.62 x 10^{-5} M NaH2PO4· H2O, and 1.06 x 10^{-4} M Na2SiO3 · 9 H2O (NCMA; National Center for Marine Algae and Microbiota).

P. tricornutum strain CCMP632 was obtained from the Provasoli-Guillard National Center for Marine Algae and Microbiota (NCMA) (East Boothbay, ME). *P. tricornutum* cells were grown in non-shaking L1 medium at 22^{0} C with a light intensity of 50 umol/m^2/s until mid-exponential phase, and 100μL of such *P. tricornutum* cell culture was transferred to 2ml L1 medium in 15ml Falcon tubes with a tapered bottom. Overnight *Baccilus* culture (100 uL), or control medium, or nutrients were respectively added into the same 2ml L1 medium. Co-cultures were grown non-shaking at 22^{o} C with a light intensity of 50 umol/m^2/s. *P. tricornutum* cells at any growth stage could stimulated by the addition of stimulating agent.

All cell counts of *P. tricornutum* were performed using a Hauser Scientific Levy Hemacytometer. 7.5uL of cell culture was loaded into the well. Cells occupying the 1mm

x 1mm x .1uL grid were counted in the experiment. The cell counts were then scaled up to indicate "number of *P. tricornutum* cells per mL".

3.2.3 Identification of the growth stimulating bacterium

The faster growth culture of *P. tricornutum* was streaked on LB medium and grown overnight at 37^{o}C, revealing two morphologically distinct types of colonies. The 16S rDNA region of the bacterial genome was amplified using primers F 5' GTGYCAGCMGCCGCGGTAA 3'/ R 5' GGACTACNVGGGTWTCTAAT 3' based on instructions at the Earth Microbiome Project (http://press.igsb.anl.gov/earthmicrobiome/protocols-and-standards/16s/). The amplicon was cloned into pCR8/GW/TOPO and sequenced using the GW1 primer in the PCR8/GW/Topo kit (Thermofisher; United States). Sanger sequencing results were BLASTed using BLASTn at NCBI, which identified the two colony types as *Staphylococcus epidermidis* and *Bacillus cereus,* respectively.

3.2.4 *Bacillus thuringiensis* cell lysate

To generate the *Bacillus thuringiensis* mother cell lysate, 1.25 mL of *Bacillus* overnight culture was added to 25mL fresh L1 medium. The nutrient poor bacterial culture was kept at RT without shaking for two weeks to enable sporulation. The culture was then spun down and the supernatant was filtered through a .22um filter to yield spore-free lysate, which can be added to the *P. tricornutum* culture. The spores in the pellet were washed three timed in DI water and resuspended in 1.25ml of L1 medium; 100uL was added to 2mL of L1 medium for co-culture with 100uL of *P. tricornutum.*

To generate mechanically lysed nonsporulating *B. thuringiensis* cells, 1.25mL of *B. thuringiensis* was removed from a 25mL overnight culture in LB, spun down, and resuspended in 350uL of L1 medium. The cellular suspension was sonicated using the Microson Ultrasonic Cell Disruptor (Misonix) at setting 12 for 10 1-sec pulses. The shredded cells were resuspended in 25mL of L1 medium and filtered through a .22 micron filter. 2mL of mechanically generate lysate was transferred into the 15ml Falcon tube followed by the addition of 100uL *P. tricornutum* culture at exponential phase.

3.2.5 Proteinase K treatment of mother cell lysate

2 mL *Bacillus* lysate was treated with 2 uL of Proteinase K (20mg/ml) (Thermofisher) and incubated overnight in a 37^{o} C incubator. Following this step, 100 µL of *P. tricornutum* culture was added to the Proteinase K treated lysate and grown in the standard *P. tricornutum* culture condition described above.

To pre-treat the *Bacillus* mother cell lysate with Proteinase K, 2 µL of Proteinase K (20mg/ml) was added to 2 ml *Bacillus* lysate, which was allowed to sit for one week at 22^{o} C. Afterwards, 80µL containing 4.1mg of glycine was added to the *Bacillus* lysate to inhibit the Proteinase K activity. At this point, 100µL *P. tricornutum* culture was added to the 2ml lysate pretreated with Proteinase K.

3.2.6 Fatty Acid analysis

2.5mL of mid-exponential *P. tricornutum* cells was added to 50mL of L1 medium or 50mL L1 medium containing *Bacillus* lysate. After 7 days, cells were collected for FA analysis. To perform the FA analysis, cells were centrifuged 13,300 rpm for 30 seconds. The pellet-containing tube was dipped in liquid nitrogen and stored at -80°C. To extract

lipids, a mixture of 628 µL methanol, 251 µL chloroform, and 251 µL water was added to the pellet. This suspension was vortexed and held at –20°C for 90 min, with further vortex at 30 and 60 min. Extracts were centrifuged at 8000 rpm for 5 min and the supernatant was transferred to a separate vial. An additional mixture of 286 µL methanol and 286 µL chloroform was added to the cell pellet. The sample was vortex mixed and held at –20°C for 30 min, centrifuged at 8000 min^{-1} for 5 min, and the supernatant was added to the previously saved supernatant. 286 µL of water was added to the combined liquid extract to achieve phase separation. The aqueous methanol layer was removed from the chloroform. The chloroform was evaporated under a gentile stream of nitrogen, and lipids were derivitized by adding 200 µL of 3 N methanolic HCl to the dried chloroform layer and heated at 70 °C for 1 h. After allowing the sample to cool to room temperature, 100 µL of hexanes were added and the sample vortex mixed. The upper hexanes layer containing the methyl-esterified lipids was collected. An additional 100 µL of hexanes was added to the acid raffinate and vortex mixed. The upper hexanes layer was again collected and combined with the first extract. 50 µg methyl heptadecanoate was added as an internal standard. All samples were analyzed using a Bruker 450-GC gas chromatograph equipped with a Varian VF-5ms (30 m × 0.25 mm × 0.25 µm) column coupled to a Bruker 300MS mass spectrometer (Bruker, Fremont, CA) in full scan, electron ionization mode. The GC oven temperature was initially set at 150°C for 2 min, raised to 205°C at 10°C min^{-1}, then raised to 230°C at 3°C min^{-1}, and finally raised to 300°C and held for 3 min at 10°C min^{-1}. This was performed by Dr. Andrew Quinn from Dr. Ganesh Sriram's lab at the University of Maryland in College Park.

3.2.7 Identification of CDPs from *B. thuringiensis* lysate

Bacillus thuringiensis strain was cultivated in 5 mL of LB medium (5 g yeast extract, 10 g peptone, and 5 g sodium chloride in 1 L distilled water) in a 15 mL falcon tube. After cultivating the strain for 3 days on a rotary shaker at 180 rpm at 30 °C, 5 mL of the *Bacillus thuringiensis* liquid culture was inoculated to 500 mL of L1 medium (1 mL $NaNO_3$ (75.0 g/L dH_2O), 1 mL $NaH_2PO_4 \cdot H_2O$ (5.0 g/L dH_2O), 1 mL $Na_2SiO_3 \cdot 9H_2O$ (30.0 g/L dH_2O) in 1 L artificial seawater) in a 1 L Pyrex media storage bottle. The *Bacillus thuringiensis* was incubated for 21 days on incubator at 22 °C, forming endospore. Then, supernatant of 8 L culture for the *Bacillus thuringiensis* was loaded on Sep-pak C_{18} cartridge and fractionated by reversed phase solvent system with 100% water, 20%, 40%, 60%, 80%, and 100% methanol/water. The growth simulation activity was detected from 100% water fraction.

To obtain active compounds, the 100% water fraction was subjected to reversed-phase prep-HPLC (Luna Phenyl-Hexyl: 250 × 21.2 mm, 5 μm) with gradient elution (5% acetonitrile/water to 20% acetonitrile/water over 40 min. after 40 min, 100% acetonitrile over 15min for washing; UV detection at 210 nm; flow rate: 10 mL/min). The fractions were collected for every 2 min from 5min to 55 min, obtaining 25 fractions. The growth stimulation activity was detected from fraction 13 (**1**) (1.5 mg) and fraction 19 (**2**) (1.2 mg), respectively.

CYCLO(L-Pro-L-OMet) (**1**). $[\alpha]_D$ -125.8 (c 0.1, MeOH); UV (MeOH) λ_{max} (log ε) 210 (4.12) nm; HRFABMS *m*/*z* 245.0972 $[M+H]^+$ (calcd for $C_{10}H_{17}N_2O_3S$ 245.0965); ^1H NMR (500 MHz, D_2O) δ_H 4.53 (t, *J* = 5.0, 1H), 4.37 (t, *J* = 8.0, 1H), 3.59-3.56 (m, 2H),

3.10-2.87 (m, 2H), 2.75 (s, 3H), 2.43-2.27 (m, 3H), 2.10 (m, 1H), 2.02-1.93 (m, 3H); ^{13}C NMR (125 MHz, D_2O) δ_C 175.2, 168.9, 61.8, 56.5, 50.3, 48.1, 39.3, 30.5, 25.3, 24.6.

CYCLO(L-Val-ΔAla) (**2**). $[\alpha]_D$ -113.2 (c 0.1, MeOH); UV (MeOH) λ_{max} (log ε) 220 (4.08) nm, 240 (3.96); HRFABMS *m/z* 169.0981 $[M+H]^+$ (calcd for $C_8H_{13}N_2O_2$ 169.0983); ^{1}H NMR (500 MHz, DMSO-d_6) δ_H 10.52 (brs, 1H), 8.36 (s, 1H), 5.17 (s, 1H), 4.77 (s, 1H), 3.83 (br, 1H), 2.12 (m, 1H), 0.92 (d, J = 7.5, 3H), 0.81 (d, J = 7.5, 3H); ^{13}C NMR (125 MHz, DMSO-d_6) δ_C 165.6, 158.7, 134.6, 98.9, 60.4, 33.2, 18.1, 16.5.

The generation of fractions, purification of fractions and identification of CDPs was performed by Dr. Munhyung Bae and Dr. Emily Meyers from Dr. Jon Clardy's lab at Harvard Medical School.

3.2.8 Synthesis of CYCLO (L-Pro-L-OMet)

Boc-L-Methionine-sulfoxide (1000 mg, 3.76 mmol) was dissolved in dichloromethane (20 mL) at room temperature. To activate terminal carboxyl acid group, *O*-(Benzotriazol-1-yl)-*N,N,N′,N′*-tetramethyluronium hexafluorophosphate (1.713 mg, 4.52 mmol) was added and stirred for 30 min. Then, L-Proline methyl ester (749 mg, 4.52 mmol) and triethylamine (0.63 mL, 4.52 mmol) were added, stirred for 18 hours at 4 °C. After 18 hours, the reaction mixture was extracted by ethyl acetate/ water system and then, ethyl acetate layer was evaporated to dryness to give 580 mg of a white oil (41% yield). This oil was dissolved in a 1 mL of dioxane at 50 °C, and 3 N hydrochloride (0.6 mL, ~4 equiv.) was added drop-wise. The reaction was stirred for 3 h, and the solvent and HCl were removed on a rotary evaporator. The mixture was lyophilized in high *vacuum*

overnight. The oil was dissolved in dimethylformamide (2 mL), and stirred at 100 °C. The cyclization reaction was quenched in 4 h as judged by LCMS. The mixture was lyophilized in high *vacuum* overnight, and the resulting oil was purified by reversed phase prep-HPLC with Luna Phenyl-Hexyl column (250 × 21.2 mm, 5 μm), using gradient solvent system (5% acetonitrile/water to 20% acetonitrile/water over 40 min. after 40 min, 100% acetonitrile over 15min for washing; UV detection at 210 nm; flow rate: 10 mL/min). The cyclo(L-Pro- L-OMet) was obtained as white oil to yield 250 mg (26.6% yield).

CYCLO(L-Pro-L-OMet) (**1**). $[\alpha]_D$ -128.5 (c 0.1, MeOH); UV (MeOH) λ_{max} (log ε) 210 (4.12) nm; HRFABMS *m*/*z* 245.0972 $[M+H]^+$ (calcd for $C_{10}H_{17}N_2O_3S$ 245.0965); ^1H NMR (500 MHz, D_2O) δ_H 4.53 (t, *J* = 5.0, 1H), 4.37 (t, *J* = 8.0, 1H), 3.59-3.56 (m, 2H), 3.10-2.87 (m, 2H), 2.75 (s, 3H), 2.43-2.27 (m, 3H), 2.10 (m, 1H), 2.02-1.93 (m, 3H); ^{13}C NMR (125 MHz, D_2O) δ_C 175.2, 168.9, 61.8, 56.5, 50.3, 48.1, 39.3, 30.5, 25.3, 24.6.

The synthesis of Cyclo L-Pro-L-OMet was performed by Dr. Munhyung Bae from Dr. Jon Clardy's lab at Harvard Medical School.

3.2.9 *P. tricornutum* cellular iron concentration

P. tricornutum cellular iron concentration was analyzed using a Ferrozine protocol as previously described (Reimer, et al. 2004). 10mL *P. tricornutum* grown in L1 medium and 10ml of *P. tricornutum* grown in *B. thuringiensis* lysate culture were started on day 0, and 1ml of *P. tricornutum* was harvested from both cultures for cell counts and intracellular iron quantification every day.

3.3 RESULTS

3.3.1 *Bacillus cereus group* bacteria stimulate *P. tricornutum* growth under co-culture condition

During experiments with cultures of *P. tricornutum* in standard L1 medium, a fast growing culture was discovered due to its obvious green color and higher *P. tricornutum* cell density (Figure 3.1). Further, bacterial cells and spores were observed in this culture (Figure 3.1C) indicating contamination by bacteria. After streaking the culture on LB medium, two distinct types of bacterial colonies were observed. 16S rDNA was amplified from these two types bacteria and sequenced. Blast search in NCBI revealed their

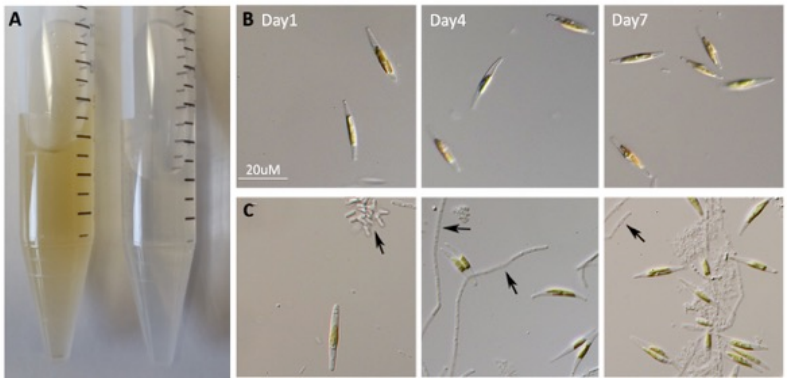

Figure 3.1: Images of *P. tricornutum* culture under microscope.
A) Photo of 5 day *P. tricornutum* cultures. The left tube is a co-culture containing *P. tricornutum* and unknown bacteria, and the right tube is an axenic culture of *P. tricornutum*. (B) Images of axenic culture with *P. tricornutum* cells in L1 medium at day 1, 4, and 7. (C) Images of *P. tricornutum* co-cultured with unknown bacteria. Arrows point to bacterium spores.

identities as *Bacillus cereus group* and *Staphylococcus sp,* respectively (Figure 3.2*)*.

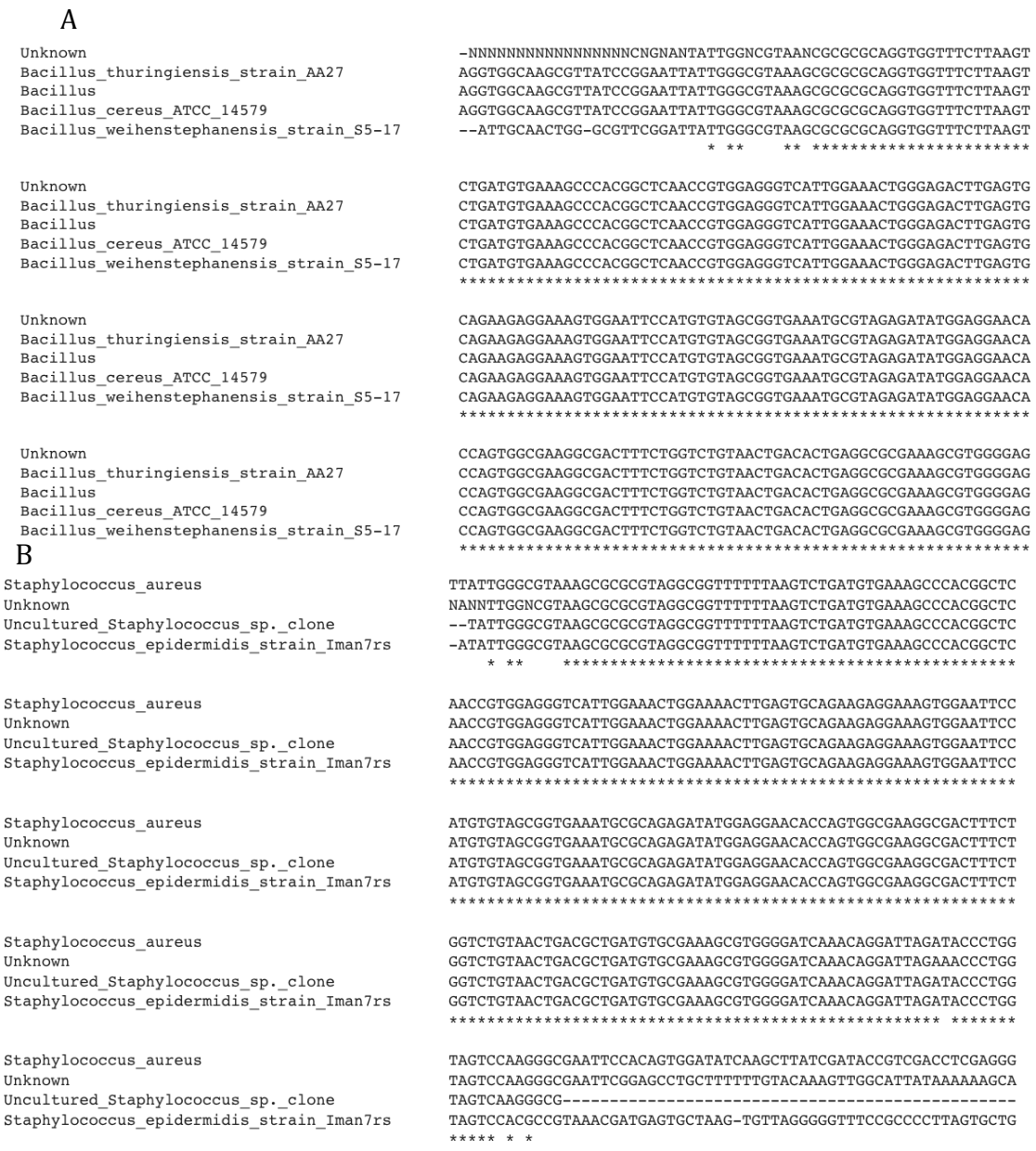

Figure 3.2: Partial 16S rDNA sequence alignment of bacteria found in contaminated *P.tricornutum* culture. A) Top BLAST hits identifies *B.cereus* group species. B) Top BLAST hit identifies *Staphylococcus sp.*

To investigate which one of the two bacteria was responsible for enhancing *P. tricornutum* growth, *P. tricornutum* cultures were inoculated respectively with *Bacillus cereus group, Staphylococcus sp,* both bacteria combined, and L1 medium only (axenic control). The *P. tricornutum* culture containing *Bacillus cereus* group showed a higher growth rate than the axenic culture, and at a similar rate as the combined bacterial culture

(Figure 3.2A).

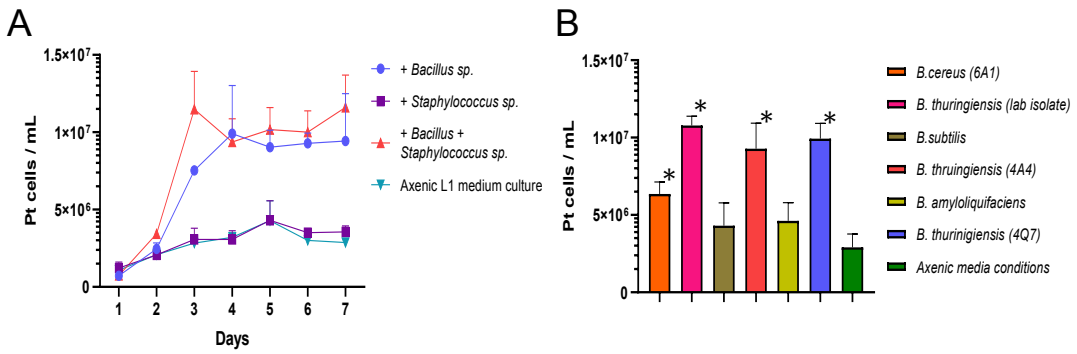

Figure 3.2: *Bacillus cereus* clade of bacteria stimulate the growth of marine diatom *Phaeodactylum tricornutum* during co-culture. **a.** Growth curve of *P. tricornutum (Pt)* when co-cultured with *Staphylococcus* sp., *Bacillus sp.,* combined bacteria, or in L1 medium (axenic condition). The bacteria were added to the *P .tricornutum* culture at day 1. The *P. tricornutum* cell number (Y-axis) was quantified at each day (X-axis). **b.** Several species of the *Bacillus cereus* clade *(*blue bar*)* and *Bacillus subtilis* clade (orange bar) were tested for their ability to stimulate *P. tricornutum* growth. *P. tricornutum* cells (Y-axis) were counted at day 6 of co-culture. Each culturing condition contained 3 replicates. Error bars are ± 1 SD. B).

At day 3, it yielded 2-3 folds more *P. tricornutum* cells than the axenic condition but the growth rate plateaued soon after. In contrast, the *P. tricornutum* culture inoculated with *Staphylococcus sp* displayed the same growth rate as the axenic culture (Figure 3.2). Our result suggests that it is the *Bacillus cereus* group microbe capable of promoting *P. tricornutum* growth.

Bacillus cereus group is composed of genetically similar but pathologically distinct bacteria (Rasko, et al. 2005; Fernández-No, et al. 2013). Because of the high sequence similarity in the 16S region, we were unable to distinguish them with the 16S rDNA sequence. Among the blast top hits are *Bacillus thuringiensis,* used commercially as an insecticide*, Bacillus cereus,* a soil microbe, and *Bacillus anthracis*, the causative agent of anthrax (Figure S1A) (Lecadet, et al. 1999; Jernigan, et al. 2002). To determine which

Bacillus cereus group microbe is responsible for stimulating *P. tricornutum* growth, four species in the *Bacillus cereus* clade and two species of the neighboring clade *Bacillus subtilis* were tested (Figure 3.2B) in co-cultured with *P. tricornutum*. All *Bacillus cereus* species, particularly *Bacillus thuringiensis* subsp *thuringiensis* (BGSC 4A4), *Bacillus thuringiensis subsp. Israelensis* (BGSC 4Q7), and the lab isolate, showed the ability to stimulate *P. tricornutum* growth. However, the two *B. subtilis species, B. subtilis* and *B. amyloliquefaciens,* did not show stimulating effect (Figure 3.2B). This suggests that the growth stimulating capability may be specific to the *Bacillus cereus* group. Further, the similarly high stimulating ability of *B. thuringiensis israelensis* to the lab isolate suggests that the initial isolate is likely *B. thuringiensis israelensis,* which was used as a larvicide in our research laboratory.

3.3.2 *B. thuringiensis* mother cell lysate contains the stimulating agent for *P. tricornutum* growth

Bacillus undergoes sporulation upon poor nutrient stress (Rasko, et al. 2005; Veening, et al. 2008). Microscopic examination of the *P. tricornutum/B. thuringiensis* co-culture revealed the presence of spores, a sign of sporulation by *B. thuringiensis* (Figure 3.1C, arrows). To investigate if increased growth of *P. tricornutum* correlated with *B. thuringiensis* spores, *P. tricornutum* and *B. thuringiensis* were co-cultured. Over the course of 5 days *P. tricornutum* and *B. thuringiensis* spores were counted. Interestingly, as *P. tricornutum* cells increased in culture so did the number of *B. thuringiensis* spores (Figure 3.3A).

In *Bacillus,* a consequence of sporulation is mother-cell lysis (Higgins, et al. 2012). Could the growth stimulating factor of *Bacillus* be released into the culture through sporulation-mediated cell lysis? To answer this question*, P. tricornutum* was cultured under two different conditions, one containing washed *B. thuringiensis* spores and the other *B. thuringiensis* mother cell lysate whose spores were filtered and removed (Figure 4A). *P. tricornutum* cultured in the presence of *B. thuringiensis* mother cell lysate exhibited an increased *P. tricornutum* growth. In contrast, *P. tricornutum* culture with *B. thruingiensis* spores grew similarly to the L1 axenic control (Figure 3.3A).

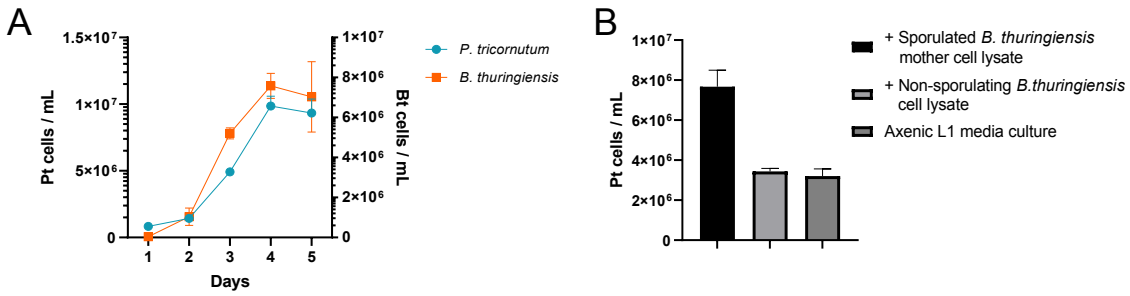

Figure 3.3 The mother-cell lysate of *Bacillus thuringiensis* contains the stimulating agent. a. *P. tricornutum* cell counts (left Y-axis) in co-cultures with *B. thuringiensis.* The number of *B. thuringiensis (Bt)* spores from the same co-culture were also counted (right Y-axis). Each culture condition has 3 replicates. Error bars are ± 1 SD. *P. tricornutum* cells were counted at day 7 after the addition of lysate. Cells counts are represented as Scientific Notation. **b.** *P. tricornutum* cell number counts in cultures containing sporulated *B. thuringiensis* cell lysate, non-sporulating *B. thuringiensis* cell lysate, and L1 medium. Each culturing condition contained 3 replicates. Error bars are ± 1 SD.

B. thuringiensis mother cell lysis during sporulation must have released a growth stimulating substance into the medium. It is however not known if sporulation merely serves to facilitate the release of the substance or also leads to the synthesis of the substance in the mother cell. To distinguish these alternative hypotheses, we mechanically lysed *B. thuringiensis* growing in nutrient-rich LB medium (without

sporulation) by sonication. The lysate was filtered and added to the *P. tricornutum* culture. The non-sporulation cell lysate had no stimulating effect (Figure 3.3B). Therefore, *B. thuringiensis* sporulation in nutrient-poor L1 medium produced and then released a growth-stimulating substance.

3.3.3 Characterization of *B. thuringiensis* mother cell lysate

What is the property of the growth-stimulating agent released by *B. thuringiensis?* The *B. thuringiensis* mother cell lysate was autoclaved and shown to lose the ability to stimulate

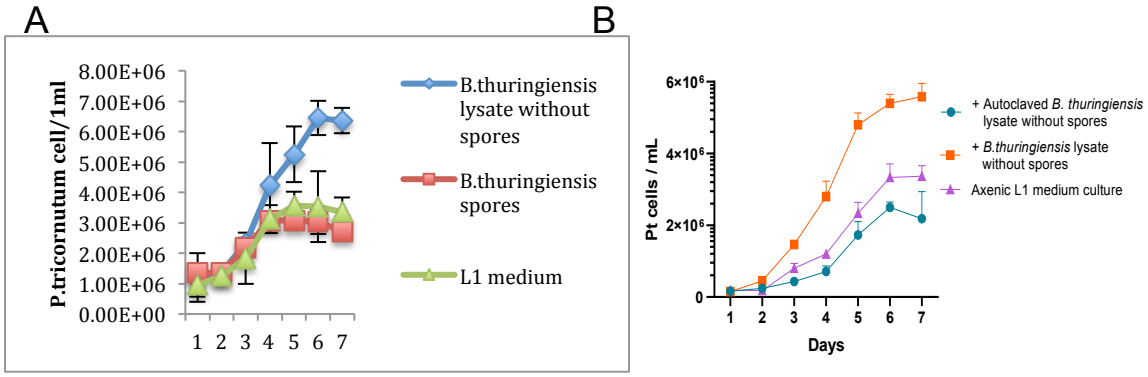

Figure 3.4 The lysate, not the spore, of *Bacillus thuringiensis* contains the stimulating agent and is heat labile. **a.** *P. tricornutum* cell counts (Y-axis) in culture with *B. thuringiensis* lysate (spores removed), the spores, and L1 medium, respectively. Each culture condition has 3 replicates. Error bars are ± 1 SD. **b.** *P. tricornutum* cell counts (Y-axis) when cultured with *B. thuringiensis* mother cell lysate, autoclaved *B. thuringiensis* mother cell lysate, or L1 medium. Mother cell lysate is made by lysis of sporulating *B. thuringiensis* cells followed by filtration that removes spores. Each culturing condition contained 3 replicates. Error bars are ± 1 SD. Cell counts (Y-axis) are represented as Scientific Notation with E = x10.

P. tricornutum growth (Figure 3.4B), suggesting that the growth-stimulating agent is heat labile. To determine if it is protein in the *B. thuringiensis* mother cell lysate with the growth stimulating activity, we treated *P. tricornutum* culture with *B. thuringiensis* lysate pretreated with Proteinase K. The *B. thuringiensis* lysate was treated with Proteinase K for 10-days, then the Proteinase K was inactivated by addition of the inhibitor glycine.

The treated lysate was then added to the *P. tricornutum* culture and shown to still maintain the growth stimulating ability (Figure 3.5). Together, our data indicate that a heat labile and proteinase K-resistant substance in the *B. thuringiensis* mother cell lysate is responsible for the growth promoting effect.

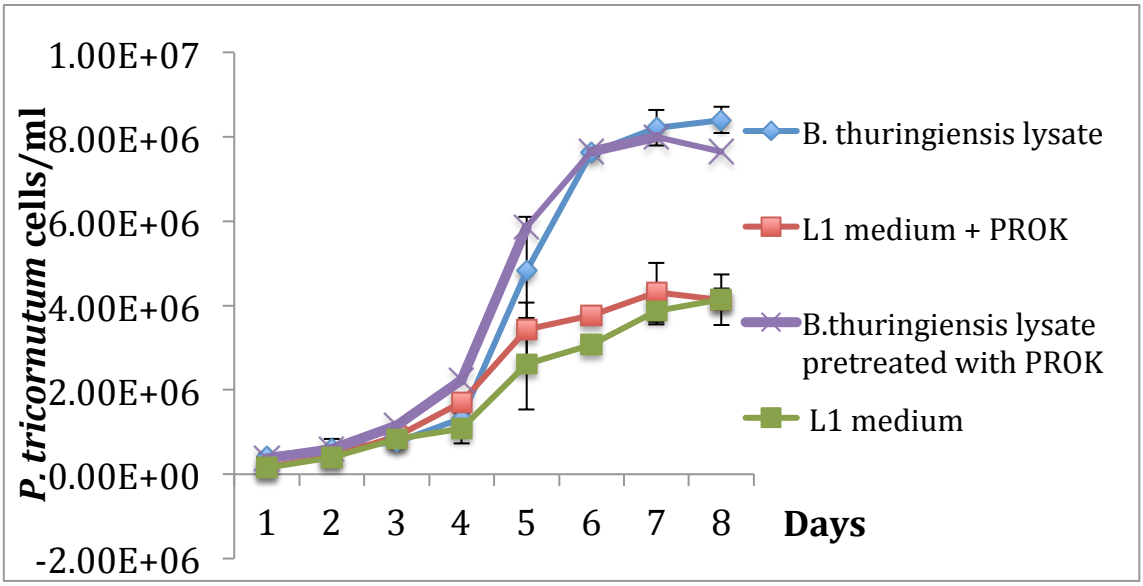

Figure 3.5 The stimulating agent is resistant to Proteinase K (PROK). *P. tricornutum* cell counts are recorded for 8 days when they are grown in L1 medium with *B. thuringiensis* lysate, L1 medium with *B. thuringiensis* lysate pretreated with PROK, and two negative controls (L1 medium and L1 medium + PROK). Each culturing condition contained 3 replicates. Error bars are ± 1 SD. Cell counts (Y-axis) are represented as Scientific Notation with E = x10.

3.3.4 The stimulated *P. tricornutum* culture shows an increased production of the beneficial fatty acids

Increasing the rate of *P. tricornutum* growth could be invaluable for the algal-based biopharma and biofuel. To assess if *P. tricornutum* still maintains the synthesis of beneficial FAs while co-cultured with *B. thuringiensis* or its cell lysate, GC-MS was used to analyze FA content of *P. tricornutum* cells. After 7 day co-culture with *B. thuriegensis*,

P. tricornutum cells were analyzed for their FA fraction. Interestingly, not only did cultures grown in the *B. thuringiensis* lysate possess a higher density than axenic culture, but also contain a higher percentage of beneficial FAs, eicosapentaenoic acid (EPA) and palmitoleic acid (Figure 3.6). Therefore, *B. thuriegensis* mother cell lysate may be applied to enhance *P. tricortunum* biomass production for biopharma and biofuel production.

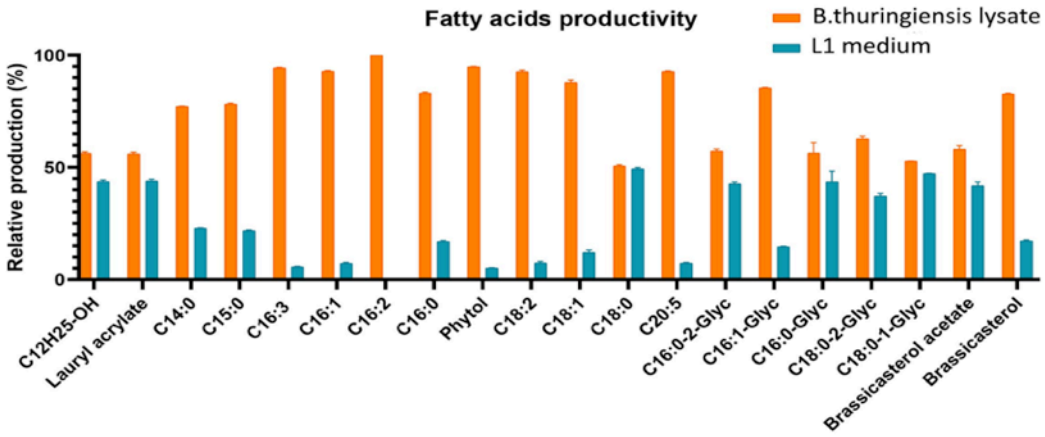

Figure 3.6: Relative productivity of fatty acids from *P. tricornutum* axenic culture and *P. tricornutum* co-cultured with *B. thuringiensis* cell lysate. Fatty acid fractions of *P. tricornutum* cultured in L1 media or in the presence of *Bacillus* lysate were assessed using GC-Mass Spectrometry. Values represent relative fatty acids production of each culture as a percentage of the intensity. *P. tricornutum* cells grown in L1 media averaged 4.35E+06 cells/mL, while cells grown in *Bacillus* lysate averaged 1.34E+07. Values were obtained from *P. tricornutum* cells after 7 days of growth.

3.3.5 Cyclic dipeptides are responsible for *P. tricornutum* growth enhancement.

We sought to determine the identity of the growth stimulating substance in the *B. thuringiensis* mother cell lysate. Bioactivity-guided fractionation was used to screen for lysate components that, when added to the *P. tricornutum* culture, resulted in growth

increases (Figure 3.7A). Twenty-five independent fractions were tested and fractions 13 and 19 were shown to have a stimulatory effect on *P. tricornutum* growth (Figure 3.6A-C). Mass Spec was used to solve the structure of fractions 13 and 19. Fractions 13 contains the Cyclic Dipeptides L-Pro-L-OMet and facture 19 contains Δ-Ala-L-Val (Figure 3.8). The generation of bioactive fractions was performed by Dr. Munhyung Bae, John Sittmann performed the screen.

3.3.6 The cyclic dipeptides (CDPs) L-Pro-L-OMet and Δ-Ala-L-Val effect *P. tricornutum* growth in a dose dependent fashion

To confirm that L-Pro-L-OMet and Δ-Ala-L-Val are the molecules with the stimulating activity, L-Pro-L-OMet was synthesized (see Methods) and Δ-Ala-L-Val was purified from a large culture (see Methods); they were respectively added to the *P. tricornutum* culture to assay for the activity. While both CDPs stimulated *P. tricornutum* at low concentrations, high concentrations of L-Pro-L-OMet (> or =10 mM) was found to inhibit *P. tricornutum* growth (Figure 3.9A).

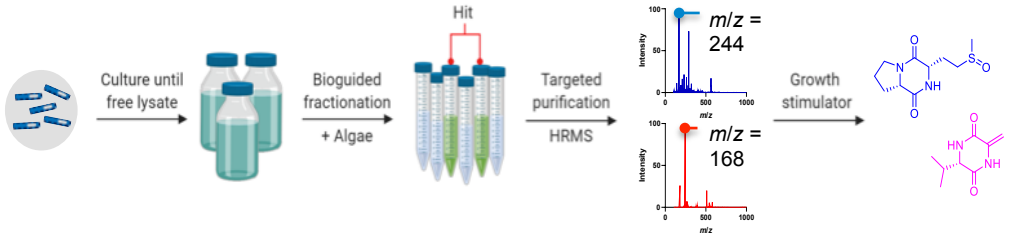

Figure 3.7: Workflow for identification of growth simulator from *B. thurengiensis*. Bacteria were cultured in L1 medium until forming free lysate. Then, supernatant of bacterial culture was subjected to SPE column. Bio-guided fractionation revealed that two fractions stimulated the growth of algae. Those fractions were characterized by their *m/z* and NMR spectroscopic data.

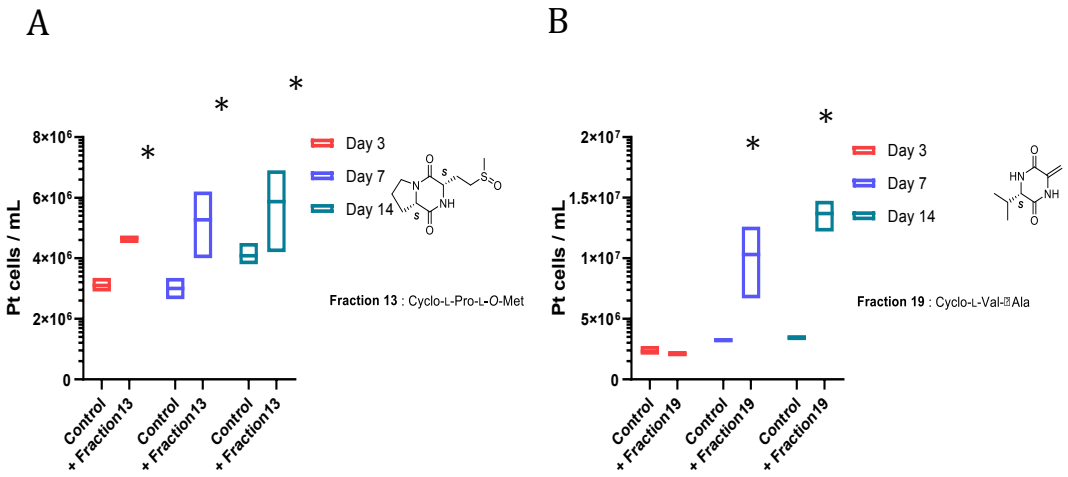

Figure 3.8: Fraction 13 and 19 significantly stimulated *P. tricornutum* growth. **a.** Fraction 13 has significant stimulating effect on *P. tricornutum* growth at day 3, 7 and 14. Fraction 13 contains 2,5-diketopiperazines Cyclo-L-Pro-L-*O*-Met. **b.** Fraction 19 shows significant stimulating effect at day 7 and 14. Fraction 19 contains Cyclo-L-ΔAla. Each culturing condition contained 3 replicates. Error bars are ± 1 SD. *P. tricornutum* cell counts (Y-axis) are represented as Scientific Notation with E = x10.

Similarly, high concentrations of Δ-Ala-L-Val at 700 uM and 350 uM failed to stimulate growth (Figure 3.7b). This observation indicates that L-Pro-L-OMet and Δ-Ala-L-Val are

likely to act as signal molecules to stimulate *P. tricornutum* growth and unlikely acting as sources of nutrient.

We also tested the minimal concentration of L-Pro-L-OMet and Δ-Ala-L-Val needed to stimulate *P. tricornutum* growth and found that L-Pro-L-OMet and Δ-Ala-L-Val lost their efficacy at a concentration of 100nM and 35nM respectively (Figure 3.9a,b).

To determine if the growth enhancement is specific to the structure of the specific CDPs. *P. tricornutum* cultures were added with 10mM, 100µM and 100nM of D-Pro+D-Met solution or 700µM, 350µM and 35nM of L-Ala+L-Val solution. *P. tricornutum* cells were counted at days 3, 6 and 9. No growth stimulation was observed with either amino acid solutions (Figure 3.10). The data suggests that L-Pro-L-OMet and Δ-Ala-L-Val may possess special bioactivities not present in mixed amino acids.

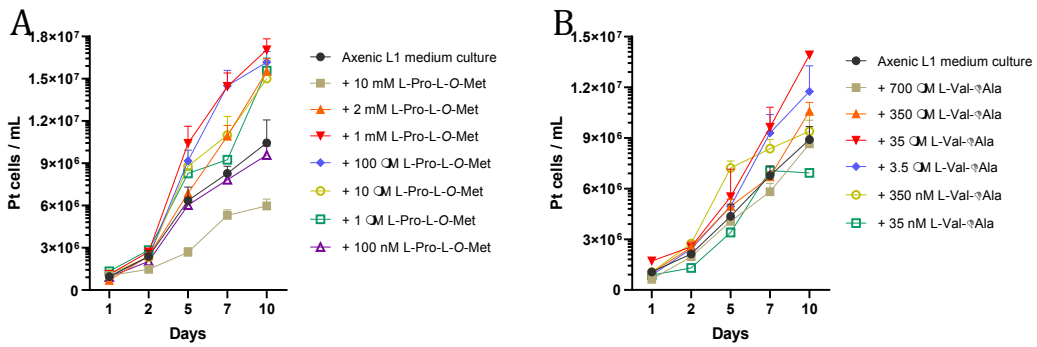

Figure 3.9: The Cyclic dipeptides (Cyclo-L-Pro-L-*O*-Met and Cyclo-L-ΔAla) stimulate *P. tricornutum* growth in a dose-dependent manner. a. *P. tricornutum* (Pt) cell counts when different concentrations of Cyclo-L-Pro-L-*O*-Met are added to the culture. (B) *P. tricornutum* cell counts when different concentrations of Cyclo-L-ΔAla are added to the culture. Each culturing condition contained 3 replicates. Error bars are ± 1 SD. Cell counts (Y-axis) are represented as Scientific Notation with E = x10.

A

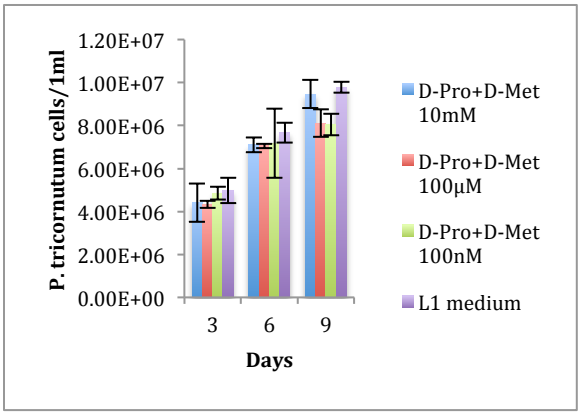

B

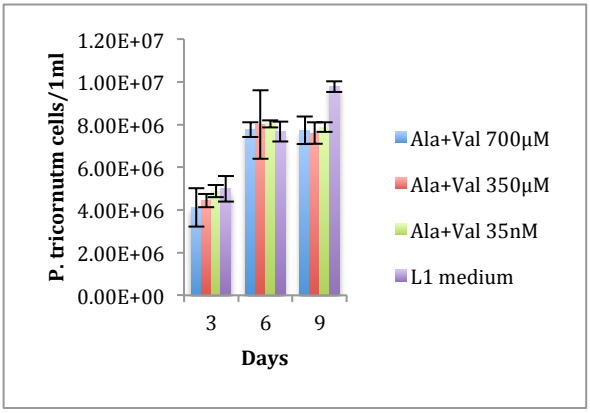

Figure 3.10: Solutions containing pairs of amino acids fail to stimulate *P. tricornutum* growth. A) D-Proline and D-Methionine were added to the *P. tricornutum* culture at 10mM, 100µM and 100nM concentrations. B) L-Alanine and L-Valine were added to the *P. tricornutum* cultures at 700µ, 350µM, and 35nM concentrations. No significant difference was observed among all conditions.

3.3.7 How does CDPs stimulate *P. tricornutum* growth?

Could CDPs help facilitate iron bioavailability? We grew *P. tricornutum* in L1 medium with no iron supplementation, with iron supplement (L1 medium + 10µM $FeCl_3$), or with *B. thuringiensis* mother cell lysate. We measured intracellular iron concentration over a 9 day period using a modified ferrozine assay (Mittra, et al. 2013). Interestingly, no significant difference was detected between the iron content of *P. tricornutum* cells grown in the presence of *B. thuringiensis* lysate and the *P. tricornutum* cells grown in L1 medium (Figure 3.12). Further, *P. tricornutum* grown in L1 medium supplemented with iron (L1 medium + 10µm $FeCl_3$) had a greater cellular concentration of iron than *P. tricornutum* cells grown in the presence of *B. thuringiensis* lysate (Figure 3.12).

Together, this suggests that the *B. thuringiensis* lysate does not appear to facilitate iron uptake.

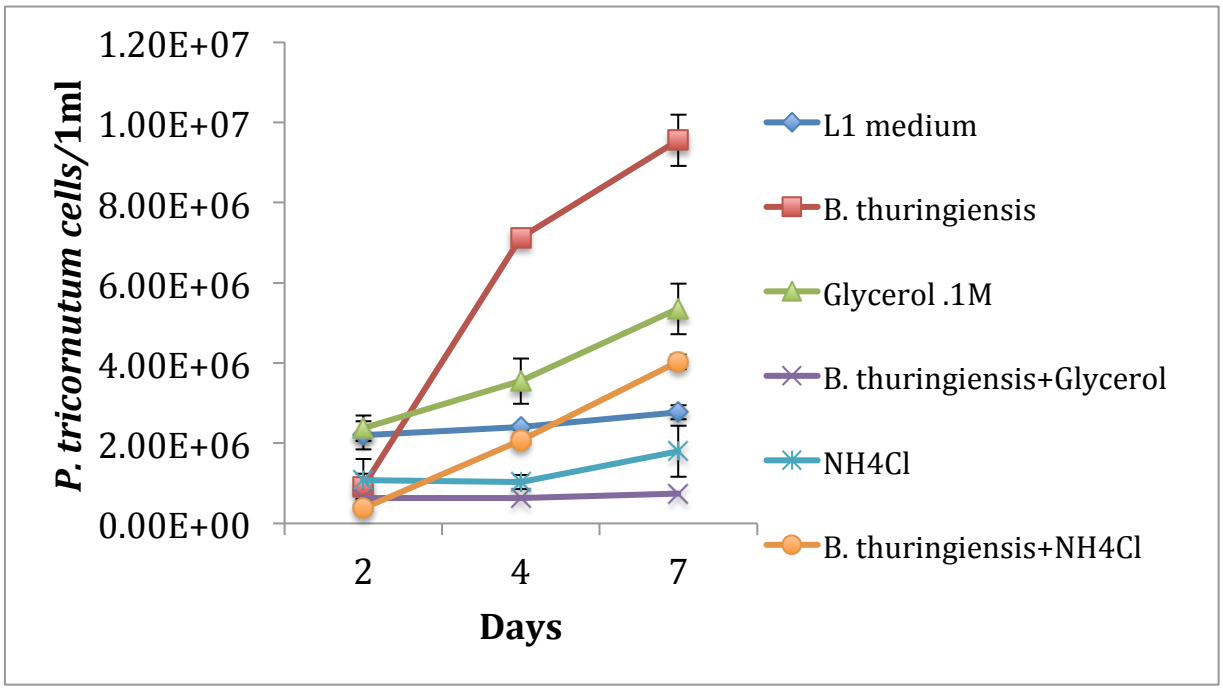

Figure 3.11: The *B. thuringiensis* produced compound may not be a source of nutrition. *P. tricornutum* cultures supplemented with carbon (glycerol) and nitrogen (NH4Cl)

3.3.8 Cyclic dipeptide's enhancement of *P. tricornutum* growth does not require cellular uptake of L-Pro-L-OMet and Δ-Ala-L-Val

Considering that CDPs may function as signaling molecules (Ortiz-Castro, et al. 2011; Gillard, et al. 2013), we sought to determine the manner in which *P. tricornutum* was interacting with L-Pro-L-OMet and Δ-Ala-L-Val. *P. tricornutum* was grown in L1 medium with 100µM L-Pro-L-OMet, 35µM Δ-Ala-L-Val or CDP-free. *P. tricornutum* cells were counted, and analyzed for CDPs on days 1, 3, 5, and 7 (Figure 3.13). *P. tricornutum* cultures were analyzed for the presence of respective CDPs in the

supernatant and cell pellet over the course of the experiment. Interestingly, while there is an increase in *P. tricornutum* cell counts in cultures containing L-Pro-L-OMet or Δ-Ala-

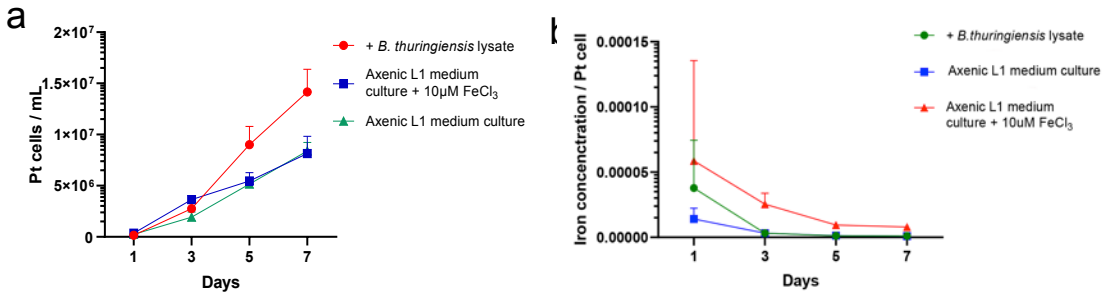

Figure 3.12. Intracellular iron content in *P. tricornutum* does not change even when grown in the presence of *B. thuringiensis* mother cell lysate. **a.** *P. tricornutum* cells grown in *B. thuringiensis*-mother cell lysate, in L1 medium, and L1 medium containing 10μM FeCl3. **b.** Ferrozine assay measuring cellular iron concentration in *P. tricornutum* cells. FeCl3 is provided as part of the L1 medium trace metal solution containing 1.17 x 10-5 M $Na_2EDTA \cdot 2H_2O$, 1.17 x 10-5 M $FeCl_3 \cdot 6H_2O$, 1.17 x 10-5 M $Na_2EDTA \cdot 2H_2O$, 9.09 x 10-7 M $MnCl_2 \cdot 4\ H_2O$, 8.00 x 10-8 M $ZnSO_4 \cdot 7H_2O$, 5.00 x 10-8 M $CoCl_2 \cdot 6H_2O$, 1.00 x 10-8 M $CuSO_4 \cdot 5H_2O$, 8.22 x 10-8 M $Na_2MoO4 \cdot 2H_2O$, 1.00 x 10-8 M H_2SeO_3, 1.00 x 10-8 M $NiSO_4 \cdot 6H_2O$, 1.00 x 10-8 M Na_3VO_4 and 1.00 x 10-8 M K_2CrO_4. Each culturing condition contained 3 replicates. Error bars are ± 1 SD. Cell counts (Y-axis) are represented as Scientific Notation with E = x10.

L-Val, CDP concentration remained unchanged in the supernatant (Figure 3.13). This result suggests that the *P. tricornutum* is unlikely absorbing CDPs into the cell. Since CDP appears to function outside the *P. tricornutum* cells, L-Pro-L-OMet and Δ-Ala-L-

Val may serve as an extracellular signaling molecule.

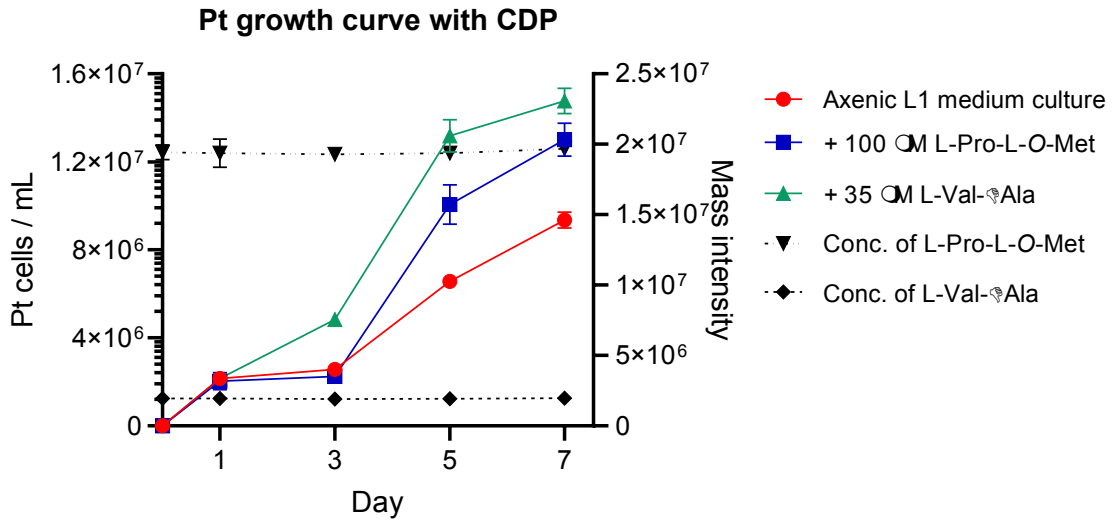

Figure 3.13: Concentrations of cyclic dipeptides in *P. tricornutum* did not change over time
While the growth rate of *P. tricornutum* was increased by cyclic dipeptides (L-proline-L-O-methionine and L-valine-Δalaine), the cyclic dipeptide level remains the same in the culture.

3.4 DISCUSSION

Due to its photosynthetic capability and high lipid content, *Phaeodactylum tricornutum* is valuable for producing biofuels and biopharma. However, the slow growth of this organism limits its potential. In this work, we showed that members of the *Bacillus cereus* group, upon sporulation, synthesize and release a heat labile but proteinase K-resistant substance capable of stimulating *P. tricornutum* growth rate and biomass accumulation without any negative impact on lipid content. Rather a measurable increase in the beneficial FAs, palmitoleic acid (C16:1) and eicosapentaenoic acid (C20:5), was observed in the stimulated culture of *P. tricornutum*. We also show that this capability is specific to the *B. cereus* group of bacteria and absent in the related *B. subtilis*.

We further showed that sporulating *B. thuringiensis* mother cell lysate is equally potent in stimulating *P. tricornutum* growth. Biofractionation of the *B. thuringiensis* mother cell lysate identifies cyclic dipeptides L-Pro-L-OMet and Δ-Ala-L-Val capable of stimulating *P. tricornutum* when added to the culture. Our work hence identified two never-before reported small CDPs synthesized in sporulating mother cells of *B. thuriegensis.* We show that these two CDPs possess signaling activities in transkingdom communications.

3.4.1 CDP biosynthesis and function

Cyclic dipeptides, also referred to as 2,5-diketopiperazines, are a biologically significant class of small molecules found in every kingdom of life (Ying, et al. 2018). To date, only two methods for CDP production have been observed in biological systems, NRPS and CDP Synthases (Gondry, et al. 2018). Non Ribosomal Peptide Synthesis (NRPS) involves a class of proteins that are capable of assembling short amino acid chains using non-proteingenic peptide intermediates (Miller and Gulick 2018). CDP Synthases, on the other hand, form CDPs by catalyzing the amino acid transfer from charged tRNA (Belin, et al. 2012).

Produced by the condensation of two α-amino acids, CDPs form a highly stable heterocyclic ring that allows for enhanced stability, protease resistance and conformational rigidity. (Giessen and Marahiel. 2015; Borthwick. 2012). Work in *Vibrio fischeri* found that the CDP L-Pro-L-Phe interfered with Aceyl Homeserine Lactone (AHL) driven Quorum Sensing (QS)(Campbell, et al. 2009). A separate study found D-Ala-L-Val and L-Pro-L-Tyr capable of activating the same AHL-QS reporter (Holden, et

al. 1999). These reports suggest that the varied structure of CDPs may allow for distinct responses in the same signaling pathway (Holden, et al. 1999). Further, a series of proline-derived CDPs produced by *Pseudomonas aeruginosa* were capable of interacting with the auxin signaling pathway in *Arabidopsis thaliana* (Ortiz-castro, et al. 2011). Due to their near ubiquity in wide range of organisms and diversity of function, CDPs may play a unique role in transkingdom signaling (Ortiz-Castro, et al. 2011).

3.4.2 Possible functions of bacterial synthesized CDPs in nature

Although *B. cereus* clade of organisms are mostly known for their impact on agriculture and human health, prior work detailing *B. cereus*-algal interactions suggests they have significant roles in the freshwater and marine environment (Liu, et al. 2017; Kataev, et al. 2012; Zhu, et al. 2016). When cultured with the freshwater alga *Chara coralline, B. cereus* secretes the pore-forming protein HLYII potentially acting to parasitize the alga (Kataev, et al. 2012). Similarly, the genome of *B. weihainsis,* another *B. cereus* microbe, contains the enzymatic pathways necessary to degrade the alga-specific polysaccharrides alginate and laminarin (Zhu, et al. 2017). In both instances, the *B. cereus* microbe is effectively farming algae for nutrients. The question remains why would *B. thuringiensis*-derived CDPs stimulate *P. tricornutum* growth?

Coexisting in the same ecological niche, bacteria may depend on algal metabolome to procure necessary nutrients, typically dissolved organic carbon (DOC) (Amin, et al. 2012, Amin, et al. 2015; Croft, et al. 2005). By releasing CDPs into the environment, bacterium may increase alga growth as a way to increase DOC production (Amin, et al.

2012). Interestingly, the spore coat of *B. cereus* is highly silicified, a characteristic shared with *P. tricornutum* cell wall (Motomura, et al. 2016; Bowler, et al. 2008). *B. cereus* uses CotB1, a spore-coat protein, to drive the biosilicification of the spore. However, it has significant homology to the diatom sliaffins, a class of proteins used in the biosilicification of diatom cell walls, suggesting similar mechanisms of silica assembly (Motomura, et a. 2016). Perhaps driving *P. tricornutum* cell division makes available more carbon and silica exudates for *B ceres* group to use. Although the current study of *B. thuriegensis* and *P. tricornutum* interaction occurs in a non-natural setting, it may mimic marine environment when CDPs were released from marine microbes related to *B. cereus*.

3.4.3 Mechanism of *B. cereus*-produced CDPs in facilitating *P. tricornutum* growth

A key unanswered question is how and why the CDPs drive *P. tricornutum* cell division. One possibility is that the bacterial CDPs may mimic in structure to molecules produced by *P. tricornutum*. For example, it may resemble and hence interfere with compounds produced by *P. tricornutum* to determine its own cell density, a process typically governed by Quorum Sensing (Miller and Bassler. 2001). In trypanosomes, the loss of the ability to sense signal molecules results in uncontrolled proliferation (Mony and Matthews. 2015). Further, CDPs have been already shown to interfere with the *Vibrio fischeri* QS pathway (Holden, et al. 1999; Campbell, et al. 2009). In a natural setting, driving *P. tricornutum* to over-proliferate could be a bacterial strategy to cause algae to grow beyond their nutritional limits, resulting in early death (Segev, et al 2016). Then marine *B. cereus* microbes could consume exudate from the dead algae (Segev, et al.

2016; Zhu, et al. 2017). However, it is currently unknown if *P. tricornutum* possesses any defined QS pathways to regulate its own cell density. Further we did not observe any *P. tricornutum* cell death during the time frame of our experiments.

Previous works have described CDPs as a potential signaling compound in the marine environment (Zhu, et al. 2017). Here we describe some of the first evidence implicating CDP signaling between bacterium and diatom. Although the exact mechanism of action remains unknown, our data suggest that L-Pro-L-OMet and ΔAla-L-Val are unlikely serving merely as nutrients for the diatom. To consider the role nutrition might play in *P. tricrontum* growth enhancement, we supplemented the *P. tricornutum* culture with a source of carbon (glycerol), nitrogen (NH_4Cl) and iron ($FeCl_3$), resources often thought to be limiting in the marine environment (Boyd, et al. 2010; Minhas, et al. 2016). In all nutrient supplement experiments, we failed to see any significant increases in *P. tricornutum* proliferation (Figure 3.11), suggesting that the carbon, nitrogen or iron are unlikely limiting *P. tricornutum* growth in our experimental condition. We also did not observe an increase in iron acquisition in *P. tricornutum* culture supplemented with the *B. cereus* lysate. HPLC MS failed to detect any change in CDP concentration in the supernatant of *P. tricorntum* culture, suggesting that CDP may not be taken into the *P. tricornutum* cells. These data suggest CDPs likely act in extracellular space to send signals to or interfere with natural signals sensed by *P. tricornutum*.

In accordance with earlier works detailing alga-bacteria interactions (Segev, et al. 2016; Amin, et al. 2015), we saw a dose dependent effect on *P. tricornutum* growth when CDPs

was applied. At a low concentration of 35nM for ΔAla-L-Val or 100nM for L-Pro-L-OMet, there is hardly any growth stimulating effect on *P. tricornutum*. The loss of stimulatory ability at the lower concentrations may be a result of the CDPs being below the critical threshold (Winzer et al. 2002). In cell to cell signaling, critical threshold is defined as the concentration a signaling molecule must be at to be effective (Winzer, et al. 2002). At concentrations of 35nM ΔAla-L-Val and 100nM L-Pro-L-OMet, these CDPs may be below the effective threshold. Optimal concentration of CDPs was shown at between 3.5μM-350μM for ΔAla-L-Val and between 1μM-2mM for L-Pro-L-OMet (Figure 7). Interestingly, inhibition of growth was observed if much higher concentration was applied such as 700 μM for ΔAla-L-Val and 10mM for L-Pro-L-OMet (Figure 3.9). Inhibition of growth is not uncommon when signaling compounds are applied at too high a concentration. Segev, et al found that the phytohormone auxin (as IAA) stimulated the growth of the alga *E. huxleyi* from 1uM to 100uM; however, at 1mM they noticed an inhibition of alga growth (Segev, et al. 2016). The decrease in growth observed at high concentrations may be a result of receptor desensitization, which occurs when a receptor is continuously exposed to its ligand at a high concentration (Woolf, et al. 2003).

In summary, we discovered organic molecules involved in mediating bacterium-diatom communication. It highlights CDPs as a highly interesting, important, and possibly a new class of language communicated between transkingdom species. With the diversity of all possible dipeptide combinations and their specific structural features, it is not hard to image the tremendous richness and pool of languages shared between specific transkingdom species that may dictate cellular behaviors ranging from cell proliferation,

QS, sexual mating, and others. From a practical viewpoint, the discovery of these CDPs may greatly facilitate culturing and biomass production of diatom and paving the way for alga-biofuel production and biopharma.

3.4.4 Future work in studying the effect of CDPs on *P.tricornutum*

Here we present novel work showing that *B. thuringiensis*-produced cyclic dipeptides stimulate *P. tricornutum* growth. Although, previous works have described CDP-based signaling, the molecular mechanisms governing how these signals are interpreted in the recipient remains unknown (Ortiz-Castro, et al. 2011; Zhu, et al. 2017). Next steps could be aimed at understanding how *P. tricornutum* recognizes and responds to the CDPs. RNA-seq comparing CDP+ and CDP- *P. tricornutum* cultures could be used to investigate what types of pathways are induced in *P. tricornutum* by the CDP. Candidate genes with roles in interpreting the CDP signal in *P. tricornutum* could be knocked out by CRISPR to determine if the stimulating effect is affected. Mutagenesis screen for *P. tricornutum* could be conducted to identify CDP-insensitive mutants. Further, analysis of the *P. tricornutum* produced FAs and methods of scaling up the stimulated *P. tricornutum* culture could determine if CDPs can serve as a new technique in increasing diatom-based biomass.

Appendix

4.1 investigating the carbon concentration mechanism in *P. tricornutum*

Diatoms are photosynthetic group of algae with critical ecological and global implications. Existing as a unicellular organism; diatoms are unique amongst other marine algae due to their silicified cell wall, known as a frustule. In addition to their unique cell biology, some diatoms are capable of a variety of metabolic pathways. Diatoms like *Phaeodactylum tricornutum,* are thought to implore a putative carbon concentrating mechanism (CCM) to fix their carbon (Zheng. 2013). The existence of a biochemical or biophysical CCM could explain how diatoms fix about 20-40% of yearly global carbon (Hopkinson, et al 2011; Zheng 2013). In collaboration with Dr. Ganesh Sriram's lab, we have investigated the carbon concentration mechanism (CCM) of *P. tricornutum*. The suspected C4 CCM in *P. tricornutum*, if proven, would provide important insights into C4 photosynthesis in diatom.

To investigate the putative C4 CCM the Sriram lab performed Isotopic Labeling Experiments (ILE) to track the metabolic flux of radiolabelled carbon (Zheng Thesis pg77. 2013). Based on their ILEs the Sriram lab identified the genes PEPC2 and PYC1, PYC2 as potentially involved in the putative *P. tricornutum* C4 CCM. While a technician in the Liu lab, my role was to develop a successful transformation protocol for *Pt* and then knockdown genes in the putative C4 pathway. The resulting *Pt* mutants were then transferred to Dr. Sriram's lab, where carbon trafficking routes were determined and compared with wild type *Pt*. I was able to establish *Pt* transformation protocol and successfully knocked down three genes by

antisense approaches. These three genes, PEPC2 PYC1, and PYC2 were suspected to function in the C4 pathway. PEPC2 was singly silenced while *PYC1* and *PYC2* were simultaneously silenced (Zheng, Thesis. 2013).

Two antisense lines targeting *PEPC2* and two antisense lines targeting *PYC1/*2 were generated. qRT-PCR showed a reduction of RNA to different levels in the silenced lines. Transgenic lines were then given to the Sriram lab and Metabolic Flux Analysis (MFA) was performed on these silenced lines to evaluate if C4 pathway is stopped or altered. Interestingly, MFA results revealed a reduction in C4 metabolites in the *PYC1-PYC2* doubly silenced lines (Quinn, Sittmann, Liu and Sriram, manuscript in preparation), suggesting that PYC1 and PYC2 may reside in a critical step of the C4 pathway in *P. tricorntum.* This work, although not directly related to my PhD thesis work, has given me training in working with *Pt* and lay the ground work for my PhD thesis.

4.2 Methods

4.2.1 Construction of *pPha-T1_antiPEPC2* plasmid

To silence the gene *Phosphoenol Pyruvate Carboxylase 2 (PEPC2)* (JGI Pid 51136), a 310 bp fragment of *PEPC2* exon 1 was PCR amplified from genomic DNA of *Phaeodactylum tricornutum* (Pt) (Strain CCMP632). The PCR primers have the HindIII and EcoRI enzyme recognition sites engineered respectively into the forward and reverse primers (Table 4.1). The 310 bp amplicon was cloned into the pCR8/GW/TOPO vector (Invitrogen, Carlsbad, CA). The *PEPC2* fragment in the newly assembled pTOPO-

PEPC2 vector was verified by sequencing and then excised with the restriction enzymes HindIII and EcoRI. The resulting *PEPC2* fragment was inserted into pPha-T1 vector (Genbank AF219942; Zaslavskaia 2001) at the same restriction enzyme sites so that the *PEPC2* fragment is in antisense orientation with respect to the fcpa promoter in the vector.

4.2.2 Construction of *pPha-T1_ eGFP* vector

eGFP was PCR amplified from the vector pk7GWIID as a template, using the forward and reverse primers Pk7GW2D_*eGFP* (Table 4.1). This fragment was cloned into pCR8/GW/TOPO and verified by sequencing. The resulting pTOPO-eGFP plasmid was cut with EcoR1. The excised eGFP fragment was inserted into the EcoR1 site of the pPha-T1 vector in sense orientation.

4.2.3 Construction of *pPha-T1_antiPYC1-PYC2* plasmid

To construct a plasmid that silences both *PYC1* and *PCY2,* a PCR fragment of *PYC1* was joined together with a PCR fragment of *PYC2* by Gibson Assembly (Gibson et al 2009). The *PYC1* fragment was amplified off exon1 of *PYC1* (JGI DOE PID 30519) and the *PYC2* fragment was amplified off exon 1 of *PYC2* (JGI DOE PID 49339) (see Table 4.2.6 for primer sequence). The pCR8/GW/TOPO vector was PCR amplified using primers *TOPO_F* and *TOPO_R*. All amplified fragments were assembled according to the NEB's protocol at (https://www.neb.com/protocols/2012/12/11/gibson-assembly-protocol-e5510). This newly formed *pTOPO_PYC1-PYC2* plasmid was verified by sequencing.

Next, the *PYC1-PYC2* fragment was PCR amplified from the *pTOPO_PYC1-PYC2* plasmid using forward and reverse primers *PYC1/2* (Table 4.1). In addition, the pPha-T1

vector was PCR amplified using *pPha-T1* primers (Table 4.1). Subsequently, the PYC1-PYC2 and pPha-T1 PCR fragments were assembled together based on the Gibson assembly protocol described above. The final vector was name *pPha-T1_antiPYC1-PYC2* with *PYC1* and *PYC2* both in the antisense orientation with respect to the fcpa promoter.

4.2.4 Transformation of *Phaeodactylum tricornutum*

Transformation was performed according to the procedure detailed in Zhang et al. (2014). Could you comment on the light condition of growth? I remember that when you just follow the published procedure, it did not work.

4.2.5 Quantitative RT-PCR

RNA was extracted from *P. tricornutum* using the RNEASY Plant Mini Kit (Qiagen, Hilden Germany). *P. tricornutum* cultures were grown to a density of 4-5 x 10^6 cells/ml and a total of 40 ml was collected and placed in a 50ml Falcon tube. Cultures were then spun down at 1500g, for 15 minutes at 4^{o}C. The pellet of *P. tricornutum* cells was re-suspended in 450 ul of Buffer RLT. The suspended cells were carefully transferred to a 1.7ml tube. Each sample was sonicated for 10 x 1 sec pulses at setting 12 using the Microson Ultrasonic Cell Disruptor (Bostonind Walpole, MA). RNA purification of the resulting lysate was carried out according to the methods outlined in the RNeasy Mini Handbook section "Purification of Total RNA from Plant Cells and Tissues and Filamentous Fungi".

Next, cDNA was synthesized using 100ng-1ug of total RNA from each of the above extractions using the *iScript cDNA Synthesis* kit (Bio-Rad, Hercules, Ca). Subsequently

qPCR was performed using the SSO-Fast Evagreen Supermix. The *ACT1* gene (JGI DOE PID 51157) served as the control. qRT-PCR primers for ACT1, *PEPC1* (JGI Pid 27976), PEPC2, *PYC1*, and the *PYC2* are listed in Table 4.1.

cDNA was diluted 10 times in H_2O, and 1ul of the dilution was used per qPCR reaction. Reactions were run on a Bio Rad CFX96 Real-Time C1000 thermalcycler. Data was analyzed using the CFX Manager software. The results were averaged from two biological replicates, each with three technical replicates. Standard deviation was calculated according to the method described at (http://www3.appliedbiosystems.com/cms/groups/mcb_support/documents/generaldocuments/cms_042380.pdf)

4.2.6 Primer table C4 CCM Project

Column1	Column2	Column3
Primer	sequence 5'-3'	Purpose
PEPC2Anti-F	GAGCTCTTTGCCCAGCTGCAGAAG	Cloning PEPC2 antisense fragment
PECP2Anti-R	GAGCTCACCGACTCCAATATTGCG	Cloning PEPC2 antisense fragment
PYC1_F_Gib_OVP	GTCTGCCGTTTCGAGAGCCTGGACCAAATCGATTC	Cloning PYC1/2 antisense fragment
PYC1_F_Topo_FW	ATGTATCGAACTCGGGTTC	Cloning PYC1/2 antisense fragment
PYC1_R_OVP_PYC2	gtccgatccgGTGCAATATCCTGGCATTG	Cloning PYC1/2 antisense fragment
PYC2_F_OVP_PYC1	gatattgcacCGGATCGGACGGTGCTTTG	Cloning PYC1/2 antisense fragment
PYC2_R	GCCTGGACCAAATCGATTCC	Cloning PYC1/2 antisense fragment
PYC2_R_Gib_OVP	TAGTCGATGATATCGAATATGTATCGAACTCGGGTTC	Cloning PYC1/2 antisense fragment
pPhaT1-F	ATTCGATATCATCGACTAATTCGAG	Cloning PYC1/2 antisense fragment

pPha-T1-R	TCTCGAAAGGCAGACAAATTTG	Cloning PYC1/2 antisense fragment
qRT PEPC2_F	GATCGAGATGGTAACCCCAACGTG	qPCR PEPC2
qRT PEPC2_R	CATCTGCCAAGGCATCCATGGCG	qPCR PEPC2
qRT PYC1_F	CCGCTGGCCATTTATTCTTACG	qPCR PYC1
qRT PYC1_2	TGGACCTTGTTCTTGACGC	qPCR PYC1
qRT PYC2_F	AAGTCACCCTTCGTCCAAG	qPCR PYC2
qRT PYC2_R	TCCAATACCTCATTCGCTTCC	qPCR PYC2
Actin_F	GAGGCAAAGCGTGGTGTTCTTAG	qPCR Actin
Actin_R	GTTGGGGAGCCTCAGTCAATAG	qPCR Actin

4.3 Results

4.3.1 qRT data shows a reduction in PEPC2 transcript abundance

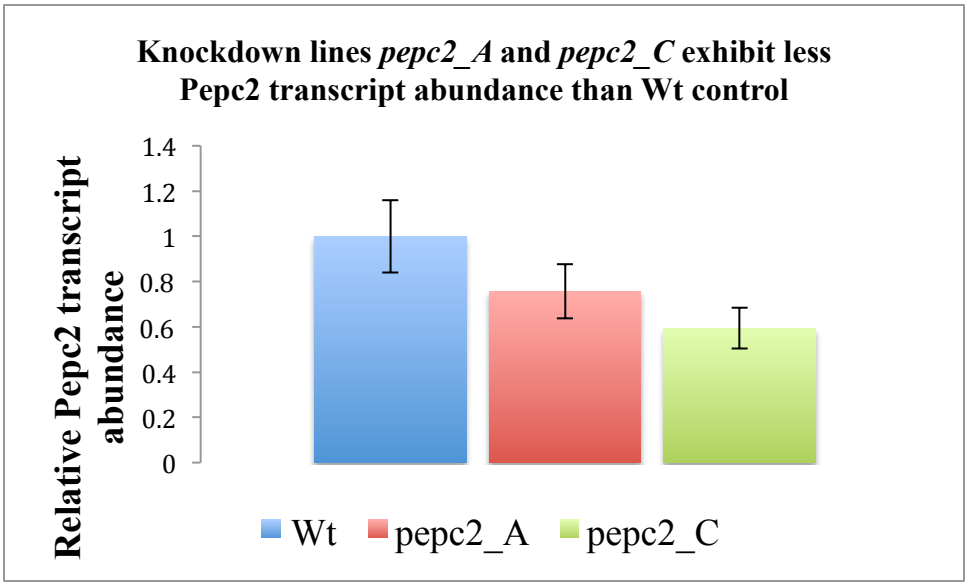

4.3.1 qRT PCR data analyzing relative *PEPC2* transcript abundance in Wt and two *pepc2* knockdown lines: Y-axis indicates the relative transcript level. ACTIN gene (JGI PID 51157) served as the control gene. Data is derived from two biological replicates, each consisting three technical replicates.

4.3.2 qRT data shows a reduction in *PYC1* and *PYC2* transcript abundance

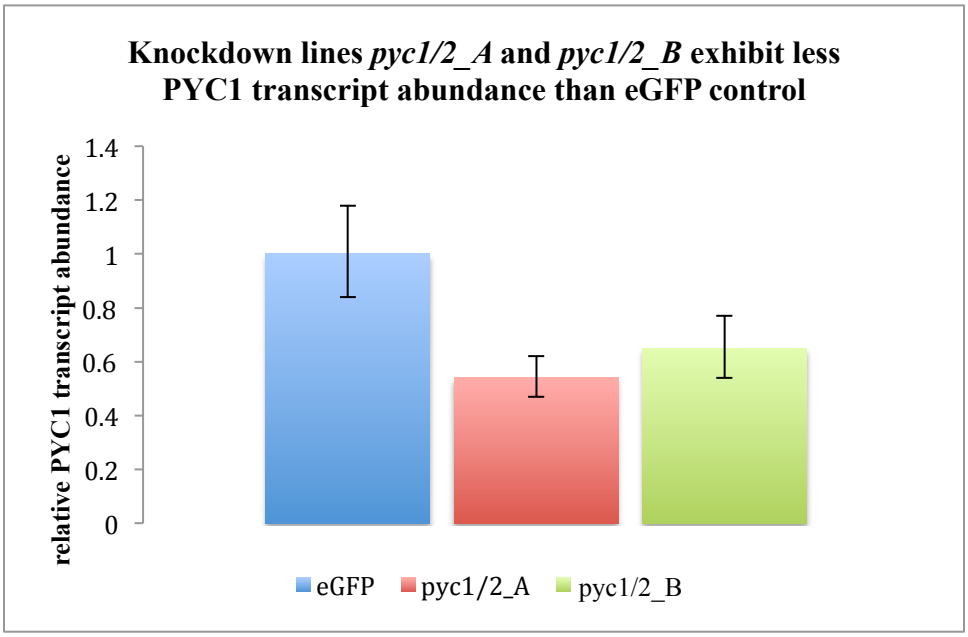

4.3.2 qRT PCR data analyzing relative *PYC1* transcript abundance in eGFP and two *pyc1/2* knockdown lines: Y-axis indicates the relative transcript level. ACTIN gene (JGI PID 51157) served as the control gene. Data is derived from two biological replicates, each consisting three technical replicates.

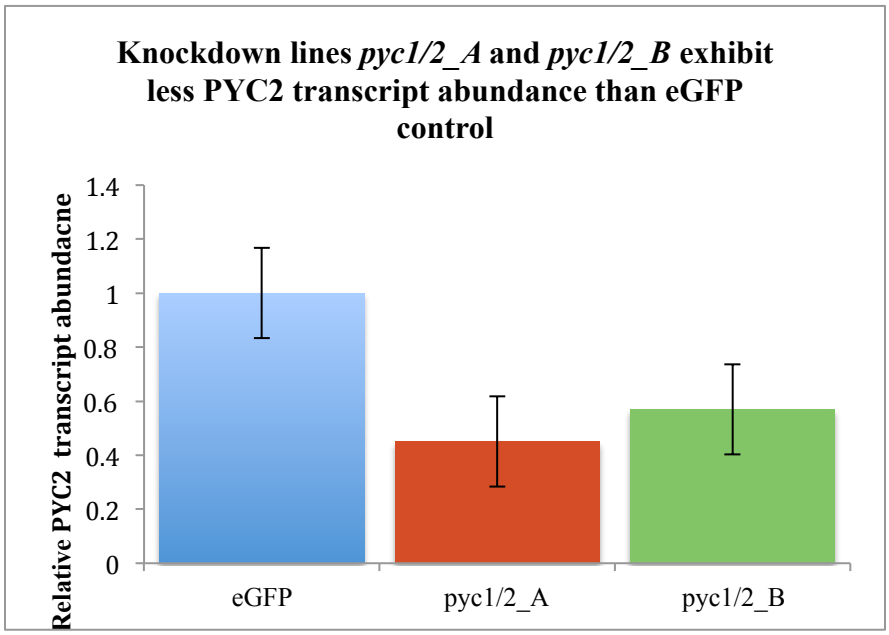

4.3.2 qRT PCR data analyzing relative *PYC2* transcript abundance in eGFP and two *pyc1/2* knockdown lines. Y-axis indicates the relative transcript level. ACTIN gene (JGI PID 51157) served as the control gene. Data is derived from two biological replicates, each consisting three technical replicates.

References

Abisado, R.G., Benomar, S., Klaus, J.R., Dandekar, A.A., and Chandler, J.R. (2018). Bacterial Quorum Sensing and Microbial Community Interactions. MBio *9*, e02331-17.

Abu-Omar, M.M., Loaiza, A., and Hontzeas, N. (2005). Reaction mechanisms of mononuclear non-heme iron oxygenases. Chem. Rev. *105*, 2227–2252.

Al-Sady, B., Ni, W., Kircher, S., Schäfer, E., and Quail, P.H. (2006). Photoactivated phytochrome induces rapid PIF3 phosphorylation prior to proteasome-mediated degradation. Mol. Cell *23*, 439–446.

Allen, A.E., LaRoche, J., Maheswari, U., Lommer, M., Schauer, N., Lopez, P.J., Finazzi, G., Fernie, A.R., and Bowler, C. (2008). Whole-cell response of the pennate diatom Phaeodactylum tricornutum to iron starvation. PNAS *105*, 10438–10443.

Àlvarez-Fernàndez, A., Abadía, J., and Abadía, A. (2006). Iron Deficiency, Fruit Yield and Fruit Quality. In Iron Nutrition in Plants and Rhizospheric Microorganisms, L.L. Barton, and J. Abadia, eds. (Springer Netherlands), pp. 85–101.

Amin, S.A., Hmelo, L.R., van Tol, H.M., Durham, B.P., Carlson, L.T., Heal, K.R., Morales, R.L., Berthiaume, C.T., Parker, M.S., Djunaedi, B., et al. (2015). Interaction and signalling between a cosmopolitan phytoplankton and associated bacteria. Nature *522*, 98–101.

Amin, S.A., Parker, M.S., and Armbrust, E.V. (2012). Interactions between Diatoms and Bacteria. Microbiol. Mol. Biol. Rev. *76*, 667–684.

Armbrust, E.V. (2009). The life of diatoms in the world's oceans. Nature *459*, 185–192.

Bai, M.-Y., Shang, J.-X., Oh, E., Fan, M., Bai, Y., Zentella, R., Sun, T., and Wang, Z.-Y. (2012). Brassinosteroid, gibberellin, and phytochrome impinge on a common transcription module in Arabidopsis. Nat Cell Biol *14*, 810–817.

Ball, A.S., Chaparian, R.R., and Kessel, J.C. van (2017). Quorum Sensing Gene Regulation by LuxR/HapR Master Regulators in Vibrios. Journal of Bacteriology *199*, e00105-17.

Barrett, S.C.H. (2015). Influences of clonality on plant sexual reproduction. PNAS *112*, 8859–8866.

Beacham, T.A., Macia, V.M., Rooks, P., White, D.A., and Ali, S.T. (2015). Altered lipid accumulation in Nannochloropsis salina CCAP849/3 following EMS and UV induced mutagenesis. Biotechnology Reports *7*, 87–94.

Beard JB, Green RL. The role of turfgrasses in environmental protection and their benefits to humans. J Environ Qual 1994; 23: 452–460.

Belin, P., Moutiez, M., Lautru, S., Seguin, J., Pernodet, J.-L., and Gondry, M. (2012). The nonribosomal synthesis of diketopiperazines in tRNA-dependent cyclodipeptide synthase pathways. Nat. Prod. Rep. *29*, 961–979.

Bellezza, I., Peirce, M.J., and Minelli, A. (2014). Cyclic dipeptides: from bugs to brain. Trends in Molecular Medicine *20*, 551–558.

Bernstein, A.M., Roizen, M.F., and Martinez, L. (2014). Purified palmitoleic acid for the reduction of high-sensitivity C-reactive protein and serum lipids: A double-blinded, randomized, placebo controlled study. Journal of Clinical Lipidology *8*, 612–617.

Borthwick, A.D. (2012). 2,5-Diketopiperazines: Synthesis, Reactions, Medicinal Chemistry, and Bioactive Natural Products. Chem. Rev. *112*, 3641–3716.

Boyer, R.F., Grabill, T.W., and Petrovich, R.M. (1988). Reductive release of ferritin iron: A kinetic assay. Analytical Biochemistry *174*, 17–22.

Bradford, E., Hancock, J.F., and Warner, R.M. (2010). Interactions of Temperature and Photoperiod Determine Expression of Repeat Flowering in Strawberry. Journal of the American Society for Horticultural Science *135*, 102–107.

Brumbarova, T., and Ivanov, R. (2014). Perls Staining for Histochemical Detection of Iron in Plant Samples. BIO-PROTOCOL *4*.

Burgess, P., and Huang, B. (2014). Growth and physiological responses of creeping bentgrass (Agrostis stolonifera) to elevated carbon dioxide concentrations. Hortic Res *1*, 14021.

Campbell, J., Lin, Q., Geske, G.D., and Blackwell, H.E. (2009). New and unexpected insights into the modulation of LuxR-type quorum sensing by cyclic dipeptides. ACS Chem. Biol. *4*, 1051–1059.

Cao, D., Cheng, H., Wu, W., Soo, H.M., and Peng, J. (2006). Gibberellin Mobilizes Distinct DELLA-Dependent Transcriptomes to Regulate Seed Germination and Floral Development in Arabidopsis. Plant Physiol *142*, 509–525.

Caruana, J.C., Sittmann, J.W., Wang, W., and Liu, Z. (2018). Suppressor of Runnerless Encodes a DELLA Protein that Controls Runner Formation for Asexual Reproduction in Strawberry. Molecular Plant *11*, 230–233.

Castillon, A., Shen, H., and Huq, E. (2007). Phytochrome Interacting Factors: central players in phytochrome-mediated light signaling networks. Trends Plant Sci. *12*, 514–521.

Chepurnov, V.A., Mann, D.G., Sabbe, K., and Vyverman, W. (2004). Experimental Studies on Sexual Reproduction in Diatoms. In International Review of Cytology, (Academic Press), pp. 91–154.

Conte, S.S., and Walker, E.L. (2011). Transporters Contributing to Iron Trafficking in Plants. Molecular Plant *4*, 464–476.

Croft, M.T., Lawrence, A.D., Raux-Deery, E., Warren, M.J., and Smith, A.G. (2005). Algae acquire vitamin B12 through a symbiotic relationship with bacteria. Nature *438*, 90–93.

Csukasi, F., Osorio, S., Gutierrez, J.R., Kitamura, J., Giavalisco, P., Nakajima, M., Fernie, A.R., Rathjen, J.P., Botella, M.A., Valpuesta, V., et al. (2011). Gibberellin biosynthesis and signalling during development of the strawberry receptacle. New Phytologist *191*, 376–390.

Davière, J.-M., and Achard, P. (2013). Gibberellin signaling in plants. Development *140*, 1147–1151.

de Lucas, M., Davière, J.-M., Rodríguez-Falcón, M., Pontin, M., Iglesias-Pedraz, J.M., Lorrain, S., Fankhauser, C., Blázquez, M.A., Titarenko, E., and Prat, S. (2008). A molecular framework for light and gibberellin control of cell elongation. Nature *451*, 480–484.

Dean, K.M., Qin, Y., and Palmer, A.E. (2012). Visualizing metal ions in cells: An overview of analytical techniques, approaches, and probes. Biochimica et Biophysica Acta (BBA) - Molecular Cell Research *1823*, 1406–1415.

Degrassi, G., Aguilar, C., Bosco, M., Zahariev, S., Pongor, S., and Venturi, V. (2002). Plant Growth-Promoting Pseudomonas putida WCS358 Produces and Secretes Four Cyclic Dipeptides: Cross-Talk with Quorum Sensing Bacterial Sensors. Curr Microbiol *45*, 250–254.

Depuydt, S., and Hardtke, C.S. (2011). Hormone signalling crosstalk in plant growth regulation. Curr. Biol. *21*, R365-373.

Dill, A., Thomas, S.G., Hu, J., Steber, C.M., and Sun, T.-P. (2004). The Arabidopsis F-box protein SLEEPY1 targets gibberellin signaling repressors for gibberellin-induced degradation. Plant Cell *16*, 1392–1405.

Eckardt, N.A. (2006). Three Arabidopsis GID1 Genes Encode Gibberellin Receptors with Overlapping Functions. Plant Cell *18*, 3353.

Faigón-Soverna, A., Harmon, F.G., Storani, L., Karayekov, E., Staneloni, R.J., Gassmann, W., Más, P., Casal, J.J., Kay, S.A., and Yanovsky, M.J. (2006). A Constitutive Shade-Avoidance Mutant Implicates TIR-NBS-LRR Proteins in Arabidopsis Photomorphogenic Development. The Plant Cell *18*, 2919–2928.

Farrow, S.C., and Facchini, P.J. (2014). Functional diversity of 2-oxoglutarate/Fe(II)-dependent dioxygenases in plant metabolism. Front Plant Sci *5*.

Feng, S., Martinez, C., Gusmaroli, G., Wang, Y., Zhou, J., Wang, F., Chen, L., Yu, L., Iglesias-Pedraz, J.M., Kircher, S., et al. (2008). Coordinated regulation of Arabidopsis thaliana development by light and gibberellins. Nature *451*, 475–479.

Franklin, K.A., and Quail, P.H. (2010). Phytochrome functions in Arabidopsis development. J. Exp. Bot. *61*, 11–24.

Freedman, N.J., and Lefkowitz, R.J. (1996). Desensitization of G protein-coupled receptors. Recent Prog. Horm. Res. *51*, 319–351; discussion 352-353.

Fuentes, S., Ljung, K., Sorefan, K., Alvey, E., Harberd, N.P., and Østergaard, L. (2012). Fruit Growth in Arabidopsis Occurs via DELLA-Dependent and DELLA-Independent Gibberellin Responses[W][OA]. Plant Cell *24*, 3982–3996.

Fukazawa, J., Ito, T., Kamiya, Y., Yamaguchi, S., and Takahashi, Y. (2015). Binding of GID1 to DELLAs promotes dissociation of GAF1 from DELLA in GA dependent manner. Plant Signal Behav *10*.

Fukazawa, J., Teramura, H., Murakoshi, S., Nasuno, K., Nishida, N., Ito, T., Yoshida, M., Kamiya, Y., Yamaguchi, S., and Takahashi, Y. (2014). DELLAs Function as Coactivators of GAI-ASSOCIATED FACTOR1 in Regulation of Gibberellin Homeostasis and Signaling in Arabidopsis. The Plant Cell *26*, 2920–2938.

Fukazawa, J., Teramura, H., Murakoshi, S., Nasuno, K., Nishida, N., Ito, T., Yoshida, M., Kamiya, Y., Yamaguchi, S., and Takahashi, Y. (2014). DELLAs Function as Coactivators of GAI-ASSOCIATED FACTOR1 in Regulation of Gibberellin Homeostasis and Signaling in Arabidopsis. The Plant Cell *26*, 2920–2938.

Gallego-Bartolomé, J., Minguet, E.G., Grau-Enguix, F., Abbas, M., Locascio, A., Thomas, S.G., Alabadí, D., and Blázquez, M.A. (2012). Molecular mechanism for the interaction between gibberellin and brassinosteroid signaling pathways in Arabidopsis. PNAS *109*, 13446–13451.

Gao, Y., Jia, L., Hu, B., Alva, A., and Fan, M. (2014). Potato Stolon and Tuber Growth Influenced by Nitrogen Form. Plant Production Science *17*, 138–143.

Gibson, D.G., Young, L., Chuang, R.-Y., Venter, J.C., Hutchison, C.A., and Smith, H.O. (2009). Enzymatic assembly of DNA molecules up to several hundred kilobases. Nat Meth *6*, 343–345.

Giessen, T.W., and Marahiel, M.A. (2014). The tRNA-Dependent Biosynthesis of Modified Cyclic Dipeptides. Int J Mol Sci *15*, 14610–14631.

Giessen, T.W., and Marahiel, M.A. (2015). Rational and combinatorial tailoring of bioactive cyclic dipeptides. Front Microbiol *6*.

Gillard, J., Frenkel, J., Devos, V., Sabbe, K., Paul, C., Rempt, M., Inzé, D., Pohnert, G., Vuylsteke, M., and Vyverman, W. (2013a). Metabolomics Enables the Structure Elucidation of a Diatom Sex Pheromone. Angewandte Chemie International Edition *52*, 854–857.

Gondry, M., Jacques, I.B., Thai, R., Babin, M., Canu, N., Seguin, J., Belin, P., Pernodet, J.-L., and Moutiez, M. (2018). A Comprehensive Overview of the Cyclodipeptide Synthase Family Enriched with the Characterization of 32 New Enzymes. Front Microbiol *9*.

Gondry, M., Sauguet, L., Belin, P., Thai, R., Amouroux, R., Tellier, C., Tuphile, K., Jacquet, M., Braud, S., Courçon, M., et al. (2009). Cyclodipeptide synthases are a family of tRNA-dependent peptide bond–forming enzymes. Nature Chemical Biology *5*, 414–420.

Griffiths, J., Murase, K., Rieu, I., Zentella, R., Zhang, Z.-L., Powers, S.J., Gong, F., Phillips, A.L., Hedden, P., Sun, T., et al. (2006). Genetic Characterization and Functional Analysis of the GID1 Gibberellin Receptors in Arabidopsis. Plant Cell *18*, 3399–3414.

Grillet, L., Mari, S., and Schmidt, W. (2014). Iron in seeds – loading pathways and subcellular localization. Front Plant Sci *4*.

Halliday, K.J., Martínez-García, J.F., and Josse, E.-M. (2009). Integration of Light and Auxin Signaling. Cold Spring Harb Perspect Biol *1*.

Hannon, M., Gimpel, J., Tran, M., Rasala, B., and Mayfield, S. (2010). Biofuels from algae: challenges and potential. Biofuels *1*, 763–784.

Hartwig, T., Corvalan, C., Best, N.B., Budka, J.S., Zhu, J.-Y., Choe, S., and Schulz, B. (2012). Propiconazole Is a Specific and Accessible Brassinosteroid (BR) Biosynthesis Inhibitor for Arabidopsis and Maize. PLOS ONE *7*, e36625.

Hartwig, T., Corvalan, C., Best, N.B., Budka, J.S., Zhu, J.-Y., Choe, S., and Schulz, B. (2012). Propiconazole is a specific and accessible brassinosteroid (BR) biosynthesis inhibitor for Arabidopsis and maize. PLoS ONE *7*, e36625.

Hayashi, K. (2012). The Interaction and Integration of Auxin Signaling Components. Plant Cell Physiol *53*, 965–975.

Hedden, P., and Thomas, S.G. (2012). Gibberellin biosynthesis and its regulation. Biochemical Journal *444*, 11–25.

Heide, O.M. (1977). Photoperiod and Temperature Interactions in Growth and Flowering of Strawberry. Physiologia Plantarum *40*, 21–26.

Helliwell, K.E., Wheeler, G.L., Leptos, K.C., Goldstein, R.E., and Smith, A.G. (2011). Insights into the Evolution of Vitamin B12 Auxotrophy from Sequenced Algal

Genomes. Mol Biol Evol *28*, 2921–2933.

Hirano, K., Asano, K., Tsuji, H., Kawamura, M., Mori, H., Kitano, H., Ueguchi-Tanaka, M., and Matsuoka, M. (2010). Characterization of the Molecular Mechanism Underlying Gibberellin Perception Complex Formation in Rice[C][W]. Plant Cell *22*, 2680–2696.

Hirsch, S., and Oldroyd, G.E. (2009). GRAS-domain transcription factors that regulate plant development. Plant Signal Behav *4*, 698–700.

Hmelo, L.R. (2017). Quorum Sensing in Marine Microbial Environments. Annual Review of Marine Science *9*, 257–281.

Holden, M.T.G., Chhabra, S.R., Nys, R.D., Stead, P., Bainton, N.J., Hill, P.J., Manefield, M., Kumar, N., Labatte, M., England, D., et al. (1999). Quorum-sensing cross talk: isolation and chemical characterization of cyclic dipeptides from Pseudomonas aeruginosa and other Gram-negative bacteria. Molecular Microbiology *33*, 1254–1266.

Hothorn, M., Belkhadir, Y., Dreux, M., Dabi, T., Noel, J.P., Wilson, I.A., and Chory, J. (2011). Structural basis of steroid hormone perception by the receptor kinase BRI1. Nature *474*, 467–471.

Huang, Y., Wang, X., Ge, S., and Rao, G.-Y. (2015). Divergence and adaptive evolution of the gibberellin oxidase genes in plants. BMC Evolutionary Biology *15*, 207.

Hughes, D.T., and Sperandio, V. (2008b). Inter-kingdom signalling: communication between bacteria and their hosts. Nat Rev Microbiol *6*, 111–120.

Hytönen, T., Elomaa, P., Moritz, T., and Junttila, O. (2009). Gibberellin mediates daylength-controlled differentiation of vegetative meristems in strawberry (Fragaria × ananassa Duch). BMC Plant Biol *9*, 18.

Ikeda, M., Fujiwara, S., Mitsuda, N., and Ohme-Takagi, M. (2012). A Triantagonistic Basic Helix-Loop-Helix System Regulates Cell Elongation in Arabidopsis. Plant Cell *24*, 4483–4497.

Jan, A., and Komatsu, S. (2006). Functional Characterization of Gibberellin-Regulated Genes in Rice Using Microarray System. Genomics Proteomics Bioinformatics *4*, 137–144.

Johansson, H., Jones, H.J., Foreman, J., Hemsted, J.R., Stewart, K., Grima, R., and Halliday, K.J. (2014). *Arabidopsis* cell expansion is controlled by a photothermal switch. Nature Communications *5*, ncomms5848.

JOHNSTON, J.S., PEPPER, A.E., HALL, A.E., CHEN, Z.J., HODNETT, G., DRABEK, J., LOPEZ, R., and PRICE, H.J. (2005). Evolution of Genome Size in

Brassicaceae. Ann Bot *95*, 229–235.

Kang, C., Darwish, O., Geretz, A., Shahan, R., Alkharouf, N., and Liu, Z. (2013). Genome-scale transcriptomic insights into early-stage fruit development in woodland strawberry Fragaria vesca. Plant Cell *25*, 1960–1978.

Kataev, A.A., Andreeva-Kovalevskaya, Z.I., Solonin, A.S., and Ternovsky, V.I. (2012). Bacillus cereus can attack the cell membranes of the alga Chara corallina by means of HlyII. Biochimica et Biophysica Acta (BBA) - Biomembranes *1818*, 1235–1241.

Kazamia, E., Czesnick, H., Nguyen, T.T.V., Croft, M.T., Sherwood, E., Sasso, S., Hodson, S.J., Warren, M.J., and Smith, A.G. (2012). Mutualistic interactions between vitamin B12-dependent algae and heterotrophic bacteria exhibit regulation. Environmental Microbiology *14*, 1466–1476.

Kim, K., Shin, J., Lee, S.-H., Kweon, H.-S., Maloof, J.N., and Choi, G. (2011). Phytochromes inhibit hypocotyl negative gravitropism by regulating the development of endodermal amyloplasts through phytochrome-interacting factors. PNAS *108*, 1729–1734.

Kumar, N., Mohandas, C., Nambisan, B., Kumar, D.R.S., and Lankalapalli, R.S. (2013). Isolation of proline-based cyclic dipeptides from Bacillus sp. N strain associated with rhabitid entomopathogenic nematode and its antimicrobial properties. World J Microbiol Biotechnol *29*, 355–364.

Lee, J., Park, J.H., Shin, Y.S., Lee, B.C., Chang, N.I., Cho, J., and Kim, S.D. (2009). Effect of dissolved organic matter on the growth of algae, Pseudokirchneriella subcapitata, in Korean lakes: The importance of complexation reactions. Ecotoxicology and Environmental Safety *72*, 335–343.

Lee, S., Lee, S., Yang, K.-Y., Kim, Y.-M., Park, S.-Y., Kim, S.Y., and Soh, M.-S. (2006a). Overexpression of PRE1 and its Homologous Genes Activates Gibberellin-dependent Responses in Arabidopsis thaliana. Plant Cell Physiol *47*, 591–600.

Lee, S., Lee, S., Yang, K.-Y., Kim, Y.-M., Park, S.-Y., Kim, S.Y., and Soh, M.-S. (2006b). Overexpression of PRE1 and its Homologous Genes Activates Gibberellin-dependent Responses in Arabidopsis thaliana. Plant Cell Physiol *47*, 591–600.

Legris, M., Klose, C., Burgie, E.S., Rojas, C.C.R., Neme, M., Hiltbrunner, A., Wigge, P.A., Schäfer, E., Vierstra, R.D., and Casal, J.J. (2016). Phytochrome B integrates light and temperature signals in Arabidopsis. Science *354*, 897–900.

Leivar, P., and Monte, E. (2014). PIFs: Systems Integrators in Plant Development. The Plant Cell *26*, 56–78.

Li, K., Yu, R., Fan, L.-M., Wei, N., Chen, H., and Deng, X.W. (2016). DELLA-mediated PIF degradation contributes to coordination of light and gibberellin signalling in *Arabidopsis*. Nature Communications *7*, 11868.

Li, Q.-F., and He, J.-X. (2013). Mechanisms of signaling crosstalk between brassinosteroids and gibberellins. Plant Signal Behav *8*.

Lin, K.-T., and Wang, L.-H. (2016). New dimension of glucocorticoids in cancer treatment. Steroids *111*, 84–88.

Liu, Z., and Franks, R.G. (2015). Molecular basis of fruit development. Front Plant Sci *6*.

Lu, Y., and Xu, J. (2015). Phytohormones in microalgae: a new opportunity for microalgal biotechnology? Trends in Plant Science *20*, 273–282.

Lucas Miguel (2014). PIFs get BRright: PHYTOCHROME INTERACTING FACTORs as integrators of light and hormonal signals. New Phytologist *202*, 1126–1141.

Lucas, M. de, Davière, J.-M., Rodríguez-Falcón, M., Pontin, M., Iglesias-Pedraz, J.M., Lorrain, S., Fankhauser, C., Blázquez, M.A., Titarenko, E., and Prat, S. (2008). A molecular framework for light and gibberellin control of cell elongation. Nature *451*, 480.

Marhold, K., Kudoh, H., Pak, J.-H., Watanabe, K., Španiel, S., and Lihová, J. (2010). Cytotype diversity and genome size variation in eastern Asian polyploid Cardamine (Brassicaceae) species. Ann Bot *105*, 249–264.

Martí, C., Orzáez, D., Ellul, P., Moreno, V., Carbonell, J., and Granell, A. (2007). Silencing of DELLA induces facultative parthenocarpy in tomato fruits. The Plant Journal *52*, 865–876.

Martínez-Cuenca, M.-R., Legaz, F., Forner-Giner, M.Á., Primo-Millo, E., and Iglesias, D.J. (2013). Bicarbonate blocks iron translocation from cotyledons inducing iron stress responses in Citrus roots. Journal of Plant Physiology *170*, 899–905.

Martins, A.O., Nunes-Nesi, A., Araújo, W.L., and Fernie, A.R. (2018). To Bring Flowers or Do a Runner: Gibberellins Make the Decision. Molecular Plant *11*, 4–6.

Martínez-García, J.F., Huq, E., and Quail, P.H. (2000). Direct Targeting of Light Signals to a Promoter Element-Bound Transcription Factor. Science *288*, 859–863.

Miller, B.R., and Gulick, A.M. (2016). Structural Biology of Non-Ribosomal Peptide Synthetases. Methods Mol Biol *1401*, 3–29.

Miller, M.B., and Bassler, B.L. (2001). Quorum Sensing in Bacteria. Annual Review of Microbiology *55*, 165–199.

Mittra, B., Cortez, M., Haydock, A., Ramasamy, G., Myler, P.J., and Andrews, N.W. (2013). Iron uptake controls the generation of Leishmania infective forms through regulation of ROS levels. J. Exp. Med. *210*, 401–416.

Moeys, S., Frenkel, J., Lembke, C., Gillard, J.T.F., Devos, V., Van den Berge, K., Bouillon, B., Huysman, M.J.J., De Decker, S., Scharf, J., et al. (2016b). A sex-inducing pheromone triggers cell cycle arrest and mate attraction in the diatom *Seminavis robusta*. Scientific Reports *6*, 19252.

Monte, E., Tepperman, J.M., Al-Sady, B., Kaczorowski, K.A., Alonso, J.M., Ecker, J.R., Li, X., Zhang, Y., and Quail, P.H. (2004). The phytochrome-interacting transcription factor, PIF3, acts early, selectively, and positively in light-induced chloroplast development. PNAS *101*, 16091–16098.

Morrissey, J., and Bowler, C. (2012). Iron Utilization in Marine Cyanobacteria and Eukaryotic Algae. Front Microbiol *3*.

Morrissey, J., and Guerinot, M.L. (2009). Iron uptake and transport in plants: The good, the bad, and the ionome. Chem Rev *109*, 4553–4567.

Morrissey, J., Baxter, I.R., Lee, J., Li, L., Lahner, B., Grotz, N., Kaplan, J., Salt, D.E., and Guerinot, M.L. (2009). The Ferroportin Metal Efflux Proteins Function in Iron and Cobalt Homeostasis in Arabidopsis. Plant Cell *21*, 3326–3338.

Mouhu, K., Kurokura, T., Koskela, E.A., Albert, V.A., Elomaa, P., and Hytönen, T. (2013). The Fragaria vesca Homolog of SUPPRESSOR OF OVEREXPRESSION OF CONSTANS1 Represses Flowering and Promotes Vegetative Growth. The Plant Cell *25*, 3296–3310.

Mozaffarian, D., Cao, H., King, I.B., Lemaitre, R.N., Song, X., Siscovick, D.S., and Hotamisligil, G.S. (2010). Circulating palmitoleic acid and risk of metabolic abnormalities and new-onset diabetes. Am J Clin Nutr *92*, 1350–1358.

Murase, K., Hirano, Y., Sun, T., and Hakoshima, T. (2008). Gibberellin-induced DELLA recognition by the gibberellin receptor GID1. Nature *456*, 459–463.

Murphy, L.A., Moore, T., and Nesnow, S. (2012). Propiconazole-enhanced hepatic cell proliferation is associated with dysregulation of the cholesterol biosynthesis pathway leading to activation of Erk1/2 through Ras farnesylation. Toxicology and Applied Pharmacology *260*, 146–154.

Neuhaus, G. (2013). Morphology and Anatomy of Vascular Plants. In Strasburger's Plant Sciences: Including Prokaryotes and Fungi, A. Bresinsky, C. Körner, J.W. Kadereit, G. Neuhaus, and U. Sonnewald, eds. (Berlin, Heidelberg: Springer), pp. 161–235.

Ni, W., Xu, S.-L., González-Grandío, E., Chalkley, R.J., Huhmer, A.F.R., Burlingame, A.L., Wang, Z.-Y., and Quail, P.H. (2017). PPKs mediate direct signal

transfer from phytochrome photoreceptors to transcription factor PIF3. Nature Communications *8*, 15236.

Nymark, M., Sharma, A.K., Sparstad, T., Bones, A.M., and Winge, P. (2016). A CRISPR/Cas9 system adapted for gene editing in marine algae. Scientific Reports *6*, 24951.

Ogawa, M., Hanada, A., Yamauchi, Y., Kuwahara, A., Kamiya, Y., and Yamaguchi, S. (2003). Gibberellin Biosynthesis and Response during Arabidopsis Seed Germination. Plant Cell *15*, 1591–1604.

Oh, E., Zhu, J.-Y., and Wang, Z.-Y. (2012). Interaction between BZR1 and PIF4 integrates brassinosteroid and environmental responses. Nat Cell Biol *14*, 802–809.

Oh, E., Zhu, J.-Y., Bai, M.-Y., Arenhart, R.A., Sun, Y., and Wang, Z.-Y. (2014). Cell elongation is regulated through a central circuit of interacting transcription factors in the Arabidopsis hypocotyl. ELife *3*.

Oh, K., Matsumoto, T., Hoshi, T., and Yoshizawa, Y. (2016). In vitro and in vivo evidence for the inhibition of brassinosteroid synthesis by propiconazole through interference with side chain hydroxylation. Plant Signaling & Behavior *11*, e1158372.

Ortiz-Castro, R., Díaz-Pérez, C., Martínez-Trujillo, M., Río, R.E. del, Campos-García, J., and López-Bucio, J. (2011). Transkingdom signaling based on bacterial cyclodipeptides with auxin activity in plants. PNAS *108*, 7253–7258.

Pacín, M., Legris, M., and Casal, J.J. (2013). COP1 re-accumulates in the nucleus under shade. Plant J. *75*, 631–641.

Pan, C., Tian, K., Ban, Q., Wang, L., Sun, Q., He, Y., Yang, Y., Pan, Y., Li, Y., Jiang, J., et al. (2017). Genome-Wide Analysis of the Biosynthesis and Deactivation of Gibberellin-Dioxygenases Gene Family in Camellia sinensis (L.) O. Kuntze. Genes (Basel) *8*.

Park, E., Kim, J., Lee, Y., Shin, J., Oh, E., Chung, W.-I., Liu, J.R., and Choi, G. (2004). Degradation of Phytochrome Interacting Factor 3 in Phytochrome-Mediated Light Signaling. Plant Cell Physiol *45*, 968–975.

Perrot-Rechenmann, C. (2010). Cellular Responses to Auxin: Division versus Expansion. Cold Spring Harb Perspect Biol *2*.

Pham, V.N., Kathare, P.K., and Huq, E. (2018). Phytochromes and Phytochrome Interacting Factors. Plant Physiology *176*, 1025–1038.

Prescott, A.G., and John, P. (1996). DIOXYGENASES: Molecular Structure and Role in Plant Metabolism. Annu. Rev. Plant Physiol. Plant Mol. Biol. *47*, 245–271.

Qiu, Y., Pasoreck, E.K., Reddy, A.K., Nagatani, A., Ma, W., Chory, J., and Chen, M.

(2017). Mechanism of early light signaling by the carboxy-terminal output module of Arabidopsis phytochrome B. Nature Communications *8*, 1905.

Quail, P.H. (2002). Phytochrome photosensory signalling networks. Nature Reviews Molecular Cell Biology *3*, 85–93.

Rantanen, M., Kurokura, T., Jiang, P., Mouhu, K., and Hytönen, T. (2015). Strawberry homologue of TERMINAL FLOWER1 integrates photoperiod and temperature signals to inhibit flowering. The Plant Journal *82*, 163–173.

Rantanen, M., Kurokura, T., Mouhu, K., Pinho, P., Tetri, E., Halonen, L., Palonen, P., Elomaa, P., and Hytönen, T. (2014). Light quality regulates flowering in FvFT1/FvTFL1 dependent manner in the woodland strawberry Fragaria vesca. Front Plant Sci *5*.

Robert, S., Zouhar, J., Carter, C., and Raikhel, N. (2007). Isolation of intact vacuoles from Arabidopsis rosette leaf–derived protoplasts. Nat. Protocols *2*, 259–262.

Rockwell, N.C., Su, Y.-S., and Lagarias, J.C. (2006). Phytochrome structure and signaling mechanisms. Annu Rev Plant Biol *57*, 837–858.

Roschzttardtz, H., Conéjéro, G., Curie, C., and Mari, S. (2009). Identification of the Endodermal Vacuole as the Iron Storage Compartment in the Arabidopsis Embryo. Plant Physiol. *151*, 1329–1338.

Ross, J.J., and Reid, J.B. (2010). Evolution of growth-promoting plant hormones. Functional Plant Biol. *37*, 795–805.

Russell, S.D. (2010). Fertilization in Angiosperms. In Plant Developmental Biology - Biotechnological Perspectives: Volume 1, E.C. Pua, and M.R. Davey, eds. (Berlin, Heidelberg: Springer Berlin Heidelberg), pp. 283–300.

Rutherford, S.T., and Bassler, B.L. (2012). Bacterial Quorum Sensing: Its Role in Virulence and Possibilities for Its Control. Cold Spring Harb Perspect Med *2*.

Ryan, R.P., and Dow, J.M. (2008). Diffusible signals and interspecies communication in bacteria. Microbiology *154*, 1845–1858.

SCAVEN, V.L., and RAFFERTY, N.E. (2013). Physiological effects of climate warming on flowering plants and insect pollinators and potential consequences for their interactions. Curr Zool *59*, 418–426.

Segev, E., Wyche, T.P., Kim, K.H., Petersen, J., Ellebrandt, C., Vlamakis, H., Barteneva, N., Paulson, J.N., Chai, L., Clardy, J., et al. (2016). Dynamic metabolic exchange governs a marine algal-bacterial interaction. ELife *5*, e17473.

Seyedsayamdost, M.R., Case, R.J., Kolter, R., and Clardy, J. (2011). The Jekyll-and-Hyde chemistry of Phaeobacter gallaeciensis. Nat Chem *3*, 331–335.

Shankaran, H., Wiley, H.S., and Resat, H. (2007). Receptor downregulation and desensitization enhance the information processing ability of signalling receptors. BMC Syst Biol *1*, 48.

Shim, J.S., Kubota, A., and Imaizumi, T. (2017). Circadian Clock and Photoperiodic Flowering in Arabidopsis: CONSTANS Is a Hub for Signal Integration. Plant Physiology *173*, 5–15.

Shin, J., Kim, K., Kang, H., Zulfugarov, I.S., Bae, G., Lee, C.-H., Lee, D., and Choi, G. (2009). Phytochromes promote seedling light responses by inhibiting four negatively-acting phytochrome-interacting factors. Proc Natl Acad Sci U S A *106*, 7660–7665.

Siriwardhana, N., Kalupahana, N.S., and Moustaid-Moussa, N. (2012). Health benefits of n-3 polyunsaturated fatty acids: eicosapentaenoic acid and docosahexaenoic acid. Adv. Food Nutr. Res. *65*, 211–222.

Slamti, L., Perchat, S., Huillet, E., and Lereclus, D. (2014). Quorum Sensing in Bacillus thuringiensis Is Required for Completion of a Full Infectious Cycle in the Insect. Toxins (Basel) *6*, 2239–2255.

Song, Y.H., Shim, J.S., Kinmonth-Schultz, H.A., and Imaizumi, T. (2015). Photoperiodic Flowering: Time Measurement Mechanisms in Leaves. Annu Rev Plant Biol *66*, 441–464.

Steber, C.M., and McCourt, P. (2001). A Role for Brassinosteroids in Germination in Arabidopsis. Plant Physiology *125*, 763–769.

Sun, T. (2008). Gibberellin Metabolism, Perception and Signaling Pathways in Arabidopsis. Arabidopsis Book *6*.

Sun, T. (2011). The Molecular Mechanism and Evolution of the GA–GID1–DELLA Signaling Module in Plants. Current Biology *21*, R338–R345.

Sutak, R., Botebol, H., Blaiseau, P.-L., Léger, T., Bouget, F.-Y., Camadro, J.-M., and Lesuisse, E. (2012a). A Comparative Study of Iron Uptake Mechanisms in Marine Microalgae: Iron Binding at the Cell Surface Is a Critical Step1[W][OA]. Plant Physiol *160*, 2271–2284.

Takeda, N., Handa, Y., Tsuzuki, S., Kojima, M., Sakakibara, H., and Kawaguchi, M. (2015). Gibberellin regulates infection and colonization of host roots by arbuscular mycorrhizal fungi. Plant Signal Behav *10*.

Tan, K.W.M., and Lee, Y.K. (2016). The dilemma for lipid productivity in green microalgae: importance of substrate provision in improving oil yield without sacrificing growth. Biotechnology for Biofuels *9*, 255.

Tenreira, T., Lange, M.J.P., Lange, T., Bres, C., Labadie, M., Monfort, A., Hernould,

M., Rothan, C., and Denoyes, B. (2017). A Specific Gibberellin 20-Oxidase Dictates the Flowering-Runnering Decision in Diploid Strawberry[OPEN]. Plant Cell *29*, 2168–2182.

Trupkin, S.A., Legris, M., Buchovsky, A.S., Rivero, M.B.T., and Casal, J.J. (2014). Phytochrome B Nuclear Bodies Respond to the Low Red to Far-Red Ratio and to the Reduced Irradiance of Canopy Shade in Arabidopsis. Plant Physiology *165*, 1698–1708.

van Tol, H.M., Amin, S.A., and Armbrust, E.V. (2017). Ubiquitous marine bacterium inhibits diatom cell division. The ISME Journal *11*, 31–42.

Vargas, C. de, Audic, S., Henry, N., Decelle, J., Mahé, F., Logares, R., Lara, E., Berney, C., Bescot, N.L., Probert, I., et al. (2015). Eukaryotic plankton diversity in the sunlit ocean. Science *348*, 1261605.

Voss, B.J., Gaddy, J.A., McDonald, W.H., and Cover, T.L. (2014). Analysis of Surface-Exposed Outer Membrane Proteins in Helicobacter pylori. J. Bacteriol. *196*, 2455–2471.

Wang, H., and Wang, H. (2015). Phytochrome Signaling: Time to Tighten up the Loose Ends. Molecular Plant *8*, 540–551.

White, M.D., and Flashman, E. (2016). Catalytic strategies of the non-heme iron dependent oxygenases and their roles in plant biology. Curr Opin Chem Biol *31*, 126–135.

Wild, M., Davière, J.-M., Regnault, T., Sakvarelidze-Achard, L., Carrera, E., Lopez Diaz, I., Cayrel, A., Dubeaux, G., Vert, G., and Achard, P. (2016). Tissue-Specific Regulation of Gibberellin Signaling Fine-Tunes Arabidopsis Iron-Deficiency Responses. Developmental Cell *37*, 190–200.

Willige, B.C., Ghosh, S., Nill, C., Zourelidou, M., Dohmann, E.M.N., Maier, A., and Schwechheimer, C. (2007). The DELLA Domain of GA INSENSITIVE Mediates the Interaction with the GA INSENSITIVE DWARF1A Gibberellin Receptor of Arabidopsis. Plant Cell *19*, 1209–1220.

Winzer, K., Hardie, K.R., and Williams, P. (2002). Bacterial cell-to-cell communication: sorry, can't talk now — gone to lunch! Current Opinion in Microbiology *5*, 216–222.

Wodniok, S., Brinkmann, H., Glöckner, G., Heidel, A.J., Philippe, H., Melkonian, M., and Becker, B. (2011). Origin of land plants: Do conjugating green algae hold the key? BMC Evol Biol *11*, 104.

Wolbang, C.M., Chandler, P.M., Smith, J.J., and Ross, J.J. (2004). Auxin from the Developing Inflorescence Is Required for the Biosynthesis of Active Gibberellins in Barley Stems. Plant Physiol *134*, 769–776.

Wu, C.-T., and Bradford, K.J. (2003). Class I chitinase and beta-1,3-glucanase are differentially regulated by wounding, methyl jasmonate, ethylene, and gibberellin in tomato seeds and leaves. Plant Physiol. *133*, 263–273.

Wuddineh, W.A., Mazarei, M., Zhang, J., Poovaiah, C.R., Mann, D.G.J., Ziebell, A., Sykes, R.W., Davis, M.F., Udvardi, M.K., and Stewart, C.N. (2015). Identification and overexpression of gibberellin 2-oxidase (GA2ox) in switchgrass (Panicum virgatum L.) for improved plant architecture and reduced biomass recalcitrance. Plant Biotechnol. J. *13*, 636–647.

Xu, F., Li, T., Xu, P.-B., Li, L., Du, S.-S., Lian, H.-L., and Yang, H.-Q. (2016). DELLA proteins physically interact with CONSTANS to regulate flowering under long days in Arabidopsis. FEBS Lett *590*, 541–549.

Yang, Y.-H., Du, L., Hosokawa, M., Miyashita, K., Kokubun, Y., Arai, H., and Taroda, H. (2017). Fatty Acid and Lipid Class Composition of the Microalga *Phaeodactylum tricornutum*. Journal of Oleo Science *66*, 363–368.

Yao, S., Lyu, S., An, Y., Lu, J., Gjermansen, C., and Schramm, A. (2019). Microalgae–bacteria symbiosis in microalgal growth and biofuel production: a review. Journal of Applied Microbiology *126*, 359–368.

Ying, J., Lin, R., Xu, P., Wu, Y., Liu, Y., and Zhao, Y. (2018). Prebiotic formation of cyclic dipeptides under potentially early Earth conditions. Sci Rep *8*, 1–8.

Zaslavskaia, L.A., Lippmeier, J.C., Shih, C., Ehrhardt, D., Grossman, A.R., and Apt, K.E. (2001). Trophic Conversion of an Obligate Photoautotrophic Organism Through Metabolic Engineering. Science *292*, 2073–2075.

Zentella, R., Zhang, Z.-L., Park, M., Thomas, S.G., Endo, A., Murase, K., Fleet, C.M., Jikumaru, Y., Nambara, E., Kamiya, Y., et al. (2007). Global Analysis of DELLA Direct Targets in Early Gibberellin Signaling in Arabidopsis. Plant Cell *19*, 3037–3057.

Zentella, R., Zhang, Z.-L., Park, M., Thomas, S.G., Endo, A., Murase, K., Fleet, C.M., Jikumaru, Y., Nambara, E., Kamiya, Y., et al. (2007). Global Analysis of DELLA Direct Targets in Early Gibberellin Signaling in Arabidopsis. Plant Cell *19*, 3037–3057.

Zhang, L.-H., and Dong, Y.-H. (2004). Quorum sensing and signal interference: diverse implications. Molecular Microbiology *53*, 1563–1571.

Zhang, Chunye, and Hanhua Hu. “High-Efficiency Nuclear Transformation of the Diatom Phaeodactylum Tricornutum by Electroporation.” *Marine Genomics*, Marine Diatoms, 16 (August 2014): 63–66. doi:10.1016/j.margen.2013.10.003

Zhou, J., Lyu, Y., Richlen, M., Anderson, D.M., and Cai, Z. (2016c). Quorum sensing is a language of chemical signals and plays an ecological role in algal-bacterial interactions. CRC Crit Rev Plant Sci *35*, 81–105.

Zhu, J.-Y., Sae-Seaw, J., and Wang, Z.-Y. (2013). Brassinosteroid signalling. Development *140*, 1615–1620.

Zhu, L.D., Li, Z.H., and Hiltunen, E. (2016). Strategies for Lipid Production Improvement in Microalgae as a Biodiesel Feedstock. Biomed Res Int *2016*.

Zribi, K., and Gharsalli, M. (2002). Effect of Bicarbonate on Growth and Iron Nutrition of Pea. Journal of Plant Nutrition *25*, 2143–2149.